

A First Order Deconfinement Transition in Large N Yang-Mills Theory on a Small S^3

Ofer Aharony^a, Joseph Marsano^{b,c}, Shiraz Minwalla^{c,b},
Kyriakos Papadodimas^{b,c} and Mark Van Raamsdonk^d

^a*Department of Particle Physics, Weizmann Institute of Science, Rehovot 76100, Israel*

^b*Jefferson Physical Laboratory, Harvard University, Cambridge, MA 02138, USA*

^c*Department of Theoretical Physics, Tata Institute of Fundamental Research,
Homi Bhabha Rd, Mumbai 400005, India*

^d*Department of Physics and Astronomy, University of British Columbia,
Vancouver, BC, V6T 1Z1, Canada*

We give an analytic demonstration that the $3 + 1$ dimensional large N $SU(N)$ pure Yang-Mills theory, compactified on a small S^3 so that the coupling constant at the compactification scale is very small, has a first order deconfinement transition as a function of temperature. We do this by explicitly computing the relevant terms in the canonical partition function up to 3-loop order; this is necessary because the leading (1-loop) result for the phase transition is precisely on the borderline between a first order and a second order transition. Since numerical work strongly suggests that the infinite volume large N theory also has a first order deconfinement transition, we conjecture that the phase structure is independent of the size of the S^3 . To deal with divergences in our calculations, we are led to introduce a novel method of regularization useful for nonabelian gauge theory on S^3 .

1. Introduction

It is widely believed that 3+1-dimensional $SU(N)$ Yang Mills theory on \mathbb{R}^3 confines at low temperatures, but is deconfined at high temperatures. Compelling numerical evidence indicates that in the absence of quarks, when all fields are in the adjoint representation, there is a sharp phase transition separating the confined and the deconfined phases, which occurs at a temperature $T \sim \Lambda_{QCD}$. Since the Yang Mills theory is strongly coupled at the transition temperature, the deconfinement phase transition is rather poorly understood. In particular, using the currently available analytic techniques it is not possible to determine even the order of the transition for $N \neq 3$; lattice simulations suggest that the transition is of second order for $N = 2$ and of first order for $N \geq 3$ (see [1,2] for the latest results for $N > 3$).

The intractability of the thermal behaviour of Yang Mills theory on \mathbb{R}^3 is related to the absence of a dimensionless coupling constant. It is thus interesting to note that Yang Mills theory compactified on an S^3 of radius R has an effective dimensionless coupling constant, $R\Lambda_{QCD}$. Indeed, when $R\Lambda_{QCD} \ll 1$, the Yang Mills coupling constant is weak even at the lowest energy scale in the theory, $E \sim 1/R$. As a consequence, at small values of $\Lambda_{QCD}R$, the thermal behaviour of this system is completely tractable¹. Unfortunately, the most interesting feature of infinite volume thermodynamics – the sharp deconfinement phase transition – is smoothed out into crossover behaviour at any finite R , assuming that N is also finite.

However, in the ‘thermodynamic’ $N \rightarrow \infty$ ’t Hooft limit (with fixed $\lambda \equiv g_{YM}^2 N$ [3]), this deconfinement phase transition remains sharp even at finite R . In this limit it is possible to study the dynamics of the deconfinement transition as a function of the effective coupling constant $R\Lambda_{QCD}$. When $R\Lambda_{QCD} \gg 1$, this system approaches the theory on \mathbb{R}^3 . On the other hand, in the opposite limit $R\Lambda_{QCD} \rightarrow 0$ the theory is weakly coupled, and may be solved exactly [4,5]; quite remarkably it turns out that this ‘free’ gauge theory undergoes a confinement-deconfinement phase transition at a temperature of order $1/R$.²

¹ More precisely, it is tractable for temperatures smaller than an upper bound that scales to infinity in the limit $\Lambda_{QCD}R \rightarrow 0$, see section 5. This would not be true if the gauge field had zero modes on the compact space, which is why we chose a sphere rather than, say, a torus.

² As discussed in [5], the $\lambda = 0$ theory must still obey a Gauss Law constraint which requires physical states to be gauge invariant. This constraint leads to nontrivial thermodynamics even at zero coupling.

At strictly zero coupling, the transition is first order, but lies precisely at the border between first and second order behaviour, as reviewed below. Consequently, to understand the nature of the transition at weak nonzero coupling, the leading effects of interaction terms must be taken into account via a perturbative calculation. This calculation is the goal of the present paper.

Before describing the calculation and our result, we recall the essential details of the story in the $\lambda = 0$ limit. It was demonstrated in [4,5] that in the limit $R\Lambda_{QCD} \rightarrow 0$ in which the theory becomes free, the thermal partition function of Yang Mills theory on a 3-sphere of radius R reduces (up to an overall constant) to an integral over a single unitary $SU(N)$ matrix³

$$Z(\beta) = \int [dU] \exp[-S_{\text{eff}}(U)], \quad (1.1)$$

where

$$S_{\text{eff}}(U) = - \sum_{n=1}^{\infty} \frac{z_V(e^{-n\beta/R})}{n} \text{Tr}(U^n) \text{Tr}(U^{-n}); \quad z_V(x) = \frac{6x^2 - 2x^3}{(1-x)^3}, \quad (1.2)$$

and $\beta \equiv 1/T$. The matrix U is the holonomy of the gauge field around the thermal circle (more precisely, $U = e^{i\beta\alpha}$ with α the zero mode of A_0 on $S^3 \times S^1$ [5]). All other modes of the theory are massive, and the effective action is obtained by integrating them out.

As usual, in the large N limit, it is convenient to replace the integral over the unitary matrix U by an integral over the eigenvalue distribution $\rho(\theta) \equiv \frac{1}{N} \sum_i \delta(\theta - \theta_i)$ (where $e^{i\theta_i}$, for $i = 1, \dots, N$, are the eigenvalues of U). Let u_n denote the n^{th} Fourier mode of the eigenvalue distribution, $u_n \equiv \int e^{in\theta} \rho(\theta) d\theta = \text{Tr}(U^n)/N$. In the large N limit, (1.1) may be rewritten as [5]

$$Z(\beta) = \int du_n d\bar{u}_n \exp \left[-N^2 \sum_{n=1}^{\infty} \frac{(1 - z_V(e^{-n\beta/R}))}{n} |u_n|^2 \right], \quad (1.3)$$

with a complicated integration boundary for the u_n 's coming from the non-negativity of $\rho(\theta)$. Equation (1.3) may be evaluated in the saddle point approximation in the large N limit. This system has one obvious saddle point located at $u_n = 0$ (for all $n \geq 1$). This saddle point is stable and dominates (1.3) whenever $(1 - z_V(e^{-n\beta/R}))$ is positive for all n , which is the case for $T < T_c = \frac{1}{R \ln(2+\sqrt{3})} \approx \frac{0.759326}{R}$.

³ We will generally ignore the distinction between $SU(N)$ and $U(N)$ groups in this paper; the only difference between their partition functions is an overall coupling-independent factor coming from the free $U(1)$ photons.

At $T = T_c$, $z_V(e^{-\beta/R}) = 1$ and the potential for u_1 in (1.3) is exactly flat (all other u_n remain massive). For $T > T_c$, the variable u_1 becomes tachyonic about the saddle point described above. At these temperatures, the system is dominated by a new saddle point, one in which u_1 has an expectation value of order unity (see [5]). Thus, free Yang Mills theory on S^3 undergoes a phase transition at $T = T_c$; the order parameter for this transition is the expectation value of the Polyakov loop u_1 (more precisely, since u_1 has an arbitrary phase, the order parameter is actually $|u_1|^2$ [5]). Since the saddle point changes discontinuously at $T = T_c$, this phase transition is of first order. However, this phase transition is extremely finely tuned⁴, in a sense we will now explain.

As described above, the exact Wilsonian effective action for the order parameter u_1 , expanded about the low temperature saddle point in the limit of zero gauge coupling, is $S_{eff} = N^2 (1 - z_V(e^{-\beta/R})) |u_1|^2$. This effective action is corrected at nonzero gauge coupling; it was argued in [5] that at nonzero coupling it takes the form⁵

$$\frac{S_{eff}}{N^2} = \left[\left(1 - z_V(e^{-\beta/R})\right) + \mathcal{O}(\lambda) \right] |u_1|^2 + \lambda^2 b(\beta) |u_1|^4 + \mathcal{O}(\lambda^4), \quad (1.4)$$

where $\lambda \equiv g_{YM}^2 N$ is the 't Hooft coupling evaluated at the energy scale $1/R$, and $b(\beta)$ is a perturbatively computable function of the temperature.

The action (1.4) describes a system that undergoes a phase transition at $T = T_c + \mathcal{O}(\lambda)$. The nature of this phase transition depends crucially on the sign of $b = b(\beta_c)$, where $\beta_c = 1/T_c$. If b is negative, the phase transition is of first order, as in the free theory. However, unlike in the free theory, this transition occurs at a lower temperature than the temperature at which u_1 in (1.4) becomes massless (the latter temperature was identified in [4,5] with the Hagedorn temperature of the large N Yang-Mills theory).

On the other hand, if b is positive, the phase transition continues to occur precisely at the temperature at which u_1 becomes massless; however, it is now of second order and is followed, at a slightly higher temperature, by another phase transition of third order, similar to that of [6] (see section 6 of [5] for more details).

The leading perturbative contribution to the value of b at the phase transition temperature is determined by a set of 2-loop and 3-loop vacuum diagrams in the Yang Mills

⁴ As one indication, the order parameter u_1 is massless at the phase transition point, a feature usually associated with second order transitions.

⁵ To obtain the explicit effective action, we first integrate out all massive modes on the sphere, and subsequently all of the other u_n modes for $n > 1$.

theory on a sphere [5]. In this paper we evaluate b by computing the relevant Feynman diagrams.

Our main result is that $b(\beta_c) \simeq -5.7 \times 10^{-4}$. Note, in particular, that b is negative; consequently, the deconfinement transition for large N $SU(N)$ Yang-Mills theory on a 3-sphere with small but nonzero $R\Lambda_{QCD}$ is of first order. As noted above, lattice simulations suggest that the large N deconfinement phase transition is also of first order in the opposite infinite-volume limit $R\Lambda_{QCD} \rightarrow \infty$. Thus, it is tempting to conjecture that the phase diagram for the large N $SU(N)$ Yang Mills theory on S^3 takes the form shown in figure 1.

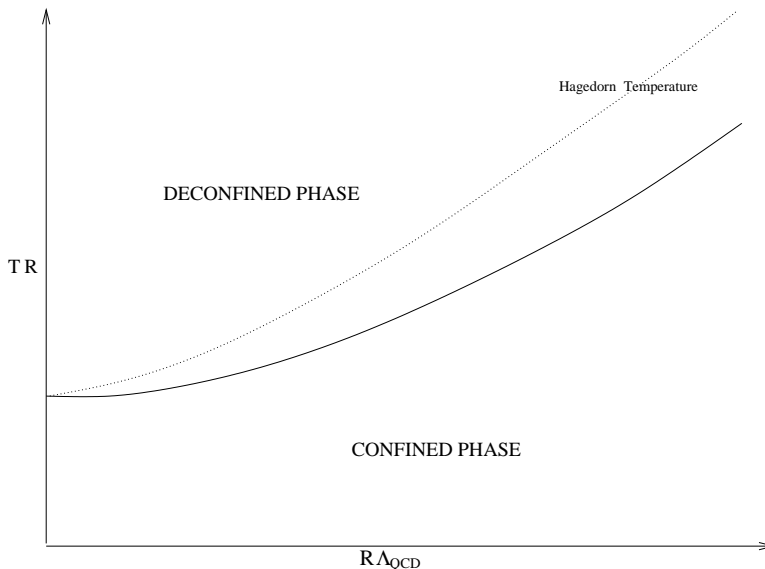


Figure 1: The simplest possible phase diagram for large N Yang Mills theory on S^3 .

The solid line in figure 1 denotes the phase transition. The dotted line describes the boundary of stability (the locus at which the coefficient of $|u_1|^2$ is zero) of the low temperature phase, which would be interpreted by a low temperature observer as a limiting or Hagedorn temperature.

Of course, the conjectured phase diagram in figure 1 merely represents the simplest phase diagram consistent with our knowledge of the behaviour of all order parameters at weak and strong coupling. It is possible that the true phase diagram is more complicated; for instance, the confined phase at small $R\Lambda_{QCD}$ could be separated from the confined phase at large $R\Lambda_{QCD}$ by a phase transition.

This paper is organized as follows. In section 2, we set up our calculation, and describe, in general terms, the procedure we employ to compute b . We then proceed in section 3 to enumerate and evaluate all diagrams that contribute to b .

The lengthy calculation we present is straightforward in principle but involves some subtleties. First, it is necessary to deal with UV divergences which show up in the perturbative computation. Due to technical difficulties associated with implementing dimensional regularization on S^3 , we have found it convenient to regularize the Feynman diagrams in a rather unusual fashion: we use a (non-gauge-invariant) momentum cut-off, and simultaneously add in a set of compensating non-gauge-invariant counterterms, such that the full theory is gauge-invariant when the cutoff is removed. This regularization procedure is described briefly in section 2.4, with a more detailed discussion, including checks, examples, and the explicit evaluation of the counterterms needed for our calculation presented in section 4 and in appendix A.

In section 5, we discuss potential problems related to the infra-red divergences associated with finite-temperature field theory. Naively there should be no trouble at finite volume, where all modes are massive. However, it turns out that there is still a breakdown of perturbation theory at sufficiently high temperatures, when the dynamically generated mass scales exceed the Kaluza-Klein scale $1/R$. Fortunately, as we argue in section 5, these effects are not important at the transition temperature and do not affect our determination of b .

In section 6, we present some conclusions and discussion.

Finally, in order to compute sums over S^3 spherical harmonics, which replace the loop integrals of the flat space theory, we needed to derive various spherical harmonic identities. These identities, together with some basic properties of the spherical harmonics for S^3 are collected in appendix B.

2. The Setup for the Perturbative Calculation

As we have described, the order of the deconfinement phase transition for pure Yang-Mills theory at small volume is determined by the sign of the quartic coefficient b in the effective action (1.4) at the $\lambda = 0$ transition temperature. In this section, we set up the calculation of this coefficient, which may be determined from leading order perturbative corrections to the matrix model action (1.2) for the $SU(N)$ pure Yang-Mills theory on S^3 . For simplicity, we will generally take the radius of the S^3 to be one; it can always be reinstated by dimensional analysis. The actual computation is presented in the next section.

2.1. Basic objective

The basic set-up for the computation was described in section 4 of [5]. We consider pure $SU(N)$ Yang-Mills theory on S^3 , at finite temperature. The thermal partition function may be computed by evaluating the Euclidean path integral with Euclidean time compactified on a circle of radius $\beta = 1/T$. The Euclidean action is given as usual by

$$\mathcal{L} = \frac{1}{4} \int_0^\beta dt \int d^3x \operatorname{tr}(F_{\mu\nu} F^{\mu\nu}). \quad (2.1)$$

For calculations on S^3 , it is convenient to work in the gauge

$$\partial_i A^i = 0, \quad (2.2)$$

where $i = 1, 2, 3$ runs over the sphere coordinates, and ∂_i are (space-time) covariant derivatives. Equation (2.2) fixes the gauge only partially; it leaves spatially independent (but time dependent) gauge transformations unfixed. We fix this residual gauge invariance by setting the constant mode of A_0 to be constant in time,

$$\partial_t \int_{S^3} A_0 = 0. \quad (2.3)$$

It will be convenient to give this (time independent) zero mode a name; we define

$$\alpha = \frac{g_{YM}}{\omega_3} \int_{S^3} A_0, \quad (2.4)$$

where ω_3 is the volume of the 3-sphere. α will play a special role in what follows, because it turns out that it is the only zero mode (mode whose action vanishes at quadratic order) in the decomposition of Yang Mills theory into Kaluza-Klein modes on $S^3 \times S^1$.

As α is a zero mode, it cannot be integrated out in perturbation theory (roughly speaking, α fluctuations are always strongly coupled in the bare action). In order to perturbatively evaluate the free energy we will therefore adopt a two step procedure. In the first step we integrate out all nonzero modes and generate an effective action for α . As described in [5], this action will be non-trivial even at zero coupling, and it is corrected in perturbation theory in λ . In the second step, we analyze the remaining integral over α .

On general grounds described in [5], the finite temperature effective action for α can be written completely in terms of the unitary matrix $U \equiv e^{i\beta\alpha}$ in the form :

$$\begin{aligned} S_{eff} = & \sum_m C_{m,-m}(x) \operatorname{tr}(U^m) \operatorname{tr}(U^{-m}) + \lambda\beta \sum_{m,n} C_{m,n,-m-n}(x) \operatorname{tr}(U^m) \operatorname{tr}(U^n) \operatorname{tr}(U^{-m-n})/N \\ & + \lambda^2\beta \sum_{m,n,p} C_{m,n,p,-m-n-p}(x) \operatorname{tr}(U^m) \operatorname{tr}(U^n) \operatorname{tr}(U^p) \operatorname{tr}(U^{-m-n-p})/N^2 + \dots, \end{aligned} \quad (2.5)$$

where $x \equiv e^{-\beta}$. Here, the coefficients obey appropriate constraints such that the action is real, and in general are corrected at higher orders in λ and $1/N$. As described in [5], the free energy F of the Yang Mills theory is then given by the matrix integral

$$e^{-\beta F} = \int [dU] e^{-S_{eff}(U)}, \quad (2.6)$$

where the Fadeev-Popov determinant corresponding to the gauge-fixing (2.3) transforms the integral over α into an integral over the gauge group with Haar measure $[dU]$.

At large N , the unitary integral may be evaluated using saddle point techniques. Defining $u_n = \text{tr}(U^n)/N$, we write the effective action in the form

$$Z = \int [du_i] e^{-N^2 S'_{eff}(u_n)}. \quad (2.7)$$

where S'_{eff} includes contributions both from S_{eff} and from the Vandermonde determinant obtained in changing to the variables u_n . The order N^2 contribution to the free energy is then given by the minimum value of $S'_{eff}(u_n)$, and the deconfinement phase transition occurs where this minimum is no longer at $|u_n| = 0$.

As described in detail in section 6 of [5], in order to compute the order of this phase transition, we have to look at $S'_{eff}(u_n)$ near the phase transition point $x_c = 2 - \sqrt{3}$ where (as shown in [4,5] and reviewed in the introduction) the mass term of u_1 changes sign, and compute the leading corrections to the potential for u_1 . The relevant terms in the action, to leading order in λ and in $x - x_c$, take the form

$$\begin{aligned} S'_{\text{eff}}(u_n) = & \mu_1(x_c - x)|u_1|^2 + \mu_2|u_2|^2 + \dots \\ & + \lambda\beta[C_{1,1,-2}(u_1^2\bar{u}_2 + \bar{u}_1^2u_2) + \dots] \\ & + \lambda^2\beta[C_{1,1,-1,-1}|u_1|^4 + \dots]. \end{aligned} \quad (2.8)$$

At large N , the effective action (1.4) for u_1 is obtained from this by classically minimizing over u_n for fixed u_1 . In particular, the variable u_2 may now be integrated out in (2.8) by setting it to its classical value

$$u_2 = -\lambda \frac{\beta_c C_{1,1,-2}}{\mu_2} u_1^2 + \mathcal{O}(\lambda^2). \quad (2.9)$$

This yields the following effective action for u_1 :

$$S'_{eff}(u_1) = \mu_1(x_c - x)|u_1|^2 + b\lambda^2|u_1|^4 + \dots, \quad (2.10)$$

where

$$b = \beta_c C_{1,1,-1,-1} - \frac{\beta_c^2 C_{1,1,-2}^2}{\mu_2}. \quad (2.11)$$

Our goal will be to compute the coefficients appearing here at the leading order in λ , and thus determine the sign of b , and the order of the transition, at weak coupling. Since an n -loop diagram has at most $n + 1$ index lines, a term in S_{eff} with m traces gets its lowest order contributions at $m - 1$ loops. Thus, the term μ_2 arises at one-loop order, $C_{1,1,-2}$ requires a two-loop computation, while $C_{1,1,-1,-1}$ requires a three-loop calculation.

2.2. Gauge-fixed action

We now set up the perturbative computation that will determine $S_{eff}(U)$, the effective action for U (which we treat as a background field). The Fadeev-Popov determinant corresponding to the gauge fixing condition (2.2) is

$$\det \partial_i D^i = \int \mathcal{D}c \mathcal{D}\bar{c} e^{-\text{tr}(\bar{c} \partial_i D^i c)}, \quad (2.12)$$

where D^i denotes a gauge covariant derivative

$$D_i c = \partial_i c - ig_{YM} [A_i, c], \quad (2.13)$$

and c and \bar{c} are complex ghosts in the adjoint representation of the gauge group. The quadratic terms in the gauge-fixed Yang-Mills action (2.1) take the form

$$- \int d^4x \text{tr} \left(\frac{1}{2} A_i (D_\tau^2 + \partial^2) A^i + \frac{1}{2} A_0 \partial^2 A_0 + \bar{c} \partial^2 c \right), \quad (2.14)$$

where ∂^2 is the Laplacian on the sphere and

$$D_\tau X \equiv \partial_0 X - i[\alpha, X]. \quad (2.15)$$

The interaction terms in (2.1) are given by

$$\begin{aligned} & \int d^4x \text{tr} (ig_{YM} D_\tau A^i [A_i, A_0] - ig_{YM} [A^i, A^0] \partial_i A_0 - ig_{YM} \partial_i A_j [A^i, A^j] + \\ & \quad \frac{g_{YM}^2}{4} [A_i, A_j] [A^j, A^i] - \frac{g_{YM}^2}{2} [A_0, A_i] [A^0, A^i] - ig_{YM} \partial_i \bar{c} [A_i, c]). \end{aligned} \quad (2.16)$$

2.3. The spherical harmonic expansion

On S^3 , integrals over spatial momenta are replaced by sums over the quantum numbers of $SO(4)$ angular momenta. It will thus be useful to expand the fields explicitly in terms

of an orthonormal basis of functions on S^3 which are angular momentum eigenstates, and write the action explicitly in terms of a standard set of integrals over these spherical harmonic functions. We denote the scalar and vector spherical harmonics on S^3 by $S^\alpha(\Omega)$ and $V_i^\beta(\Omega)$, where $\alpha = (j_\alpha, m_\alpha, m'_\alpha)$ and $\beta = (j_\beta, m_\beta, m'_\beta, \epsilon_\beta)$ are the angular momentum (and parity for the vector field) quantum numbers for the various modes. The properties of these functions are reviewed in appendix B.

We expand the modes of the fields in terms of these spherical harmonics as follows :

$$\begin{aligned} A_0(t, \theta) &= \sum_{\alpha} a^\alpha(t) S^\alpha(\theta); \\ A_i(t, \theta) &= \sum_{\beta} A_i^\beta(t) V_i^\beta(\theta); \\ c(t, \theta) &= \sum_{\alpha} c^\alpha(t) S^\alpha(\theta). \end{aligned} \tag{2.17}$$

Note that general vector functions also include modes proportional to ∇S^α , but these are eliminated by our gauge choice. Below, it will be useful to denote the complex conjugates of S^α and V_i^β by $S^{\bar{\alpha}}$ and $V_i^{\bar{\beta}}$.

In terms of these spherical harmonics, we define

$$\begin{aligned} C^{\alpha\beta\gamma} &= \int_{S^3} S^\alpha \vec{V}^\beta \cdot \vec{\nabla} S^\gamma, \\ D^{\alpha\beta\gamma} &= \int_{S^3} \vec{V}^\alpha \cdot \vec{V}^\beta S^\gamma, \\ E^{\alpha\beta\gamma} &= \int_{S^3} \vec{V}^\alpha \cdot (\vec{V}^\beta \times \vec{V}^\gamma), \end{aligned} \tag{2.18}$$

where explicit expressions for C , D and E may be found in [7] and are collected in appendix B. Note that C is antisymmetric in α and γ , D is symmetric in α and β , and E is totally antisymmetric.

Using the spherical harmonic expansions, we may now write the action for gauge-fixed pure Yang-Mills theory on S^3 explicitly in terms of modes. The quadratic action becomes

$$S_2 = \int dt \text{tr} \left(\frac{1}{2} A^{\bar{\alpha}} (-D_\tau^2 + (j_\alpha + 1)^2) A^\alpha + \frac{1}{2} a^{\bar{\alpha}} j_\alpha (j_\alpha + 2) a^\alpha + \bar{c}^{\bar{\alpha}} j_\alpha (j_\alpha + 2) c^\alpha \right). \tag{2.19}$$

In addition, we have cubic interactions

$$\begin{aligned} S_3 = g_{YM} \int dt \text{tr} & \left(i \bar{c}^{\bar{\alpha}} [A^\gamma, c^\beta] C^{\bar{\alpha}\gamma\beta} + 2i a^\alpha A^\gamma a^\beta C^{\alpha\gamma\beta} \right. \\ & \left. - i [A^\alpha, D_\tau A^\beta] a^\gamma D^{\alpha\beta\gamma} + i A^\alpha A^\beta A^\gamma \epsilon_\alpha (j_\alpha + 1) E^{\alpha\beta\gamma} \right), \end{aligned} \tag{2.20}$$

and quartic interactions

$$S_4 = g_{YM}^2 \int dt \operatorname{tr} \left(-\frac{1}{2} [a^\alpha, A^\beta] [a^\gamma, A^\delta] \left(D^{\beta\bar{\lambda}\alpha} D^{\delta\lambda\gamma} + \frac{1}{j_\lambda(j_\lambda + 2)} C^{\alpha\beta\bar{\lambda}} C^{\gamma\delta\lambda} \right) \right. \\ \left. - \frac{1}{2} A^\alpha A^\beta A^\gamma A^\delta \left(D^{\alpha\gamma\bar{\lambda}} D^{\beta\delta\lambda} - D^{\alpha\delta\bar{\lambda}} D^{\beta\gamma\lambda} \right) \right). \quad (2.21)$$

The propagators of the various fields follow from (2.19) and are given by

$$\langle \bar{c}_{ab}^\alpha(t) c_{cd}^\beta(t') \rangle = \frac{1}{j_\alpha(j_\alpha + 2)} \delta^{\alpha\beta} \delta(t - t') \delta_{ad} \delta_{cb}, \quad (2.22)$$

$$\langle a_{ab}^\alpha(t) a_{cd}^\beta(t') \rangle = \frac{1}{j_\alpha(j_\alpha + 2)} \delta^{\alpha\bar{\beta}} \delta(t - t') \delta_{ad} \delta_{cb}, \quad (2.23)$$

$$\langle A_{ab}^\alpha(t) A_{cd}^\beta(t') \rangle = \delta^{\alpha\bar{\beta}} \Delta_{j_\alpha}^{ad,cb}(t - t'). \quad (2.24)$$

Here, Δ is defined to be a periodic function of time satisfying

$$(-D_\tau^2 + (j + 1)^2) \Delta_j(t) = \delta(t) \quad (2.25)$$

where we have suppressed matrix indices. For $0 \leq t \leq \beta$, the explicit solution is given by

$$\Delta_j(t) \equiv \frac{e^{i\alpha t}}{2(j + 1)} \left(\frac{e^{-(j+1)t}}{1 - e^{i\alpha\beta} e^{-(j+1)\beta}} - \frac{e^{(j+1)t}}{1 - e^{i\alpha\beta} e^{(j+1)\beta}} \right) \quad (2.26)$$

with the value for other values of t defined by the periodicity. Here, α is shorthand for $\alpha \otimes 1 - 1 \otimes \alpha$, and a term $\alpha^n \otimes \alpha^m$ in the expansion of Δ should be understood to carry indices $(\alpha^n)^{ad} (\alpha^m)^{cb}$ in (2.24).

For our calculations, the following correlators are also useful

$$\langle D_\tau A_{ab}^\alpha(t) A_{cd}^\beta(t') \rangle = -\langle A_{ab}^\alpha(t) D_\tau A_{cd}^\beta(t') \rangle = \delta^{\alpha\bar{\beta}} D_\tau \Delta_{j_\alpha}^{ad,cb}(t - t'), \quad (2.27)$$

$$\langle D_\tau A_{ab}^\alpha(t) D_\tau A_{cd}^\beta(t') \rangle = \delta^{\alpha\bar{\beta}} \delta(t - t') \delta_{ad} \delta_{cb} - \delta^{\alpha\bar{\beta}} (j_\alpha + 1)^2 \Delta_{j_\alpha}^{ad,cb}(t - t'). \quad (2.28)$$

2.4. Regularization and counterterms

As usual with four dimensional gauge theories, certain perturbative calculations lead naively to ultraviolet divergences. In our calculation of the coefficient b in (1.4), we will find that all divergences cancel, but only after summing a collection of logarithmically divergent diagrams. It is therefore necessary to introduce a regularization scheme, and in order to obtain the correct finite result, this must respect gauge invariance.

In principle, there is no obstacle in taking the usual approach of applying dimensional regularization. In our case, this amounts to considering gauge theory on $S^3 \times S^1 \times \mathbb{R}^{d-4}$.⁶ While it is straightforward to write down the appropriate expressions for Feynman diagrams in this dimensionally regulated theory, we have found it difficult to evaluate them because of the combination of momentum sums and integrals that appear. Thus, we have found it helpful to apply a more unusual approach, which nevertheless gives precisely the answers that would have been obtained through dimensional regularization.

In practice, we apply a sharp momentum cutoff to the total angular momentum quantum number for modes on the sphere. This does not respect gauge invariance. However, as explained originally by 't Hooft [8] in his series of classic papers on the renormalizability of Yang Mills theory, a non gauge invariant regularization yields gauge invariant results when employed with a bare Yang Mills action that includes an appropriate set of non-gauge-invariant counterterms. As we describe in section 4, these counterterms may be determined by demanding that simple Green's functions evaluated using the cutoff and counterterms agree with the same Green's functions evaluated using dimensional regularization. Apart from curvature-dependent counterterms (which do not contribute to our calculation), this comparison may be carried out in flat space, since all counterterms must be local.

In section 4, we present the calculation to determine the precise coefficients for all counterterms necessary in our calculation, together with a more complete discussion of the regularization scheme and a variety of consistency checks. In the end, we should expect non-zero coefficients for all counterterms with dimension less than or equal to four which respect $SO(3)$ invariance.

3. The Perturbative Computation

In this section, we proceed to calculate the coefficients in (2.8) necessary to determine the order of the deconfinement transition at weak coupling. We have

$$\begin{aligned} e^{-S_{eff}(U)} &= \int [da][dA][dc] e^{-S(\alpha, a, A, c)} \\ &= e^{-S_{eff}^{1 loop}} \langle e^{-S_3 - S_4} \rangle, \end{aligned} \tag{3.1}$$

⁶ As we describe in section 4, in order that all momentum sums/integrals are rendered finite when employing dimensional regularization in Coulomb gauge, it is necessary to analytically continue both the number of dimensions which participate in the Coulomb gauge condition, and the number of dimensions which do not, a procedure referred to as split dimensional regularization.

where the expectation value in the last line is evaluated in the free theory with propagators given in section 2. The required leading order contributions to μ_2 , $C_{1,1,-2}$, and $C_{1,1,-1,-1}$ appear at one, two, and three loops respectively.

3.1. Simplifying the action by integrating out A_0 and c

Since the action is quadratic in a and c , these may be integrated out explicitly to yield additional interaction vertices for the A 's. The first contribution arises from loops of a or c . For the calculation up to three loops that we are interested in here, the relevant vertices in the resulting effective action (combining a and c loops) are a quadratic vertex

$$A_2 = g_{YM}^2 N \delta(0) \frac{D^{\gamma_1 \alpha \beta} D^{\gamma_2 \bar{\alpha} \bar{\beta}}}{j_\beta(j_\beta + 2)} \text{tr}(A^{\gamma_1} A^{\gamma_2}), \quad (3.2)$$

a cubic vertex

$$A_3 = -2i g_{YM}^3 N \delta(0) \frac{C^{\bar{\alpha} \gamma_1 \bar{\beta}} D^{\gamma_2 \delta \beta} D^{\gamma_3 \bar{\delta} \alpha}}{j_\alpha(j_\alpha + 2) j_\beta(j_\beta + 2)} \text{tr}(A^{\gamma_1} A^{\gamma_2} A^{\gamma_3}), \quad (3.3)$$

and a quartic vertex

$$\begin{aligned} A_4 = -g_{YM}^4 N \delta(0) & \left(3 \frac{C^{\alpha \gamma_1 \bar{\beta}} C^{\beta \gamma_2 \bar{\rho}} D^{\gamma_3 \lambda \rho} D^{\gamma_4 \bar{\lambda} \bar{\alpha}}}{j_\alpha(j_\alpha + 2) j_\beta(j_\beta + 2) j_\rho(j_\rho + 2)} + \frac{1}{2} \frac{D^{\gamma_1 \lambda \alpha} D^{\gamma_2 \bar{\lambda} \beta} D^{\gamma_3 \rho \bar{\beta}} D^{\gamma_4 \bar{\rho} \bar{\alpha}}}{j_\alpha(j_\alpha + 2) j_\beta(j_\beta + 2)} \right) \\ & \times \left(\text{tr}(A^{\gamma_1} A^{\gamma_2} A^{\gamma_3} A^{\gamma_4}) + \frac{1}{N} \text{tr}(A^{\gamma_1} A^{\gamma_2}) \text{tr}(A^{\gamma_3} A^{\gamma_4}) \right. \\ & \left. + \frac{1}{N} \text{tr}(A^{\gamma_1} A^{\gamma_3}) \text{tr}(A^{\gamma_2} A^{\gamma_4}) + \frac{1}{N} \text{tr}(A^{\gamma_1} A^{\gamma_4}) \text{tr}(A^{\gamma_2} A^{\gamma_3}) \right). \end{aligned} \quad (3.4)$$

We have included here only terms that can contribute to planar diagrams. Note that all of these are proportional to a divergent factor $\delta(0)$, and so any diagrams containing these vertices must eventually cancel.⁷ Note also that since these vertices arise from loops, they have additional factors of $g_{YM}^2 N$ compared to (2.20), (2.21). Therefore, inserting any one of these vertices into a diagram counts as an additional loop.

In addition to these, we have vertices arising from open strings of a 's containing two vertices linear in a and some number of vertices quadratic in a . These start at quartic

⁷ The divergence associated with $\delta(0)$ terms may be regulated using a momentum cutoff in the S^1 direction. We have checked that in the properly regulated theory, the naive cancellations of $\delta(0)$ terms described below persist without introducing any new finite contributions.

order, and for our three loop calculation, we will need the quartic, quintic, and sextic vertices. These are

$$\begin{aligned}
B_4 &= \frac{g_{YM}^2}{2} \frac{D^{\alpha_1 \beta_1 \gamma} D^{\alpha_2 \beta_2 \bar{\gamma}}}{j_\gamma(j_\gamma + 2)} \text{tr}([A^{\alpha_1}, D_\tau A^{\beta_1}][A^{\alpha_2}, D_\tau A^{\beta_2}]), \\
B_5 &= -ig_{YM}^3 \frac{D^{\alpha_1 \beta_1 \lambda} C^{\bar{\lambda} \gamma \bar{\sigma}} D^{\alpha_2 \beta_2 \sigma}}{j_\lambda(j_\lambda + 2)j_\sigma(j_\sigma + 2)} \text{tr}([A^{\alpha_1}, D_\tau A^{\beta_1}][A^\gamma, [A^{\alpha_2}, D_\tau A^{\beta_2}]]), \\
B_6 &= \frac{g_{YM}^4}{2} \left(3 \frac{D^{\alpha_1 \beta_1 \sigma} C^{\bar{\sigma} \gamma_1 \tau} C^{\bar{\tau} \gamma_2 \lambda} D^{\alpha_2 \beta_2 \bar{\lambda}}}{j_\lambda(j_\lambda + 2)j_\sigma(j_\sigma + 2)j_\tau(j_\tau + 2)} + \frac{D^{\alpha_1 \beta_1 \sigma} D^{\gamma_1 \lambda \bar{\sigma}} D^{\gamma_2 \bar{\lambda} \bar{\tau}} D^{\alpha_2 \beta_2 \tau}}{j_\sigma(j_\sigma + 2)j_\tau(j_\tau + 2)} \right) \\
&\quad \text{tr}([A^{\alpha_1}, D_\tau A^{\beta_1}], A^{\gamma_1} [[A^{\alpha_2}, D_\tau A^{\beta_2}], A^{\gamma_2}]).
\end{aligned} \tag{3.5}$$

Using these effective vertices, it is straightforward to check that all divergent contributions proportional to $\delta(0)$ cancel. Any diagram with a vertex A_2 will cancel the $\delta(0)$ part of a similar diagram with A_2 replaced with a B_4 having its two covariant derivative legs contracted. Similarly, any diagram with a vertex A_3 will cancel the $\delta(0)$ part of a similar diagram with A_3 replaced with a B_5 having its two covariant derivative legs contracted. Finally, any diagram containing A_4 will cancel against a combination of two diagrams: one with A_4 replaced by B_6 with its two covariant derivative legs contracted, and one with A_4 replaced by two B_4 's with the four covariant derivative legs contracted into a loop.

Thus, all $\delta(0)$ terms coming from the A_n vertices cancel out, and it is easy to check that there are no additional $\delta(0)$ terms coming from diagrams with B_n vertices apart from those needed to cancel the A_n vertex diagrams. As a result, we may proceed with the calculation by keeping only the transverse photons A^α , and evaluating all diagrams built from the original cubic and quartic vertices in the transverse photons plus the additional vertices B_4 , B_5 , and B_6 , ignoring any terms proportional to $\delta(0)$.

The diagrams contributing to the free energy at one, two and three loop orders, after having integrated out A_0 and c , are shown in figure 2. The B -type vertices are denoted by circles.

3.2. 1-Loop

The one-loop computation of the path integral was described in [5]. The result (writing only the leading terms in the large N limit) is

$$S_{eff}(U) = \frac{11\beta N^2}{120} - \sum_{n=1}^{\infty} \frac{z_V(x^n)}{n} \text{tr}(U^n) \text{tr}(U^{-n}), \tag{3.6}$$

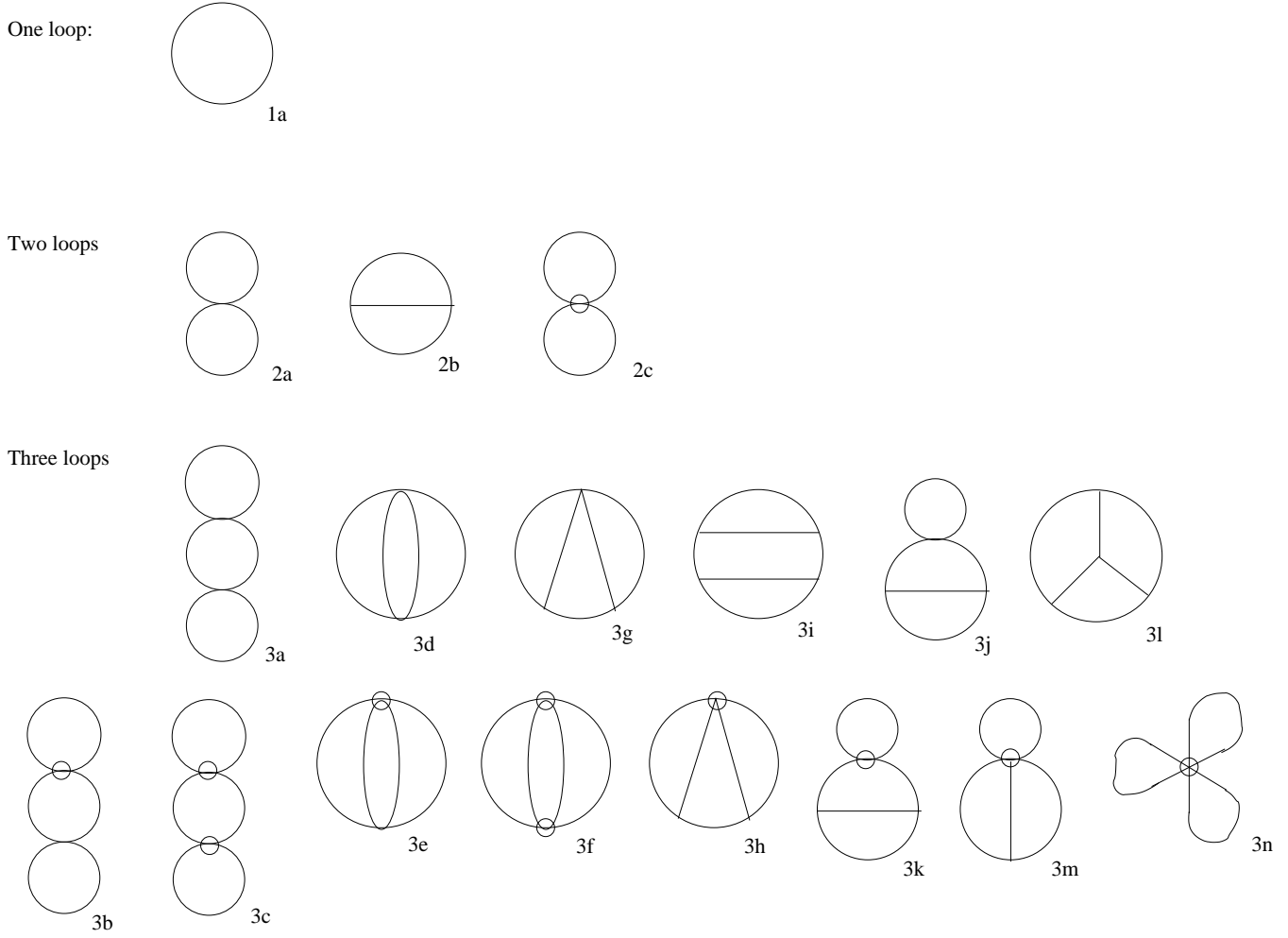


Figure 2: The diagrams contributing to the free energy up to 3-loop order. In this figure we present a particular planar form for each diagram, but in some cases the same diagram may also be drawn in the plane in different ways. There is also an additional counter-term diagram that will be discussed later.

where $z_V(x)$ is the single-particle partition function for a free vector field on S^3 , given by

$$z_V(x) = \frac{6x^2 - 2x^3}{(1-x)^3}. \quad (3.7)$$

Changing variables to $u_n = \text{tr}(U^n)/N$ and including the additional Vandermonde determinant from the measure, we have

$$S'_{eff}(u_n) = \frac{11\beta}{120} + \sum_{n=1}^{\infty} \frac{1}{n} (1 - z_V(x^n)) |u_n|^2, \quad (3.8)$$

and thus

$$\mu_2(x_c) = \frac{1}{2} (1 - z_V(x_c^2)) \approx 0.481125. \quad (3.9)$$

3.3. Two Loops

In this section we compute the coefficient $C_{1,1,-2}$ in (2.8) by evaluating the three two-loop diagrams of figure 2. Note that since the propagators depend only on the relative time between vertices, it is always possible to change variables so that the integrand is independent of one of the time variables. The integral over this variable then gives an overall factor of β so it is convenient to define $F(U) = S_{eff}(U)/\beta$. In terms of the propagators and spherical harmonic integrals defined above, we find that the three two-loop contributions to F are⁸ (with summation over the spherical harmonic indices α , β and γ implied)

$$\begin{aligned}
F_{2a} &= -\frac{g_{YM}^2}{2} (D^{\alpha\beta\gamma} D^{\bar{\alpha}\bar{\beta}\bar{\gamma}} - D^{\alpha\bar{\alpha}\gamma} D^{\beta\bar{\beta}\bar{\gamma}}) \Delta_{j_\alpha}(0, \alpha_{ab}) \Delta_{j_\beta}(0, \alpha_{ac}), \\
F_{2b} &= -\frac{g_{YM}^2}{6} \epsilon_\alpha(j_\alpha + 1) \widehat{E}^{\alpha\beta\gamma} \widehat{E}^{\bar{\alpha}\bar{\beta}\bar{\gamma}} \int dt \Delta_{j_\alpha}(t, \alpha_{ab}) \Delta_{j_\beta}(t, \alpha_{bc}) \Delta_{j_\gamma}(t, \alpha_{ca}), \\
F_{2c} &= g_{YM}^2 \frac{D^{\alpha\beta\gamma} D^{\bar{\alpha}\bar{\beta}\bar{\gamma}}}{j_\gamma(j_\gamma + 2)} (D_\tau \Delta_{j_\alpha}(0, \alpha_{ac}) D_\tau \Delta_{j_\beta}(0, \alpha_{ab}) + (j_\beta + 1)^2 \Delta_{j_\alpha}(0, \alpha_{bc}) \Delta_{j_\beta}(0, \alpha_{ab})),
\end{aligned} \tag{3.10}$$

where we have defined

$$\widehat{E}^{\alpha\beta\gamma} \equiv E^{\alpha\beta\gamma} (\epsilon_\alpha(j_\alpha + 1) + \epsilon_\beta(j_\beta + 1) + \epsilon_\gamma(j_\gamma + 1)). \tag{3.11}$$

In the expressions above, each of the propagators contributes factors of α to two of the three index loops, which we label by a, b , and c . The notation α_{ab} indicates that for the tensor products $(\alpha \otimes 1 - 1 \otimes \alpha)$ appearing in the propagator, the first and second elements of the tensor product appear in the traces associated with index loops a and b respectively.

The expressions (3.10) involve sums over products of spherical harmonic integrals. In all cases here and below, the sums over quantum numbers m, m' and ϵ may be carried out explicitly using the formulae in appendix B. To express the results, it is useful, following [7], to define some functions which appear in integrals of products of spherical harmonics

$$R_2(x, y, z) = \frac{(-1)^{\sigma'}}{\pi} \left[\frac{(x+1)(z+1)(\sigma' - x)(\sigma' - y)(\sigma' - z)(\sigma' + 1)}{(y+1)} \right]^{1/2}, \tag{3.12}$$

⁸ Recall that in diagram 2c, we ignore the part proportional to $\delta(0)$.

$$\begin{aligned}
R_{3\epsilon_x\epsilon_z}(x, y, z) &= \frac{(-1)^{\sigma+(\epsilon_x+\epsilon_z)/2}}{\pi} \left(\frac{(y+1)}{32(x+1)(z+1)} \right)^{\frac{1}{2}} \\
&\quad \cdot ((\epsilon_x(x+1) + \epsilon_z(z+1) + y + 2)(\epsilon_x(x+1) + \epsilon_z(z+1) + y) \\
&\quad \quad (\epsilon_x(x+1) + \epsilon_z(z+1) - y)(\epsilon_x(x+1) + \epsilon_z(z+1) - y - 2))^{\frac{1}{2}}, \\
R_{4\epsilon_x\epsilon_y\epsilon_z}(x, y, z) &= \frac{(-1)^{\sigma'+1}}{\pi} \text{sign}(\epsilon_x + \epsilon_y + \epsilon_z) \left(\frac{(\sigma'+1)(\sigma'-x)(\sigma'-y)(\sigma'-z)}{4(x+1)(y+1)(z+1)} \right)^{\frac{1}{2}} \\
&\quad \cdot ((\epsilon_x(x+1) + \epsilon_y(y+1) + \epsilon_z(z+1) + 2)(\epsilon_x(x+1) + \epsilon_y(y+1) + \epsilon_z(z+1) - 2))^{\frac{1}{2}}, \\
\widehat{R}_{4\epsilon_x\epsilon_y\epsilon_z}(x, y, z) &= R_{4\epsilon_x\epsilon_y\epsilon_z}(x, y, z)(\epsilon_x(x+1) + \epsilon_y(y+1) + \epsilon_z(z+1)),
\end{aligned} \tag{3.13}$$

where the right-hand sides of the equations are defined to be non-zero only if the triangle inequality $|x-z| \leq y \leq x+z$ holds, and if $\sigma \equiv (x+y+z)/2$ (in R_3) and $\sigma' \equiv (x+y+z+1)/2$ (in R_2 and R_4) are integers. We also define $R_{3+} \equiv R_{3++} = R_{3--}$, $R_{3-} \equiv R_{3+-} = R_{3-+}$, $R_{4+} \equiv R_{4+++}$ and $R_{4-} \equiv R_{4+-}$.

With these definitions, we find after performing the sums over m , m' and ϵ , that

$$\begin{aligned}
F_{2a} &= \frac{2g_{YM}^2}{3\pi^2} j_\alpha(j_\alpha + 2)j_\beta(j_\beta + 2)\Delta_{j_\alpha}(0, \alpha_{ab})\Delta_{j_\beta}(0, \alpha_{ac}), \\
F_{2b} &= -g_{YM}^2 \left(\frac{1}{3}(j_\alpha + j_\beta + j_\gamma + 3)^2 R_{4+}^2(j_\alpha, j_\beta, j_\gamma) + (j_\alpha + j_\beta - j_\gamma + 1)^2 R_{4-}^2(j_\alpha, j_\beta, j_\gamma) \right) \\
&\quad \int dt \Delta_{j_\alpha}(t, \alpha_{ab})\Delta_{j_\beta}(t, \alpha_{bc})\Delta_{j_\gamma}(t, \alpha_{ca}), \\
F_{2c} &= \frac{2g_{YM}^2}{j_\gamma(j_\gamma + 2)} (R_{3+}^2(j_\alpha, j_\gamma, j_\beta) + R_{3-}^2(j_\alpha, j_\gamma, j_\beta)) \\
&\quad (D_\tau \Delta_{j_\beta}(0, \alpha_{ab})D_\tau \Delta_{j_\alpha}(0, \alpha_{ac}) + (j_\beta + 1)^2 \Delta_{j_\alpha}(0, \alpha_{bc})\Delta_{j_\beta}(0, \alpha_{ab})).
\end{aligned} \tag{3.14}$$

These expressions are all to be summed over the j 's, with the sums unconstrained in F_{2a} , and constrained in F_{2b} and F_{2c} by the rules given above.

As described above, in order to analyze the phase transition we need to compute the specific term in $F_{2a} + F_{2b} + F_{2c}$ of the form

$$C_{1,1,-2} g_{YM}^2 (\text{tr}(U)\text{tr}(U)\text{tr}((U^\dagger)^2) + \text{tr}(U^2)\text{tr}(U^\dagger)\text{tr}(U^\dagger)), \tag{3.15}$$

and to determine the coefficient $C_{1,1,-2}$ at the deconfinement temperature of the free Yang-Mills theory, $x_c = 2 - \sqrt{3}$. For each diagram, we therefore expand the product of propagators in powers of U , and sum the coefficients of all terms of the form (3.15).

For F_{2a} , all sums may be done explicitly, and we find

$$\begin{aligned}
F_{2a} = & \frac{g_{YM}^2}{24\pi^2} \sum_{n,m \geq 0} \tilde{F}(x^n) \tilde{F}(x^m) (\text{tr}(U^m) \text{tr}(U^n) \text{tr}(U^{-n-m}) + \{m \rightarrow -m\} + \\
& \{n \rightarrow -n\} + \{m, n \rightarrow -m, -n\}) \\
& + \frac{g_{YM}^2}{3\pi^2} \left(\sum \frac{j(j+2)}{(j+1)} \right) \sum_n \tilde{F}(x^n) N \text{tr}(U^n) \text{tr}(U^{-n}) + \frac{g_{YM}^2}{6\pi^2} \left(\sum \frac{j(j+2)}{(j+1)} \right)^2 N^3,
\end{aligned} \tag{3.16}$$

where we have left the divergent sums (which will not be relevant for the computation we are doing in this paper) explicit. The function \tilde{F} is related to the single particle partition function z_V by

$$\tilde{F}(e^{-\beta}) = \int_{\beta}^{\infty} da z_V(e^{-a}), \tag{3.17}$$

or explicitly

$$\tilde{F}(x) = 2 \ln(1-x) + \frac{2x}{(1-x)^2}. \tag{3.18}$$

Thus, the contribution to $C_{1,1,-2}$ from F_{2a} is

$$C_{2a} = \frac{1}{24\pi^2} (\tilde{F}(x) \tilde{F}(x) + 2\tilde{F}(x) \tilde{F}(x^2)). \tag{3.19}$$

For the other two cases we could not compute the sums explicitly, but it is not difficult to numerically evaluate the desired coefficient at the transition temperature $x_c = 2 - \sqrt{3}$. We find that the contributions of the three diagrams to $C_{1,1,-2}$ are given by

$$\begin{aligned}
C_{2a} &= 6.53536 \times 10^{-4}, \\
C_{2b} &= -22.87088 \times 10^{-4}, \\
C_{2c} &= 9.16396 \times 10^{-4},
\end{aligned} \tag{3.20}$$

so that the total coefficient is

$$C_{1,1,-2} = -7.1716 \times 10^{-4}. \tag{3.21}$$

3.4. Three Loops

The leading contribution to the coefficient $C_{1,1,-1,-1}$ in (2.8) comes from the fourteen three-loop diagrams of figure 2. We first give the expressions for each diagram in terms of propagators and spherical harmonic integrals. For diagram 3a, we find

$$\begin{aligned}
F_{3a} = & -\frac{g_{YM}^4}{2} (D^{\alpha\gamma\lambda} D^{\bar{\alpha}\delta\bar{\lambda}} D^{\beta\delta\tau} D^{\bar{\beta}\bar{\gamma}\bar{\tau}} - 2D^{\alpha\bar{\alpha}\lambda} D^{\gamma\delta\bar{\lambda}} D^{\beta\bar{\gamma}\tau} D^{\bar{\beta}\delta\bar{\tau}} + D^{\alpha\bar{\alpha}\lambda} D^{\gamma\delta\bar{\lambda}} D^{\beta\bar{\beta}\tau} D^{\bar{\gamma}\delta\bar{\tau}}) \\
& \int dt \Delta_{j_\alpha}(0, \alpha_{ab}) \Delta_{j_\gamma}(t, \alpha_{ca}) \Delta_{j_\delta}(t, \alpha_{ac}) (\Delta_{j_\beta}(0, \alpha_{ad}) + \Delta_{j_\beta}(0, \alpha_{dc})).
\end{aligned} \tag{3.22}$$

For diagram 3b, we find

$$\begin{aligned}
F_{3b} = & g_{YM}^4 (D^{\alpha\gamma\lambda} D^{\bar{\alpha}\delta\bar{\lambda}} - D^{\alpha\bar{\alpha}\lambda} D^{\gamma\delta\bar{\lambda}}) \frac{D^{\bar{\gamma}\beta\rho} D^{\bar{\delta}\bar{\beta}\bar{\rho}}}{j_\rho(j_\rho + 2)} \\
& \left\{ \Delta_{j_\alpha}(0, \alpha_{ab})(D_\tau \Delta_{j_\beta}(0, \alpha_{ad}) + D_\tau \Delta_{j_\beta}(0, \alpha_{dc})) \right. \\
& \quad \int dt (D_\tau \Delta_{j_\gamma}(t, \alpha_{ac}) \Delta_{j_\delta}(t, \alpha_{ca}) - \Delta_{j_\gamma}(t, \alpha_{ac}) D_\tau \Delta_{j_\delta}(t, \alpha_{ca})) \\
& \quad + \Delta_{j_\alpha}(0, \alpha_{ab})(\Delta_{j_\beta}(0, \alpha_{ad}) + \Delta_{j_\beta}(0, \alpha_{dc})) \\
& \quad \left. \int dt ((j_\beta + 1)^2 \Delta_{j_\gamma}(t, \alpha_{ac}) \Delta_{j_\delta}(t, \alpha_{ca}) - D_\tau \Delta_{j_\gamma}(t, \alpha_{ac}) D_\tau \Delta_{j_\delta}(t, \alpha_{ca})) \right\}. \tag{3.23}
\end{aligned}$$

For diagram 3c, the result is

$$\begin{aligned}
F_{3c} = & -\frac{g_{YM}^4}{2} \frac{D^{\alpha\gamma\lambda} D^{\bar{\alpha}\delta\bar{\lambda}} D^{\bar{\gamma}\beta\rho} D^{\bar{\delta}\bar{\beta}\bar{\rho}}}{j_\lambda(j_\lambda + 2) j_\rho(j_\rho + 2)} \\
& \int dt (\Delta_{j_\beta}(0, \alpha_{ad}) + \Delta_{j_\beta}(0, \alpha_{dc})) \\
& \quad \left\{ ((j_\alpha + 1)^2 (j_\beta + 1)^2 + (j_\gamma + 1)^2 (j_\delta + 1)^2) \Delta_{j_\alpha}(0, \alpha_{ab}) \Delta_{j_\delta}(t, \alpha_{ac}) \Delta_{j_\gamma}(t, \alpha_{ca}) \right. \\
& \quad - (j_\beta + 1)^2 D_\tau \Delta_{j_\gamma}(t, \alpha_{ca}) (4D_\tau \Delta_{j_\alpha}(0, \alpha_{ab}) \Delta_{j_\delta}(t, \alpha_{ac}) + 2\Delta_{j_\alpha}(0, \alpha_{ab}) D_\tau \Delta_{j_\delta}(t, \alpha_{ac})) \\
& \quad \left. - 2(j_\delta + 1)^2 \Delta_{j_\alpha}(0, \alpha_{ab}) \Delta_{j_\delta}(0, \alpha_{ac}) \right\} \\
& + \int dt (D_\tau \Delta_{j_\beta}(0, \alpha_{ad}) + D_\tau \Delta_{j_\beta}(0, \alpha_{dc})) \\
& \quad \left\{ (j_\gamma + 1)^2 \Delta_{j_\gamma}(t, \alpha_{ca}) (4D_\tau \Delta_{j_\delta}(t, \alpha_{ac}) \Delta_{j_\alpha}(0, \alpha_{ab}) + 2\Delta_{j_\delta}(t, \alpha_{ac}) D_\tau \Delta_{j_\alpha}(0, \alpha_{ab})) \right. \\
& \quad - 2D_\tau \Delta_{j_\alpha}(0, \alpha_{ab}) D_\tau \Delta_{j_\delta}(t, \alpha_{ac}) D_\tau \Delta_{j_\gamma}(t, \alpha_{ca}) \\
& \quad \left. - 2(D_\tau \Delta_{j_\alpha}(0, \alpha_{ab}) \Delta_{j_\delta}(0, \alpha_{ac}) + 2\Delta_{j_\alpha}(0, \alpha_{ab}) D_\tau \Delta_{j_\delta}(0, \alpha_{ac})) \right\}. \tag{3.24}
\end{aligned}$$

For diagram 3d, we find

$$\begin{aligned}
F_{3d} = & -\frac{g_{YM}^4}{4} D^{\alpha\gamma\lambda} D^{\beta\delta\bar{\lambda}} D^{\bar{\alpha}\bar{\gamma}\rho} D^{\bar{\beta}\bar{\delta}\bar{\rho}} \\
& \int dt \Delta_{j_\alpha}(t, \alpha_{ab}) \Delta_{j_\beta}(t, \alpha_{bc}) (2\Delta_{j_\gamma}(t, \alpha_{cd}) \Delta_{j_\delta}(t, \alpha_{da}) + \Delta_{j_\delta}(t, \alpha_{cd}) \Delta_{j_\gamma}(t, \alpha_{da})) \\
& -\frac{g_{YM}^4}{4} D^{\alpha\beta\lambda} D^{\gamma\delta\bar{\lambda}} D^{\bar{\gamma}\bar{\beta}\rho} D^{\bar{\alpha}\bar{\delta}\bar{\rho}} \\
& \int dt \Delta_{j_\alpha}(t, \alpha_{ab}) \Delta_{j_\beta}(t, \alpha_{bc}) (\Delta_{j_\gamma}(t, \alpha_{cd}) \Delta_{j_\delta}(t, \alpha_{da}) - 4\Delta_{j_\delta}(t, \alpha_{cd}) \Delta_{j_\gamma}(t, \alpha_{da})). \tag{3.25}
\end{aligned}$$

Evaluating diagram 3e, we obtain

$$\begin{aligned}
F_{3e} = & g_{YM}^4 (2D^{\alpha\delta\lambda} D^{\beta\gamma\bar{\lambda}} - D^{\alpha\beta\lambda} D^{\gamma\delta\bar{\lambda}} - D^{\alpha\gamma\lambda} D^{\beta\delta\bar{\lambda}}) \frac{D^{\bar{\gamma}\delta\rho} D^{\bar{\alpha}\beta\bar{\rho}}}{j_\rho(j_\rho + 2)} \\
& \int dt \left\{ D_\tau \Delta_{j_\alpha}(t, \alpha_{ba}) \Delta_{j_\beta}(t, \alpha_{ad}) \Delta_{j_\gamma}(t, \alpha_{cb}) D_\tau \Delta_{j_\delta}(t, \alpha_{dc}) \right. \\
& \left. - \Delta_{j_\alpha}(t, \alpha_{ba}) D_\tau \Delta_{j_\beta}(t, \alpha_{ad}) \Delta_{j_\gamma}(t, \alpha_{cb}) D_\tau \Delta_{j_\delta}(t, \alpha_{dc}) \right\}. \tag{3.26}
\end{aligned}$$

Diagram 3f gives

$$\begin{aligned}
F_{3f} = & -\frac{g_{YM}^4}{2} \frac{D^{\alpha\gamma\lambda} D^{\beta\delta\bar{\lambda}} D^{\bar{\alpha}\bar{\gamma}\rho} D^{\bar{\beta}\bar{\delta}\bar{\rho}}}{j_\lambda(j_\lambda + 2) j_\rho(j_\rho + 2)} \\
& \left[4\Delta_{j_\alpha}(0, \alpha_{ab}) D_\tau \Delta_{j_\delta}(0, \alpha_{cd}) D_\tau \Delta_{j_\beta}(0, \alpha_{da}) \right. \\
& \quad - 2((j_\beta + 1)^2 + (j_\delta + 1)^2) \Delta_{j_\alpha}(0, \alpha_{ab}) \Delta_{j_\delta}(0, \alpha_{cd}) \Delta_{j_\beta}(0, \alpha_{da}) \\
& \quad + \int dt \left\{ \Delta_{j_\alpha}(t, \alpha_{ab}) \Delta_{j_\gamma}(t, \alpha_{bc}) \Delta_{j_\delta}(t, \alpha_{cd}) \Delta_{j_\beta}(t, \alpha_{da}) \right. \\
& \quad \quad (j_\gamma + 1)^2 ((j_\delta + 1)^2 + (j_\beta + 1)^2) \\
& \quad \quad + 2D_\tau \Delta_{j_\alpha}(t, \alpha_{ab}) D_\tau \Delta_{j_\gamma}(t, \alpha_{bc}) D_\tau \Delta_{j_\delta}(t, \alpha_{cd}) D_\tau \Delta_{j_\beta}(t, \alpha_{da}) \\
& \quad \quad \left. - 4(j_\gamma + 1)^2 \Delta_{j_\alpha}(t, \alpha_{ab}) \Delta_{j_\gamma}(t, \alpha_{bc}) D_\tau \Delta_{j_\delta}(t, \alpha_{cd}) D_\tau \Delta_{j_\beta}(t, \alpha_{da}) \right\} \\
& - \frac{g_{YM}^4}{2} \frac{D^{\alpha\beta\lambda} D^{\gamma\delta\bar{\lambda}} D^{\bar{\alpha}\bar{\gamma}\rho} D^{\bar{\beta}\bar{\delta}\bar{\rho}}}{j_\lambda(j_\lambda + 2) j_\rho(j_\rho + 2)} \\
& \left[4D_\tau \Delta_{j_\alpha}(0, \alpha_{ab}) D_\tau \Delta_{j_\gamma}(0, \alpha_{bc}) \Delta_{j_\beta}(0, \alpha_{da}) \right. \\
& \quad - 2(j_\alpha + 1)^2 \Delta_{j_\alpha}(0, \alpha_{ab}) \Delta_{j_\gamma}(0, \alpha_{bc}) \Delta_{j_\beta}(0, \alpha_{da}) \\
& \quad - 2\Delta_{j_\alpha}(0, \alpha_{ab}) D_\tau \Delta_{j_\gamma}(0, \alpha_{bc}) D_\tau \Delta_{j_\beta}(0, \alpha_{da}) \\
& \quad + \int dt \left\{ D_\tau \Delta_{j_\alpha}(t, \alpha_{ab}) D_\tau \Delta_{j_\gamma}(t, \alpha_{bc}) D_\tau \Delta_{j_\delta}(t, \alpha_{cd}) D_\tau \Delta_{j_\beta}(t, \alpha_{da}) \right. \\
& \quad \quad + (j_\alpha + 1)^2 (j_\delta + 1)^2 \Delta_{j_\alpha}(t, \alpha_{ab}) \Delta_{j_\gamma}(t, \alpha_{bc}) \Delta_{j_\delta}(t, \alpha_{cd}) \Delta_{j_\beta}(t, \alpha_{da}) \\
& \quad \quad + 2(j_\delta + 1)^2 \Delta_{j_\alpha}(t, \alpha_{ab}) D_\tau \Delta_{j_\gamma}(t, \alpha_{bc}) \Delta_{j_\delta}(t, \alpha_{cd}) D_\tau \Delta_{j_\beta}(t, \alpha_{da}) \\
& \quad \quad \left. - 4(j_\delta + 1)^2 D_\tau \Delta_{j_\alpha}(t, \alpha_{ab}) D_\tau \Delta_{j_\gamma}(t, \alpha_{bc}) \Delta_{j_\delta}(t, \alpha_{cd}) \Delta_{j_\beta}(t, \alpha_{da}) \right\}]. \tag{3.27}
\end{aligned}$$

For diagram 3g, we find

$$\begin{aligned}
F_{3g} = & g_{YM}^4 \widehat{E}^{\alpha\delta\rho} \widehat{E}^{\gamma\beta\bar{\rho}} (D^{\bar{\alpha}\bar{\gamma}\lambda} D^{\bar{\beta}\bar{\delta}\bar{\lambda}} - \frac{1}{2} D^{\bar{\alpha}\bar{\beta}\lambda} D^{\bar{\gamma}\bar{\delta}\bar{\lambda}} - \frac{1}{2} D^{\bar{\alpha}\bar{\delta}\lambda} D^{\bar{\beta}\bar{\gamma}\bar{\lambda}}) \\
& \int dt dt' \Delta_{j_\beta}(t', \alpha_{da}) \Delta_{j_\gamma}(t', \alpha_{cd}) \Delta_{j_\delta}(t, \alpha_{bc}) \Delta_{j_\alpha}(t, \alpha_{ab}) \Delta_{j_\rho}(t' - t, \alpha_{ac}), \tag{3.28}
\end{aligned}$$

where \widehat{E} was defined in the previous subsection. Diagram 3h evaluates to

$$\begin{aligned}
F_{3h} = & g_{YM}^4 \frac{1}{j_\lambda(j_\lambda + 2)} D^{\alpha\gamma\lambda} D^{\beta\delta\bar{\lambda}} \widehat{E}^{\bar{\alpha}\bar{\gamma}\rho} \widehat{E}^{\bar{\delta}\bar{\beta}\bar{\rho}} \\
& \int dt_1 dt_2 D_\tau \Delta_{j_\alpha}(t_1, \alpha_{ab}) \Delta_{j_\gamma}(t_1, \alpha_{bc}) \Delta_{j_\rho}(t_1 - t_2, \alpha_{ca}) \\
& \quad (\Delta_{j_\delta}(t_2, \alpha_{cd}) D_\tau \Delta_{j_\beta}(t_2, \alpha_{da}) - D_\tau \Delta_{j_\delta}(t_2, \alpha_{cd}) \Delta_{j_\beta}(t_2, \alpha_{da})) \\
& + g_{YM}^4 \frac{1}{j_\lambda(j_\lambda + 2)} D^{\alpha\beta\lambda} D^{\gamma\delta\bar{\lambda}} \widehat{E}^{\bar{\alpha}\bar{\gamma}\rho} \widehat{E}^{\bar{\delta}\bar{\beta}\bar{\rho}} \\
& \int dt_1 dt_2 D_\tau \Delta_{j_\alpha}(t_1, \alpha_{ab}) \Delta_{j_\beta}(t_2, \alpha_{da}) \Delta_{j_\rho}(t_1 - t_2, \alpha_{ca}) \\
& \quad (\Delta_{j_\delta}(t_2, \alpha_{cd}) D_\tau \Delta_{j_\gamma}(t_1, \alpha_{bc}) - D_\tau \Delta_{j_\delta}(t_2, \alpha_{cd}) \Delta_{j_\gamma}(t_1, \alpha_{bc})).
\end{aligned} \tag{3.29}$$

Diagram 3i gives

$$\begin{aligned}
F_{3i} = & -\frac{g_{YM}^4}{4} \widehat{E}^{\alpha\beta\rho} \widehat{E}^{\bar{\alpha}\sigma\bar{\beta}} \widehat{E}^{\bar{\sigma}\delta\bar{\gamma}} \widehat{E}^{\bar{\delta}\bar{\rho}\bar{\gamma}} \\
& \int dt_1 dt_2 dt_3 \Delta_{j_\alpha}(t_1 - t_2, \alpha_{ab}) \Delta_{j_\beta}(t_1 - t_2, \alpha_{bc}) \Delta_{j_\gamma}(t_3, \alpha_{cd}) \\
& \quad \Delta_{j_\delta}(t_3, \alpha_{da}) \Delta_{j_\rho}(t_1 - t_3, \alpha_{ca}) \Delta_{j_\sigma}(t_2, \alpha_{ac}).
\end{aligned} \tag{3.30}$$

For diagram 3j, we find

$$\begin{aligned}
F_{3j} = & g_{YM}^4 (D^{\alpha\rho\lambda} D^{\beta\bar{\rho}\bar{\lambda}} - D^{\rho\bar{\rho}\lambda} D^{\alpha\beta\bar{\lambda}}) \widehat{E}^{\bar{\alpha}\tau\sigma} \widehat{E}^{\bar{\beta}\bar{\sigma}\bar{\tau}} \\
& \int dt dt' \Delta_{j_\rho}(0, \alpha_{ab}) \Delta_{j_\beta}(t - t', \alpha_{ac}) \Delta_{j_\sigma}(t', \alpha_{ad}) \Delta_{j_\alpha}(t, \alpha_{ca}) \Delta_{j_\tau}(t', \alpha_{dc}).
\end{aligned} \tag{3.31}$$

Diagram 3k yields

$$\begin{aligned}
F_{3k} = & g_{YM}^4 \frac{1}{j_\lambda(j_\lambda + 2)} D^{\alpha\beta\lambda} D^{\bar{\alpha}\gamma\bar{\lambda}} \widehat{E}^{\bar{\beta}\bar{\rho}\sigma} \widehat{E}^{\bar{\gamma}\bar{\sigma}\bar{\rho}} \\
& \int dt_1 dt_2 \Delta_{j_\rho}(t_1 - t_2, \alpha_{cd}) \Delta_{j_\sigma}(t_1 - t_2, \alpha_{da}) \\
& \quad \{ 2D_\tau \Delta_{j_\alpha}(0, \alpha_{ab}) \Delta_{j_\beta}(t_1, \alpha_{ac}) D_\tau \Delta_{j_\gamma}(t_2, \alpha_{ca}) \\
& \quad + \Delta_{j_\alpha}(0, \alpha_{ab}) D_\tau \Delta_{j_\beta}(t_1, \alpha_{ac}) D_\tau \Delta_{j_\gamma}(t_2, \alpha_{ca}) \\
& \quad - (j_\alpha + 1)^2 \Delta_{j_\alpha}(0, \alpha_{ab}) \Delta_{j_\beta}(t_1, \alpha_{ac}) \Delta_{j_\gamma}(t_2, \alpha_{ca}) \}.
\end{aligned} \tag{3.32}$$

For diagram 3l, we obtain

$$\begin{aligned}
F_{3l} = & -\frac{g_{YM}^4}{12} \widehat{E}^{\alpha\beta\tau} \widehat{E}^{\bar{\beta}\gamma\rho} \widehat{E}^{\bar{\gamma}\bar{\alpha}\sigma} \widehat{E}^{\bar{\rho}\bar{\sigma}\bar{\tau}} \\
& \int dt_1 dt_2 dt_3 \Delta_{j_\alpha}(t_2 - t_3, \alpha_{ab}) \Delta_{j_\beta}(t_3 - t_1, \alpha_{ac}) \Delta_{j_\gamma}(t_1 - t_2, \alpha_{ad}) \\
& \quad \Delta_{j_\rho}(t_1, \alpha_{dc}) \Delta_{j_\sigma}(t_2, \alpha_{bd}) \Delta_{j_\tau}(t_3, \alpha_{cb}).
\end{aligned} \tag{3.33}$$

For diagram 3m, we find

$$\begin{aligned}
F_{3m} = & 4g_{YM}^4 \frac{D^{\alpha\beta\lambda} C^{\bar{\lambda}\bar{\alpha}\rho} D^{\gamma\delta\bar{\rho}} \widehat{E}^{\bar{\beta}\bar{\gamma}\bar{\delta}}}{j_\lambda(j_\lambda+2)j_\rho(j_\rho+2)} \\
& \int dt (D_\tau \Delta_{j_\alpha}(0, \alpha_{ab}) \Delta_{j_\beta}(t, \alpha_{ca}) - \Delta_{j_\alpha}(0, \alpha_{ab}) D_\tau \Delta_{j_\beta}(t, \alpha_{ca})) \\
& \quad (\Delta_{j_\gamma}(t, \alpha_{dc}) D_\tau \Delta_{j_\delta}(t, \alpha_{ad}) - D_\tau \Delta_{j_\gamma}(t, \alpha_{dc}) \Delta_{j_\delta}(t, \alpha_{ad})) \\
& + 2g_{YM}^4 \frac{D^{\alpha\delta\lambda} C^{\bar{\lambda}\beta\bar{\rho}} D^{\gamma\bar{\delta}\bar{\rho}} \widehat{E}^{\bar{\alpha}\bar{\gamma}\bar{\beta}}}{j_\lambda(j_\lambda+2)j_\rho(j_\rho+2)} \\
& \int dt \{ D_\tau \Delta_{j_\alpha}(t, \alpha_{ab}) \Delta_{j_\beta}(t, \alpha_{bd}) D_\tau \Delta_{j_\gamma}(t, \alpha_{da}) \Delta_{j_\delta}(0, \alpha_{ca}) \\
& \quad + 2D_\tau \Delta_{j_\alpha}(t, \alpha_{ab}) \Delta_{j_\beta}(t, \alpha_{bd}) \Delta_{j_\gamma}(t, \alpha_{da}) D_\tau \Delta_{j_\delta}(0, \alpha_{ca}) \\
& \quad - (j_\delta + 1)^2 \Delta_{j_\alpha}(t, \alpha_{ab}) \Delta_{j_\beta}(t, \alpha_{bd}) \Delta_{j_\gamma}(t, \alpha_{da}) \Delta_{j_\delta}(0, \alpha_{ca}) \}.
\end{aligned} \tag{3.34}$$

Finally, diagram 3n gives the result

$$\begin{aligned}
F_{3n} = & g_{YM}^4 \frac{D^{\alpha\gamma\rho} D^{\beta\bar{\gamma}\sigma}}{j_\rho(j_\rho+2)j_\sigma(j_\sigma+2)} \left(3 \frac{C^{\bar{\rho}\bar{\alpha}\lambda} C^{\bar{\lambda}\bar{\beta}\bar{\sigma}}}{j_\lambda(j_\lambda+2)} + 3 \frac{C^{\bar{\rho}\bar{\beta}\lambda} C^{\bar{\lambda}\bar{\alpha}\bar{\sigma}}}{j_\lambda(j_\lambda+2)} + D^{\bar{\alpha}\bar{\lambda}\bar{\rho}} D^{\bar{\beta}\bar{\lambda}\bar{\sigma}} + D^{\bar{\alpha}\bar{\lambda}\bar{\sigma}} D^{\bar{\beta}\bar{\lambda}\bar{\rho}} \right) \\
& \{ D_\tau \Delta_{j_\alpha}(0, \alpha_{cb}) \Delta_{j_\gamma}(0, \alpha_{ac}) D_\tau \Delta_{j_\beta}(0, \alpha_{ad}) \\
& \quad + 2D_\tau \Delta_{j_\alpha}(0, \alpha_{cb}) D_\tau \Delta_{j_\gamma}(0, \alpha_{ac}) \Delta_{j_\beta}(0, \alpha_{ad}) \\
& \quad - (j_\gamma + 1)^2 \Delta_{j_\alpha}(0, \alpha_{cb}) \Delta_{j_\gamma}(0, \alpha_{ac}) \Delta_{j_\beta}(0, \alpha_{ad}) \} \\
& - g_{YM}^4 \frac{D^{\alpha\gamma\rho} D^{\beta\bar{\gamma}\sigma}}{j_\rho(j_\rho+2)j_\sigma(j_\sigma+2)} \left(3 \frac{C^{\bar{\rho}\bar{\alpha}\lambda} C^{\bar{\lambda}\bar{\beta}\bar{\sigma}}}{j_\lambda(j_\lambda+2)} + D^{\bar{\alpha}\bar{\lambda}\bar{\rho}} D^{\bar{\beta}\bar{\lambda}\bar{\sigma}} \right) \\
& \{ D_\tau \Delta_{j_\alpha}(0, \alpha_{ab}) \Delta_{j_\gamma}(0, \alpha_{ac}) D_\tau \Delta_{j_\beta}(0, \alpha_{ad}) \\
& \quad + 2D_\tau \Delta_{j_\alpha}(0, \alpha_{ab}) D_\tau \Delta_{j_\gamma}(0, \alpha_{ac}) \Delta_{j_\beta}(0, \alpha_{ad}) \\
& \quad + (j_\gamma + 1)^2 \Delta_{j_\alpha}(0, \alpha_{ab}) \Delta_{j_\gamma}(0, \alpha_{ac}) \Delta_{j_\beta}(0, \alpha_{ad}) \} \\
& - g_{YM}^4 \frac{D^{\alpha\gamma\rho} D^{\bar{\alpha}\bar{\gamma}\sigma}}{j_\rho(j_\rho+2)j_\sigma(j_\sigma+2)} \left(3 \frac{C^{\bar{\rho}\bar{\beta}\lambda} C^{\bar{\lambda}\bar{\beta}\bar{\sigma}}}{j_\lambda(j_\lambda+2)} + D^{\lambda\bar{\beta}\bar{\rho}} D^{\bar{\lambda}\bar{\beta}\bar{\sigma}} \right) \\
& \{ 2D_\tau \Delta_{j_\alpha}(0, \alpha_{ab}) D_\tau \Delta_{j_\gamma}(0, \alpha_{ad}) \Delta_{j_\beta}(0, \alpha_{bc}) \\
& \quad + ((j_\alpha + 1)^2 + (j_\gamma + 1)^2) \Delta_{j_\alpha}(0, \alpha_{ab}) \Delta_{j_\gamma}(0, \alpha_{ad}) \Delta_{j_\beta}(0, \alpha_{bc}) \}.
\end{aligned} \tag{3.35}$$

3.5. Evaluation of three-loop diagrams

We now evaluate the coefficient $C_{1,1,-1,-1}$ of $\beta g_{YM}^4 |\text{tr}(U)|^4$ in (2.5) arising from the three loop diagrams computed above. The expressions for the diagrams are of the general

form:

$$F = \sum_{j,m,\epsilon} S'(j, m, \epsilon) I'(j), \quad (3.36)$$

where S' is the term containing all spherical harmonic factors (C, D, E) and I' is the term involving the propagators and the integrals over t . S' depends on the j 's, m 's and ϵ 's of the spherical harmonics but I' only on the j 's. Using the identities of appendix B we can perform the sum over the m 's and ϵ 's analytically and find $S(j) = \sum_{m,\epsilon} S'(j, m, \epsilon)$. Then, the diagram can be written as a sum over j 's

$$F = \sum_j S(j) I'(j). \quad (3.37)$$

We then expand $I'(j)$ in powers of $\text{tr}(U^n)$ and determine $I(j)$, the coefficient of $|\text{tr}(U)|^4$ in this expansion. The contribution to b from this diagram may then be written in the form

$$C_{1,1,-1,-1} = \sum_j S(j) I(j). \quad (3.38)$$

We can find S for any diagram by using the identities given in appendix B, and the corresponding integral I can be found in the Mathematica file [9]. The sum (3.38) over j 's is the only part of the calculation that we have generally had to perform numerically.

Diagram 3a is the simplest and we can actually calculate it analytically. The expression (3.22) above may be simplified using the angular momentum sums of appendix B. We find

$$C_{1,1,-1,-1}^{3a} = -\frac{1}{18\pi^4} \sum_{a,b,c} \frac{a(a+2)b(b+2)c(c+2)}{(a+1)(b+1)(c+1)^3} x^{a+b+2} \left\{ (x^{c+1} + 1)(x^{c+1} + 2) - (c+1) \ln(x)(2x^{2c+2} + 3x^{c+1}) \right\}. \quad (3.39)$$

Note that this sum contains a logarithmic divergence in the sum over c when taking the x -independent term (equal to 2) in the curly brackets.

Such logarithmic divergences appear in the contribution to $C_{1,1,-1,-1}$ from most of our 3-loop diagrams, since there are terms where only two of the three unconstrained sums over loop momenta have exponential damping factors. These divergences arise from *non-planar* 1-loop subdiagrams, as we explain in the next section when we discuss the corresponding counterterms.

In practice, when doing the computation we will place a cutoff J on the angular momentum sums. We can then write the result with a cutoff in the form

$$C_{1,1,-1,-1}(J) = \alpha \sum_{c=1}^J \frac{1}{c+1} + C_{1,1,-1,-1}^{finite} + \mathcal{O}(1/J), \quad (3.40)$$

where α is the coefficient of the logarithmic divergence, which we can define by

$$\alpha = \lim_{J \rightarrow \infty} (J+1)(C_{1,1,-1,-1}(J) - C_{1,1,-1,-1}(J-1)), \quad (3.41)$$

and⁹

$$C_{1,1,-1,-1}^{finite} \equiv \lim_{J \rightarrow \infty} (C_{1,1,-1,-1}(J) - \alpha \sum_{c=1}^J \frac{1}{c+1}). \quad (3.42)$$

In particular, from the expression above for the 3a sum (3.39) we find

$$\alpha_{3a} = -\frac{1}{9\pi^4} \left(\frac{x}{(1-x)^2} + \log(1-x) \right)^2 = -4.0356 \times 10^{-5}, \quad C_{1,1,-1,-1}^{3a,finite} = -3.666 \times 10^{-7}, \quad (3.43)$$

where we have evaluated α_{3a} and $C_{1,1,-1,-1}^{3a,finite}$ at the transition point $x_c = 2 - \sqrt{3}$ [5].

For the 13 remaining diagrams, we were unable to evaluate the sum over j in (3.38) analytically. However, we have performed the sum numerically (at the phase transition temperature), and we will present the results in section 3.7.

3.6. Counterterm diagrams

We have seen that the contributions to $C_{1,1,-1,-1}$ arising from individual 3-loop diagrams contain logarithmic divergences. It turns out that all of these must cancel in the sum over diagrams. To see this, note first that no single-trace counterterm can contribute to the coefficient of $|\text{tr}(U)|^4$, since such a contribution requires four index loops, while planar counterterm diagrams at order λ^2 are two loop diagrams with only three index loops. In fact, the only possible counterterm contribution comes from double-trace counterterms¹⁰ of the form $\text{tr}(AA)\text{tr}(AA)$, which give rise to diagrams of the form shown in figure 3. But no such counterterm is gauge invariant, so in any gauge invariant regularization scheme

⁹ To improve numerical convergence we use Aitken's method : if $\lim_{n \rightarrow \infty} a_n = r$ then $\lim_{n \rightarrow \infty} \frac{a_n a_{n+2} - a_{n+1}^2}{a_n + a_{n+2} - 2a_{n+1}} = r$, but the convergence of the second sequence is faster.

¹⁰ See, for instance, [10,11] for recent discussions of how double-trace terms can contribute at leading order in the large N limit.

(such as dimensional regularization), there are no counterterm contributions at all, and all divergences must cancel in the sum over diagrams. Our regularization scheme does not respect gauge invariance, but the coefficients of logarithmic divergences are insensitive to the regularization scheme, so we must still find that all divergences cancel.¹¹

The preceding argument does not mean that we can ignore counterterms altogether. Indeed, the finite contribution resulting from the sum over diagrams does depend on the regularization scheme, and it is crucial to include the contributions of finite counterterms in order to obtain the correct result. The counterterms that can contribute take the form

$$L_{CT} = \left(\frac{\lambda}{N}\right)^2 \frac{1}{\pi^2} (c_1 \text{tr}(A_i A_i) \text{tr}(A_j A_j) + 2c_2 \text{tr}(A_i A_j) \text{tr}(A_i A_j)), \quad (3.44)$$

where c_1 and c_2 will be finite numerical coefficients chosen so that the results of calculations in our scheme match with results using dimensional regularization.

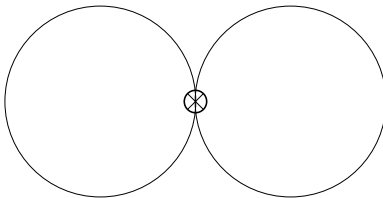


Figure 3: Counterterm contribution to the free energy at order λ^2 .

At order λ^2 , this vertex contributes to the free energy via counterterm graphs of the form depicted in figure 3. Following the same procedure as in the previous subsections, it is not difficult to isolate the coefficient C_c of $g_{YM}^4 |\text{tr}(U)^4|$ in the contribution of this diagram to the free energy :

$$C_c = \frac{1}{\pi^2} \sum_{\alpha, \gamma, \kappa} (c_1 D^{\alpha \bar{\alpha} \kappa} D^{\gamma \bar{\gamma} \bar{\kappa}} + 2c_2 D^{\alpha \gamma \kappa} D^{\bar{\alpha} \bar{\gamma} \bar{\kappa}}) \frac{1}{j_\alpha + 1} \frac{1}{j_\gamma + 1} x^{j_\alpha + j_\gamma + 2}. \quad (3.45)$$

Using spherical harmonic identities from appendix B and performing the sum we find:

$$C_c = \frac{2}{\pi^4} \left(c_1 + \frac{2}{3} c_2 \right) \left[\frac{x}{(1-x)^2} + \ln(1-x) \right]^2, \quad (3.46)$$

which may be conveniently written as

$$C_c = -(18c_1 + 12c_2) \alpha_{3\alpha}, \quad (3.47)$$

¹¹ In comparing with dimensional regularization, the coefficient of $1/\epsilon$ poles will be proportional to the coefficient of the logarithmic divergence in a cutoff scheme.

where α_{3a} is as in (3.43).

In order to determine the counterterm coefficients c_1 and c_2 , it is enough to look at the simplest correlator to which the counterterms (3.44) contribute, namely the nonplanar one-loop four point function on \mathbb{R}^4 with two external legs attached to each of the index loops. As we describe in detail in section 4.4 and appendix A.5 below, the coefficients are determined by demanding that the combination of logarithmically divergent one-loop diagrams (shown in figure 6) with the counterterm diagrams reproduces the result for the same correlator evaluated in dimensional regularization. For our regularization scheme with a sharp cutoff, we find

$$c_1 = c_2 = \frac{1}{60}, \quad (3.48)$$

so that

$$C_c = -\frac{1}{2}\alpha_{3a}. \quad (3.49)$$

This net contribution from the counterterm diagrams is all we need to complete our calculation. However, it turns out that a very useful check of our three loop results arises from splitting up the counterterm contribution into pieces associated with the individual one loop diagrams of figure 6. Note that each of these is logarithmically divergent, and appears as a nonplanar subdiagram in exactly one of the three loop vacuum diagrams of figure 2 (obtained by joining up the four free vector lines of the one loop diagram in pairs in such a way that we obtain a planar three-loop diagram, and replacing any a or c lines with the corresponding effective vertex). Thus, the logarithmic divergences in the contribution to b from three loop vacuum diagrams are directly related to logarithmic divergences in a specific set of non-planar one-loop four point diagrams.¹² If we denote by L_{CT}^X the counterterm Lagrangian density necessary to make this particular set of one-loop diagrams agree with dimensional regularization, then the combination of the three loop diagram X and the counterterm diagrams associated with L_{CT}^X should be finite, providing a check on the divergent part of each individual 3-loop diagram.

In addition to the overall result (3.49) we therefore define partial contributions C_c^X arising from the counterterm diagrams associated with a given three loop diagram X .

¹² The coefficient of $|\text{tr}(U)|^4$ has no additional divergences from planar one-loop subdiagrams of the three-loop diagrams, since we have seen that there are no single-trace counterterms that could cancel them (or remove the regulator dependence of the finite results if any such divergences cancelled upon summing diagrams).

These will generally have both a logarithmically divergent piece, and a finite piece, and take the form¹³

$$C_c^X = \alpha_c^X \ln \left(\frac{J}{R\mu} \right) + C_c^{X \text{ finite}}. \quad (3.50)$$

The values of α_c and C_c^{finite} for each diagram are tabulated in the next section together with our results for the three loop diagrams.

3.7. Results

In this section, we tabulate our numerical results for the contributions to $C_{1,1,-1,-1}$. For each three-loop diagram, we give the coefficient α of the logarithmic divergence and the remaining finite piece, as defined in (3.41) and (3.42). We also give the coefficients α_c and C_c^{finite} for the logarithmically divergent and finite parts of the associated counterterm diagrams, as defined in (3.50). We find:

Diagram	$\alpha/\alpha_{3\alpha}$	$C_{1,1,-1,-1}^{\text{finite}}$	$\alpha_c/\alpha_{3\alpha}$	$C_c^{\text{finite}}/\alpha_{3\alpha}$
3a	1	-3.666×10^{-7}	-1	-107/120
3b	-1	-4.805×10^{-5}	1	13/60
3c	-3/4	2.224×10^{-5}	3/4	1/20
3d	5/4	2.21×10^{-5}	-5/4	-47/60
3e	1/2	-5.85×10^{-5}	-1/2	-7/30
3f	-9/4	-2.69×10^{-4}	9/4	3/5
3g	-3	1.15×10^{-4}	3	1/5
3h	0	1.91×10^{-4}	0	-1/10
3i	5/2	-6.6×10^{-4}	-5/2	1/12
3j	-3	2.414×10^{-4}	3	11/10
3k	1/2	1.42×10^{-4}	-1/2	7/60
3l	5/4	$-1. \times 10^{-4}$	-5/4	1/24
3m	2	4.6×10^{-5}	-2	1/15
3n	1	-9.2×10^{-5}	-1	-29/30
Sum	0	-4.5×10^{-4}	0	-1/2

¹³ The constants $\mathcal{A}_1, \mathcal{A}_2, \mathcal{A}_3, \mathcal{A}_4$ appearing in Appendix A all evaluate to the same value with the choice of damping function (essentially a step function) used here, while the UV cutoff M is simply J/R .

The numerical results in the middle column of the table are all accurate at least within the number of digits appearing in the table. We estimate the maximal total numerical error of our result for the sum to be less than 3×10^{-5} . This accuracy could be improved with additional computer time, but we found no reason to do this since we are only interested in the sign of b . Note that the sum of all divergent contributions vanishes (without including counterterms).

Note that, in the table above, $\alpha^X + \alpha_c^X = 0$ for every diagram X ; that is, the sum of any three-loop vacuum graph and its associated counterterm graphs is finite. This sum depends on the renormalization scale μ (see (3.42) and (3.50)) but should be independent of the regulating function $R(q)$ ¹⁴. This μ -dependence vanishes upon summing all diagrams¹⁵, leaving us with the scheme-independent answer

$$C_{1,1,-1,-1} = -4.5 \times 10^{-4} - \alpha_{3a}/2 = -4.3 \times 10^{-4}. \quad (3.51)$$

3.8. Effective potential

We can now put together our results for the terms of interest in our effective potential (2.8) for the eigenvalues, evaluated at the deconfinement temperature:

$$\begin{aligned} \mu_2 &= 4.8112 \times 10^{-1}, \\ \beta_c C_{1,1,-2} &= -9.4447 \times 10^{-4}, \\ \beta_c C_{1,1,-1,-1} &= -5.7 \times 10^{-4}. \end{aligned} \quad (3.52)$$

From (2.11) we find that the coefficient b in the effective potential (2.10) for u_1 is

$$\begin{aligned} b &= \beta_c C_{1,1,-1,-1} - \frac{\beta_c^2 C_{1,1,-2}^2}{\mu_2} \\ &\simeq -5.7 \times 10^{-4} - 1.854 \times 10^{-6} \\ &\approx -5.7 \times 10^{-4}. \end{aligned} \quad (3.53)$$

¹⁴ In order to verify this independence – and as a check on the logic of our regularization scheme and our numerics – we have recomputed α/α_{3a} , $C_{1,1,-1,-1}^{\text{finite}}$, α_c/α_{3a} and $C_c^{\text{finite}}/\alpha_{3a}$ for diagrams 3a, 3b, 3c, 3g and 3n with a different regulating function (we took $R(q/M)$ to be a double step function, $R(x) = 1$ for $x < 1$, $R(x) = \frac{1}{2}$ for $1 < x < 2$ and $R(x) = 0$ for $x > 2$). We evaluated these quantities analytically for diagram 3a and numerically for all the other diagrams. As expected, in every case the coefficient of the logarithmic divergence α/α_{3a} and α_c/α_{3a} was unchanged in this new regulating scheme. Also, as expected, while finite parts of each diagram and its associated counterterm yielded different values in this new regulating scheme, the sum of every diagram with its associated counterterm graphs was unmodified.

¹⁵ This follows because $\sum_{\{\text{diagrams } X\}} \alpha^X = \sum_{\{\text{diagrams } X\}} \alpha_c^X = 0$.

Note that b is the sum of two terms, one of which is manifestly negative. In (3.53), however, the dominant contribution came from the first term which, in principle, could have been either positive or negative. This suggests that there could exist also theories for which $b > 0$; we will discuss this further in the final section.

Since we have, after a laborious calculation, determined that $b < 0$, we may conclude that the large N deconfinement transition of pure Yang-Mills theory on a small S^3 is of first order.

4. A Gauge Invariant Regularization Scheme on S^3

In the previous section we have computed a set of two and three loop Feynman diagrams to determine a particular term (b in equation (1.4)) in the Wilsonian effective action for finite temperature Yang Mills theory on S^3 . We found that while b is finite, individual diagrams that contribute to b diverge logarithmically. In order to obtain the finite physical value of b we needed to sum contributions from the various diagrams, at which point the logarithmic divergence cancels and we are left with the finite result of interest. The process of isolating a finite piece from the difference of divergent sub pieces is delicate, and will yield the correct answer only if the regularization procedure respects gauge invariance. In this section we will expand on the discussion of section 2.4 to describe in more detail the regularization procedure that we employ in our computation.

As described above, computations of Yang Mills theory on S^3 are most simply performed in the Coulomb gauge $\partial_i A^i = 0$, where the index i runs over the three spatial indices of the S^3 . Further, we found it most convenient to regularize all diagrams by truncating the spherical harmonic sums at spherical harmonic number n (in flat space this corresponds to imposing a hard momentum cut off at momentum $E(n)/R$ where $E(n) \sim n$ is the energy of the n^{th} spherical harmonic mode). This regularization scheme is not gauge invariant, but should yield gauge invariant results when employed with a bare Yang Mills action that includes an appropriate set of non-gauge-invariant counterterms. The appropriate counterterms may, in principle, be uniquely determined (up to the usual ambiguity in the definition of the Yang Mills coupling constant) by demanding that correlation functions computed by this theory obey the Ward identities that follow from gauge invariance, together with local Lorentz invariance.

In this section we will explicitly determine some of the counterterms that will render our non-gauge-invariant regularization scheme effectively gauge-invariant. These counterterms fall into two classes; counterterms that would be needed even in flat space, and

counterterms that are proportional to the spacetime curvature. It will turn out that no counterterm of the second type (those proportional to spacetime curvature) contributes to the computation of b , so we will content ourselves with determining only those counterterms that appear even in flat space. These counterterms may be determined rather simply by choosing them to ensure that certain Green's functions (following 't Hooft we use the $A_\mu(p)A_\nu(-p)$ two-point function, as well as a four-point function of gauge fields) agree with the same Green's functions evaluated using dimensional regularization¹⁶.

In §4.1 we explain our regularization method in detail and give a simple example of how it works. Sections 4.2 and 4.3 are devoted to tests of the validity of our regularization scheme. In §4.2 we determine all quadratic counterterms of the first type (those that appear in flat space) to order λ . Even though these counterterms do not actually contribute to our main computation in this paper, we use them to test the validity of our regularization procedure. First, we verify in §4.3 that our results are consistent with the Slavnov-Taylor identity and with Lorentz invariance. As another test, in appendix A.3 we verify that our results lead to the correct free energy at infinite volume to order λ . Finally, in §4.4 we proceed to use the same methods to compute the counterterms that we actually need for the computation of b ; these are a set of double-trace counterterms at order λ^2 .

4.1. General discussion and a simple example

The regularization we will analyze in this section is a slightly more general regularization scheme than the sharp cutoff which was used in the computation of the previous section. We include damping functions $R(\sqrt{q^2}/M)$ and $\tilde{R}(q_0/\Lambda)$ for the momentum of each internal A_i line of a given diagram, and damping functions $\bar{R}(\sqrt{q^2}/\bar{M})$ and $\tilde{\bar{R}}(q_0/\bar{\Lambda})$ ($q^2 \equiv q_i q_i$, $i = 1, 2, 3$, and we take $\bar{\Lambda} \gg \Lambda$, $\bar{M} \gg M$, $\Lambda \gg M$ and $\bar{\Lambda} \gg \bar{M}$ for convenience) for the momentum of each internal A_0 or ghost line. These functions are chosen so that $R(0) = \bar{R}(0) = \tilde{R}(0) = \tilde{\bar{R}}(0) = 1$, $R'(0) = \bar{R}'(0) = \tilde{R}'(0) = \tilde{\bar{R}}'(0) = 0$, and

¹⁶ More precisely, we compare with a form of dimensional regularization that is tailored to deal with Yang Mills theory in the Coulomb gauge. This so-called split dimensional regularization scheme [12,13,14,15] separately extends the number of dimensions participating in the Coulomb gauge condition (from 3 to $3 - \epsilon$) and the number of other dimensions (from 1 to $1 - \epsilon'$). One may worry that this regularization procedure is not Lorentz invariant (since integrals over temporal and spatial momenta end up being regulated differently), however the breaking of Lorentz invariance really comes from our choice of gauge rather than the regularization scheme. In practice, we will apply split dimensional regularization in the limit where $\epsilon' \rightarrow 0$.

$R(x \rightarrow \infty) = \bar{R}(x \rightarrow \infty) = \tilde{R}(x \rightarrow \infty) = \tilde{\tilde{R}}(x \rightarrow \infty) = 0$. We choose to treat A_0 and ghost lines differently from A_i lines because, in our calculation of b , it was convenient to integrate out A_0 and the ghosts directly in the action. This can be done with no regularization subtleties in diagrams with both A_0 /ghost lines and A_i lines, provided that we take the scale $\bar{M} \gg M$ and $\bar{\Lambda} \gg \Lambda$. We will sometimes be lazy with our notation and write $R(\sqrt{q^2}/M)$ ($\bar{R}(\sqrt{q^2}/\bar{M})$) as $R(q/M)$ ($\bar{R}(q/\bar{M})$).

In perturbation theory, correlation functions are obtained by evaluating all contributing Feynman diagrams, each of which may be written as an integral over internal momenta. In general these integrals diverge and must be regulated; in this section we will explain how one may convert the simple minded regularization scheme described in the previous paragraph into dimensional regularization by an appropriate choice of non gauge invariant counterterms. In the rest of this subsection we will demonstrate our method on a ‘toy’ regularized integral¹⁷

$$I = \int \frac{d^3 q dq_0}{(2\pi)^4} \frac{R(\frac{q}{M})R(\frac{p-q}{M})}{q^2 + q_0^2}, \quad (4.1)$$

and its counterpart in split dimensional regularization (SDR)

$$I = \int_{SDR} \frac{d^3 q dq_0}{(2\pi)^4} \frac{1}{q^2 + q_0^2}. \quad (4.2)$$

The q_0 integral in (4.1), (4.2) is finite (which is why we ignored the \tilde{R} regulators in (4.1)) and may easily be done to yield (from now on we suppress explicit reference to the regulator in intermediate steps)

$$I = \frac{1}{16\pi^3} \int \frac{d^3 q}{q}. \quad (4.3)$$

In split dimensional regularization (4.3) evaluates to zero, whereas in the damping function regularization scheme (4.1) evaluates to¹⁸

$$\alpha(p) = M^2 C_2 + \frac{p^2}{6} F_2 - \frac{p^2}{24\pi^2}, \quad (4.4)$$

¹⁷ This integral is slightly different in form from those that will appear in our actual expressions below; in particular the integrand contains a single propagator but two copies of the regulator function. Thus, it should merely be thought of as a simple divergent integral that illustrates all the complications that arise in the actual process of regularization.

¹⁸ The finite piece arises because $\int_0^\infty dq R(q) R'(q) = -\frac{1}{2}$.

where we have defined

$$\begin{aligned} C_2 &= \frac{1}{4\pi^2} \int_0^\infty dq q R(q)^2, \\ F_2 &= \frac{1}{4\pi^2} \int_0^\infty dq q R(q) R''(q). \end{aligned} \quad (4.5)$$

Thus, in order that our damping scheme agrees with dimensional regularization, we should introduce a counterterm that contributes $-\alpha(p)$.

Not every integral we encounter will be simple enough to explicitly evaluate in split dimensional regularization (as I of (4.1) was). However, it will always be possible to decompose the integrals of interest into the sum of a complicated but convergent integral and an easily evaluated divergent integral; this will be sufficient to determine the corresponding counterterms. As an illustration, we reevaluate the counterterm corresponding to the integral I in a perversely convoluted manner. Under the change of variables $q \rightarrow p - q$ (an allowed variable change in both regularization schemes), I becomes

$$I = \int \frac{d^4 q}{(2\pi)^4} \frac{1}{(p - q)^2 + (p_0 - q_0)^2}. \quad (4.6)$$

Performing the q_0 integration as above yields

$$\frac{1}{16\pi^3} \int \frac{d^3 q}{\sqrt{(p - q)^2}} = \frac{1}{16\pi^3} \int \frac{d^3 q}{q} \left(1 + \frac{q \cdot p}{q^2} - \frac{p^2}{2q^2} + \frac{3(q \cdot p)^2}{2q^4} + \dots \right). \quad (4.7)$$

We may now rewrite (4.6) as a sum over a manifestly convergent piece and an easily evaluated divergent piece as¹⁹

$$\begin{aligned} I &= \frac{1}{16\pi^3} \int \frac{d^3 q}{\sqrt{(p - q)^2}} \\ &= \frac{1}{16\pi^3} \int d^3 q \left(\frac{1}{\sqrt{(p - q)^2}} - \frac{1}{\sqrt{q^2}} \left[1 + \frac{q \cdot p}{q^2} - \frac{p^2}{2(q^2 + a^2)} + \frac{3(q \cdot p)^2}{2q^2(q^2 + a^2)} \right] \right) \\ &\quad + \frac{1}{16\pi^3} \int \frac{d^3 q}{\sqrt{q^2}} \left(1 + \frac{q \cdot p}{q^2} - \frac{p^2}{2(q^2 + a^2)} + \frac{3(q \cdot p)^2}{2q^2(q^2 + a^2)} \right) \end{aligned} \quad (4.8)$$

In (split) dimensional regularization with $d = 3 - \epsilon$, the second line evaluates to

$$\begin{aligned} \frac{1}{32\pi^3} \int \frac{d^3 q}{\sqrt{q^2}(q^2 + a^2)} \left[\frac{3(q \cdot p)^2}{q^2} - p^2 \right] &= \lim_{d \rightarrow 3} \frac{p^2}{32\pi^3} \left(\frac{3}{d} - 1 \right) \int \frac{d^d q}{\sqrt{q^2}(q^2 + a^2)} \\ &= \lim_{\epsilon \rightarrow 0} \frac{p^2}{32\pi^3} \left(\frac{\epsilon}{3 - \epsilon} \right) \left(\frac{4\pi}{\epsilon} + \mathcal{O}(\epsilon^0) \right) \\ &= \frac{p^2}{24\pi^2}. \end{aligned} \quad (4.9)$$

¹⁹ We introduce a parameter a in order to avoid artificially introducing IR singularities.

On the other hand, in the cut off scheme it evaluates to

$$M^2 C_2 + \frac{p^2}{6} F_2, \quad (4.10)$$

and (4.10) is equal to (4.9) upon the addition of the counterterm $-\alpha(p)$.

In this particular example, the convergent part of (4.8) is easy to evaluate (it is equal to $\frac{-p^2}{24\pi^2}$), but this is not true in more complicated examples, and was not needed in order to evaluate the counterterm.

Of course, the separation of (4.8) into a divergent and a convergent part is ambiguous. In our work ahead we will find it convenient to fix this ambiguity by demanding that the divergent piece (which we call the regulator dependent piece below) should evaluate to zero in split dimensional regularization²⁰. With this convention, the counterterm associated with any diagram is simply minus the regulator dependent integral evaluated in the cutoff regulator scheme.

4.2. Single-trace quadratic flat-space counterterms at order λ

As an explicit example, we can now proceed to compute the regulator-dependent piece of the gauge boson self-energy $\Pi_{\mu\nu} = -\frac{1}{2}\langle A_\mu A_\nu \rangle$. To set our conventions, we write the Yang-Mills action as

$$S = \frac{1}{4} \int d^4x \operatorname{tr}(F_{\mu\nu} F^{\mu\nu}). \quad (4.11)$$

The momentum space Coulomb gauge ($\partial_i A_i = 0$) propagators take the form

$$\langle A_i^{ab} A_j^{cd} \rangle = \delta^{ad} \delta^{bc} \left(\frac{q^2 g_{ij} - q_i q_j}{q^2 (q^2 + q_0^2)} \right), \quad \langle A_0^{ab} A_0^{cd} \rangle = \delta^{ad} \delta^{bc} \left(\frac{1}{q^2} \right). \quad (4.12)$$

In addition, the gauge fixing procedure introduces a set of complex adjoint ghosts c, \bar{c} with Lagrangian

$$\mathcal{L}_{ghost} = -\operatorname{tr}(\bar{c} \partial^i D_i c), \quad (4.13)$$

where $D_i = \partial_i - ig_{YM}[A_i, *]$ is the gauge covariant derivative. The propagator for the ghosts is identical to that of the A_0 fields,

$$\langle \bar{c}^{ab} c^{cd} \rangle = \delta^{ad} \delta^{bc} \left(\frac{1}{q^2} \right). \quad (4.14)$$

²⁰ With this convention, the regulator dependent piece in the example of the previous paragraphs is the second term in (4.8) minus $\frac{p^2}{24\pi^2}$.

In the computations of this section we do not explicitly integrate out A_0 and c as we did in the previous section; of course this does not affect the results.

In Appendix A.1 we define several regulator-dependent constants and functions of external momentum that arise in our calculation. In Appendix A.2 we depict the diagrams contributing to the gauge boson self-energy, and list our results for their regulator-dependent contributions (defined above). Adding these together yields the following result for the regulator-dependent contribution to the gauge boson self-energy (see Appendix A.1 for notation) :

$$\begin{aligned}
\frac{1}{\lambda}\Pi_{ik}^{(RD)} &= \frac{1}{8\pi^2} \ln\left(\frac{M}{\mu}\right) [p_i p_k - (p^2 + p_0^2)g_{ik}] - \frac{1}{15} (p^2 g_{ik} + 4p_i p_k) F_2 \\
&+ \frac{1}{6\pi^2} (p_i p_k - p^2 g_{ik}) - \frac{p_0^2}{24\pi^2} g_{ik} + M^2 g_{ik} \left(2C_1 - \frac{2}{3}C_2\right) \\
&+ \frac{1}{24\pi^2} p_0^2 g_{ik} \ln\left(\frac{\mathcal{A}_2}{\mathcal{A}_1^4}\right) + \frac{1}{40\pi^2} p^2 g_{ik} \ln\left(\frac{\mathcal{A}_1^4}{\mathcal{A}_2^9}\right) + \frac{1}{120\pi^2} p_i p_k \ln\left(\frac{\mathcal{A}_2^{31}}{\mathcal{A}_1^{16}}\right) \\
&+ 2\bar{\Lambda}\bar{M}\bar{B}_1\bar{C}_1 g_{ik} + \Lambda M B_1 [\delta_i^m \delta_k^n - g^{mn} g_{ik}] (H_1)_{mn} \\
&- \bar{\Lambda}\bar{M}\bar{B}_2 (\bar{H}_2)_{ik},
\end{aligned} \tag{4.15}$$

$$\frac{1}{\lambda}\Pi_{i0}^{(RD)} = \frac{7}{24\pi^2} p_0 p_i \ln\left(\frac{M}{\mu}\right) + \frac{5}{72\pi^2} p_0 p_i + \frac{1}{24\pi^2} p_0 p_i \ln\left(\frac{\mathcal{A}_1^8}{\mathcal{A}_2}\right), \tag{4.16}$$

$$\frac{1}{\lambda}\Pi_{00}^{(RD)} = -\frac{11}{24\pi^2} p^2 \ln\left(\frac{M}{\mu}\right) - \frac{p^2}{3} F_2 - \frac{1}{72\pi^2} p^2 + 2M^2 (C_1 - C_2) + \frac{1}{24\pi^2} p^2 \ln\left(\frac{\mathcal{A}_2^5}{\mathcal{A}_1^{16}}\right). \tag{4.17}$$

From the discussion above, the required quadratic counterterm Lagrangian must be chosen to precisely cancel these regulator dependent contributions, in order to give agreement with dimensional regularization. Thus, we must have

$$\mathcal{L}_{ct} = -\text{tr}(A^\mu A^\nu) \Pi_{\mu\nu}^{(RD)}. \tag{4.18}$$

In the next subsection, we perform two consistency checks on these results.

4.3. The Slavnov-Taylor identity and $SO(4)$ invariance

In this subsection, we first use the fact that our result for the self-energy must be consistent with gauge invariance and $SO(4)$ symmetry at short distances to demonstrate the consistency of our results for the logarithmic divergences in (4.15)- (4.17). In particular,

since the logarithmically divergent and finite contributions must satisfy various Slavnov-Taylor identities for these symmetries independently, we can determine the structure of the former without any knowledge of the latter.

We begin by considering the Slavnov-Taylor identity relevant for the gauge symmetry in Coulomb gauge. As usual, we start with the Euclidean gauge-fixed action

$$S = \int d^4x \left\{ \mathcal{L}_{YM} + \frac{1}{2\epsilon} (\nabla_i A^i)^2 - \bar{c} \nabla_i D_i c \right\} \quad (4.19)$$

and take $\epsilon \rightarrow 0$ to get the Coulomb gauge. The BRST charge Q satisfies

$$\begin{aligned} [Q, A_\mu] &= D_\mu c, \\ \{Q, c\} &= ic^2, \\ \{Q, \bar{c}\} &= \frac{1}{\epsilon} \nabla_i A_i. \end{aligned} \quad (4.20)$$

To obtain the Slavnov-Taylor identity, we study the partition function with sources added for the operators generated by the BRST transformation

$$Z[J_\mu, \xi, K_\mu, L] = \int \exp \left\{ -S + \int d^4x (J_\mu A_\mu + \bar{\xi} c + \bar{c} \xi + K_\mu [Q, A_\mu] - L \{Q, c\}) \right\}. \quad (4.21)$$

Performing the change of variables $A \rightarrow A + [\bar{c}Q, A]$, $c \rightarrow c + [\bar{c}Q, c]$, $\bar{c} \rightarrow \bar{c} + [\bar{c}Q, \bar{c}]$ in the path integral, we eventually obtain the standard identity

$$\frac{\delta \hat{\Gamma}}{\delta A_\mu} \frac{\delta \hat{\Gamma}}{\delta K_\mu} + \frac{\delta \hat{\Gamma}}{\delta c} \frac{\delta \hat{\Gamma}}{\delta L} = 0, \quad (4.22)$$

where $\hat{\Gamma}$ is the 1PI effective action less the gauge fixing term. From this, we may easily derive a 1-loop Slavnov-Taylor identity relating the self-energy, $\Pi_{\mu\nu}$, and the coefficient Φ_μ of the $K_\mu c$ term of $\hat{\Gamma}$:

$$\partial_\mu \Pi_{\mu\nu} + (-\partial^2 g_{\mu\nu} + \partial_\mu \partial_\nu) \Phi_\mu = 0. \quad (4.23)$$

An analogous relation arising from $SO(4)$ invariance is difficult to obtain since we are working in a noncovariant gauge. Fortunately, a simple restriction that arises by requiring $SO(4)$ -invariance of the S-matrix will be enough for our purposes. The specific condition

that we will impose is the existence of a double pole in the full propagator at zero momentum. This requirement, combined with the weaker Slavnov-Taylor identity $\partial_\mu \partial_\nu \Pi_{\mu\nu} = 0$, restricts the local part of $\Pi_{\mu\nu}$ to be of the form

$$\begin{aligned}\Pi_{ij} &= C ([p^2 + p_0^2]g_{ij} - p_i p_j) \\ \Pi_{i0} &= D p_i p_0 \\ \Pi_{00} &= -(C + 2D)p^2\end{aligned}\tag{4.24}$$

where C and D are dimensionless constants. It is easy to demonstrate, using the definition of Φ_μ , that the full Slavnov-Taylor identity (4.23) fixes $C + D$, leaving one degree of freedom that is in principle determined by a wave function renormalization condition. The logarithmic divergences must have this structure independent of the finite contribution to the local part of $\Pi_{\mu\nu}$. That our result (4.15)- (4.17) is consistent with these conditions is easy to verify.

As a second, and less formal consistency check, we have used our regularization scheme, together with the counterterms (4.18), to compute a physical quantity; the two-loop free energy of Yang-Mills theory at infinite volume²¹. The counterterms computed in the previous subsection play a crucial role in our calculation, which we present in detail in appendix A.3. Our final answer, $F_{2-loop} = V\lambda T^4/72$, agrees with the previously computed result (using dimensional regularization in Feynman gauge) [16]. We regard this as a rather nontrivial check of our regularization scheme.

4.4. The $\text{tr}(A_i A_j)\text{tr}(A_k A_l)$ counterterms

We have seen in section 3.6 that the counterterms required to evaluate b take the form of double-trace terms quartic in the spatial components of the gauge field. We will now follow the method of the previous subsection (requiring the order λ^2/N^2 contribution to the four point function $\langle A_i A_j A_k A_l \rangle$ to agree with the result obtained by (split) dimensional regularization) to evaluate the coefficients of the two possible counterterms of this form, given in (3.44).

The one loop diagrams contributing to the nonplanar part of the four-point correlator are depicted in figure 6 in appendix A.5. It follows from power counting that the leading divergence in each of these diagrams is logarithmic. As a consequence, the regulator

²¹ As far as we are aware, this is the first time that this computation has been done in Coulomb gauge using any regulating scheme.

dependent part of each of these diagrams may be evaluated with all external momenta set to zero and has a divergent part proportional to the single integral

$$\int \frac{d^3 q}{4\pi\sqrt{q^2}(q^2 + a^2)}. \quad (4.25)$$

In Appendix A.5 we list the coefficient of this divergent integral computed for each of the diagrams with a particular index structure²². To obtain the full expression, we must also sum over distinct permutations of indices. We list the results $R_{ijkl}^{(*)}$ (for the coefficient of the integral (4.25)), as well as the corresponding contribution to the counterterm, diagram by diagram in Appendix A.5.

Summing over the expressions in Appendix A.5 we find that the sum of the diagrams depicted in Appendix A evaluates to

$$\frac{d-3}{2\pi^2} \left[1 - \frac{4d-1}{d(d+2)} \right] \int \frac{d^3 q}{4\pi\sqrt{q^2}(q^2 + a^2)} + \text{finite}. \quad (4.26)$$

Notice that the first term in (4.26) is simply zero in the cut off regulator scheme (on setting $d = 3$). However, in dimensional regularization this term evaluates to

$$\left(-\frac{2\epsilon}{15\pi^2} + \mathcal{O}(\epsilon^2) \right) \times \frac{1}{\epsilon} = -\frac{2}{15\pi^2}. \quad (4.27)$$

It follows that perturbative computations in the damping function scheme must be accompanied by the counterterm

$$\mathcal{L}_{CT} = \left(\frac{\lambda^2}{N^2} \right) \left(\frac{1}{120\pi^2} \ln \left(\frac{\mathcal{A}_1^4 \mathcal{A}_2^3 \mathcal{A}_4^{15}}{\mathcal{A}_3^{22}} \right) + \frac{1}{60\pi^2} \right) [\text{tr}(A_i A_i) \text{tr}(A_j A_j) + 2\text{tr}(A_i A_j) \text{tr}(A_i A_j)], \quad (4.28)$$

where the \mathcal{A} s are regulator dependent constants defined in appendix A.1. For the sharp cutoff used in section 3, all \mathcal{A} 's give the same result, so the term involving \mathcal{A} 's evaluates to zero.

²² We keep the number of spatial dimensions, d , explicit (as opposed to setting $d = 3$), in order to determine the finite counterterm needed to bring our result into agreement with that of (split) dimensional regularization.

5. Validity of Perturbation Theory

In this section we will determine the precise regime of validity of perturbation theory for pure Yang Mills theory on a sphere of radius R , in order to make sure that the computation we described above is valid. Naively, perturbation theory is good whenever $\Lambda_{QCD}R \ll 1$, since the running coupling constant is then small at all scales above the scale $1/R$ of the classical mass gap. In thermal Yang Mills theory it turns out that this expectation is modified by IR divergences; as we explain below, perturbation theory is valid at small $\Lambda_{QCD}R$ only for $TR \ll \frac{1}{\lambda(T)}$, where $\lambda(T)$ is the running 't Hooft coupling at the energy scale T . It follows in particular that for $\Lambda_{QCD}R \ll 1$ perturbation theory is good at $TR \sim 1$, which is the regime of interest for this paper.

5.1. Review of IR divergences in flat space

In this subsection we review the well known effects of IR divergences on thermal Yang Mills theory in flat space; see [17] and references therein for more details.

Perturbative computations in Yang Mills theory on $\mathbb{R}^3 \times S^1$ (where the S^1 is a thermal circle) are beset by IR divergences, as is easily seen from power counting. IR divergences arise from the $\omega = 0$ sector (ω is the Euclidean energy) of the theory. Consider a Feynman diagram made up entirely of $\omega = 0$ modes. Let q be the scale of spatial momenta in such a diagram. Each additional loop is accompanied by a factor of $\frac{\lambda T}{q^4}$ (from vertices and propagators) times q^3 (from phase space), giving a net factor of $\frac{\lambda T}{q}$. Consequently, higher loop graphs are increasingly infrared divergent.

These infrared divergences are cured by the fact that the gauge field A is effectively massive. Working in Feynman gauge, the one loop self energy of the A_0 field at zero energy and momentum, $\Pi_{00}(0, \vec{0})$, is nonzero and of order λT^2 . As a consequence, A_0 is effectively massive with mass of order $m_{el} = \sqrt{\Pi_{00}(0, \vec{0})} \sim \sqrt{\lambda}T$. Consequently, infrared divergences in loops involving A_0 are cut off at this mass; thus, the effective loop counting parameter for A_0 loops with $\omega = 0$ is $\frac{\lambda T}{m_{el}} \sim \sqrt{\lambda}$. So, A_0 IR divergences change the perturbative expansion parameter from λ to $\sqrt{\lambda}$. The first fractional power of λ that appears in the expansion of the free energy is $\lambda^{\frac{3}{2}}$ (from a one loop graph using a mass corrected propagator for A_0). The next fractional power, $\lambda^{\frac{5}{2}}$, follows from the electric mass regularization of a 3-loop IR divergence.

IR divergences involving the spatial gauge field A_i are more serious. It turns out that the A_i self energy at zero momentum vanishes at one loop, but is nonvanishing at two

loops. As a consequence, the effective mass for A_i is of order $m_{mag} \sim \sqrt{\lambda^2 T^2} = T\lambda$. IR divergences involving spatial A_i fields are cut off by this mass; as a consequence the effective loop counting parameter for loops involving spatial A_i is of order one. Graphs of low enough order do not suffer from spatial IR divergences; however, a detailed investigation reveals that an infinite number of graphs contribute to the free energy at order λ^3 and higher. In summary, the free energy may be expanded up to order $\lambda^{\frac{5}{2}}$; all coefficients in the expansion of the free energy to this order are perturbatively computable, and have been computed (see [18] and references therein). Higher order terms are, in principle, inaccessible to perturbative analysis.

The generation of an electric mass simply reflects the fact that the high temperature dynamics of Yang Mills theory deconfines. Indeed, space is filled with a plasma of charged particles of density $\sim T^3$. As each of these particles carries a charge $\sqrt{\lambda}$, the screening length of this plasma is $1/\sqrt{\lambda}T$, explaining the magnitude of m_{el} described above.

The generation of a magnetic mass may be explained from the observation that Yang Mills theory on $\mathbb{R}^3 \times S^1$ reduces, at high temperatures, to a (Euclidean) 3 dimensional Yang Mills theory with an effective Yang Mills coupling constant λT , coupled to an adjoint scalar field of much larger mass $\sqrt{\lambda}T$. The low energy dynamics of this theory is simply that of pure 3 dimensional Yang Mills theory, which non-perturbatively develops a mass gap of order λT .

5.2. IR behaviour on S^3

We now turn to a study of the IR behaviour of Yang Mills theory on S^3 . Yang Mills theory on S^3 has a mass gap $1/R$ even classically. As a consequence, even ignoring the dynamical mass generation, the power counting arguments of the previous subsection indicate that (assuming $TR \gg 1$) loops of low energy A_0 and A_i fields are both weighted by the effective coupling

$$\lambda_{eff} \sim \lambda TR \simeq m_{mag}R. \quad (5.1)$$

Perturbation theory is valid when this effective coupling is small. When $m_{mag}R \sim 1$ this effective coupling is of order one, and perturbation theory breaks down ²³.

In summary, finite temperature Yang Mills perturbation theory on S^3 is useful provided both that $\Lambda_{QCD}R \ll 1$ and that temperatures are low enough so that $\lambda(T)TR \ll 1$.

²³ Once naive perturbation theory breaks down, the effects of dynamical mass generation are important. In this regime the correct way to proceed is to mimic the flat space analysis, and to shift the bare quadratic action by $A_\mu \Pi_{\mu\nu}(0,0)A_\nu$, where the first index of Π refers to the energy and the second to the spherical harmonic number on S^3 . At low enough temperatures this effective

6. Conclusions

In this paper we have computed the leading perturbative correction to the thermal partition function of pure $SU(N)$ Yang-Mills theory on S^3 around the phase transition point, and found that it leads to a first order deconfinement phase transition. The analysis, requiring diagrams with up to 3 loops, is quite complicated, and the interesting result is a single number (3.53) which governs the order of the phase transition. As described above, we have subjected our formalism to various consistency checks, including the cancellation of all divergent contributions, but we do not have any way to independently verify the correctness of our final result (3.53). It would be useful to have an independent computation of (3.53) as a check of our results.

In the pure Yang-Mills theory on S^3 we found that b is negative; a similar result was found in the corresponding analysis of various quantum mechanical systems [19,20]. It would be interesting to compute the sign of b in other $3 + 1$ dimensional (or lower dimensional) field theories, and to see how it depends on the matter content and on the various coupling constants of the theory. In particular, we are planning to compute the value of b in the $3 + 1$ dimensional $\mathcal{N} = 4$ supersymmetric Yang-Mills theory on S^3 , to see if the order of the deconfinement phase transition at weak coupling is the same as the first order behaviour found at strong coupling [21,22].

Since b is negative in all examples that have been analyzed so far, one might conjecture that for some reason it always has to be negative. However, it is easy to see that this is not the case, at least when one adds additional scalar fields with arbitrary couplings. For example, let us consider a $0 + 1$ or $1 + 1$ dimensional gauge theory with a massive adjoint scalar field Φ , with a potential of the form

$$V(\Phi) = \text{tr}(m^2\Phi^2 + c_4g_{YM}^2\Phi^4 + c_6g_{YM}^4\Phi^6 + c_8g_{YM}^6\Phi^8), \quad (6.1)$$

where the c_i are kept fixed in the 't Hooft large N limit. By analyzing the vacuum diagrams up to 3-loop order, it is easy to see that c_6 contributes linearly to b at order λ^2 (through a

mass is of order $1/R$, while at higher temperatures the effective mass crosses over to its flat space value. For instance, the effective A_i mass is of order $1/R$ for $\lambda TR \ll 1$, but is given by m_{mag} for $\lambda TR \gg 1$. Consequently, for $T \gg 1/\lambda R$, the flat space analysis of the previous subsection applies, and perturbation theory breaks down. Were we to ignore the dynamically generated contribution to the masses, we would be faced with a paradox. The free energy would receive contributions proportional to increasingly high powers of R , in conflict with extensivity.

diagram similar to $3n$ of figure 2), while c_8 only contributes to b at higher orders. Thus, for given values of m^2 and c_4 , we can achieve any sign for the leading perturbative contribution to b just by varying c_6 . We may need to choose c_6 to be negative for this, but we can always choose c_8 to be large enough so that $\Phi = 0$ is still the unique minimum of (6.1). In higher dimensions we have not yet been able to find a similar example involving purely single-trace interactions, but a potential term of the form $cg_{YM}^2 \text{tr}(\Phi^2)^2/N$ may be shown by similar arguments to lead to arbitrary values for b (already at order λ). Thus, large N weakly coupled deconfinement phase transitions may generally be of either first order or second order.

Acknowledgements

We would like to thank N. Arkani-Hamed, A. Dabholkar, R. Gopakumar, D. Gross, C. Korthals Altes, H. Liu, J. Maldacena, G. Mandal, L. Motl, A. Neitzke, R. Pisarski, J. Polchinski, E. Rabinovici, A. Sen, G. Semenoff, S. Shenker, A. Strominger, M. Teper, S. Trivedi, S. Wadia, L. Yaffe, and X. Yin, as well as everybody else that encouraged us to go through with this computation. OA would like to thank Harvard University, UBC, KITP, the Aspen Center for Physics, the Fields Institute, the Perimeter Institute, and the second Crete regional meeting on String Theory for hospitality during the course of this long project. JM would like to thank UBC, IAS, and KITP for hospitality during various stages of this work. SM would like to thank the second Crete regional meeting on String Theory, the Indian Institute for the Cultivation of Sciences, and KITP for hospitality while this work was in progress. KP would like to thank KITP for hospitality while this work was in progress. The work of OA was supported in part by the Israel-U.S. Binational Science Foundation, by the Israel Science Foundation (grant number 1399/04), by the Braun-Roger-Siegl foundation, by the European network HPRN-CT-2000-00122, by a grant from the G.I.F., the German-Israeli Foundation for Scientific Research and Development, and by Minerva. The work of JM was supported in part by an NSF Graduate Research Fellowship. The work of SM was supported in part by DOE grant DE-FG01-91ER40654, NSF career grant PHY-0239626, a Sloan fellowship, and a Harvard Junior Fellowship. The work of KP was supported in part by DOE grant DE-FG01-91ER40654. The work of MVR was supported in part by NSF grant PHY-9870115, by funds from the Stanford Institute for Theoretical Physics, by NSERC grant 22R81136 and by the Canada Research Chairs programme.

Appendix A. Details Related to Regularization

In this appendix, we provide many of the details behind calculations discussed in sections 3 and 4.

A.1. Definitions of useful regulator-dependent constants and functions

We start by presenting definitions for the various constants which encode the dependence of the results in section 4 on the regularization functions R , \tilde{R} , \bar{R} and $\tilde{\tilde{R}}$. We also define three functions of external momentum that will arise in the expressions for individual diagrams presented later in this appendix.

$$\ln\left(\frac{\mathcal{A}_n M}{\mu}\right) = \int_0^\infty dq \frac{\sqrt{q^2} R^n(q)}{q^2 + \frac{\mu^2}{M^2}} \quad (\text{A.1})$$

$$\begin{aligned} B_1 &= \frac{1}{2\pi} \int_{-\infty}^\infty dq_0 \tilde{R}(q_0) \\ \bar{B}_1 &= \frac{1}{2\pi} \int_{-\infty}^\infty dq_0 \tilde{\tilde{R}}(q_0) \\ \bar{B}_2 &= \frac{1}{2\pi} \int_{-\infty}^\infty dq_0 \tilde{\tilde{R}}(q_0)^2 \\ C_1 &= \frac{1}{4\pi^2} \int_0^\infty dq q R(q) \\ \bar{C}_1 &= \frac{1}{4\pi^2} \int_0^\infty dq q \bar{R}(q) \\ C_2 &= \frac{1}{4\pi^2} \int_0^\infty dq q R(q)^2 \\ F_2 &= \frac{1}{4\pi^2} \int_0^\infty dq q R(q) R''(q) \end{aligned} \quad (\text{A.2})$$

$$\begin{aligned} (H_1)_{ij}(p) &= \int \frac{d^3 q}{(2\pi)^3} \frac{q_i q_j}{q^2 \left(\frac{p}{M} - q\right)^2} R(q) \\ (\bar{H}_2)_{ij}(p) &= \int \frac{d^3 q}{(2\pi)^3} \frac{q_i q_j}{q^2 \left(\frac{p}{M} - q\right)^2} \bar{R}(\sqrt{q^2}) \bar{R}\left(\sqrt{\left(\frac{p}{M} - q\right)^2}\right) \\ (\bar{J}_2)_i(p) &= \int \frac{d^3 q}{(2\pi)^3} \frac{q_i}{q^2 \left(\frac{p}{M} - q\right)^2} \bar{R}(\sqrt{q^2}) \bar{R}\left(\sqrt{\left(\frac{p}{M} - q\right)^2}\right) \end{aligned} \quad (\text{A.3})$$

Note the parameter μ appearing in the definition of the constants \mathcal{A}_i . This parameter is needed when splitting logarithmically divergent integrals in order to avoid introducing artificial IR divergences into the “regularized” pieces. Moreover, μ is identified with the

scale associated to (split) dimensional regularization when comparing results obtained in that scheme with those obtained in ours.

A.2. Diagram by diagram contribution to the regulator dependent piece of $\Pi_{\mu\nu}$

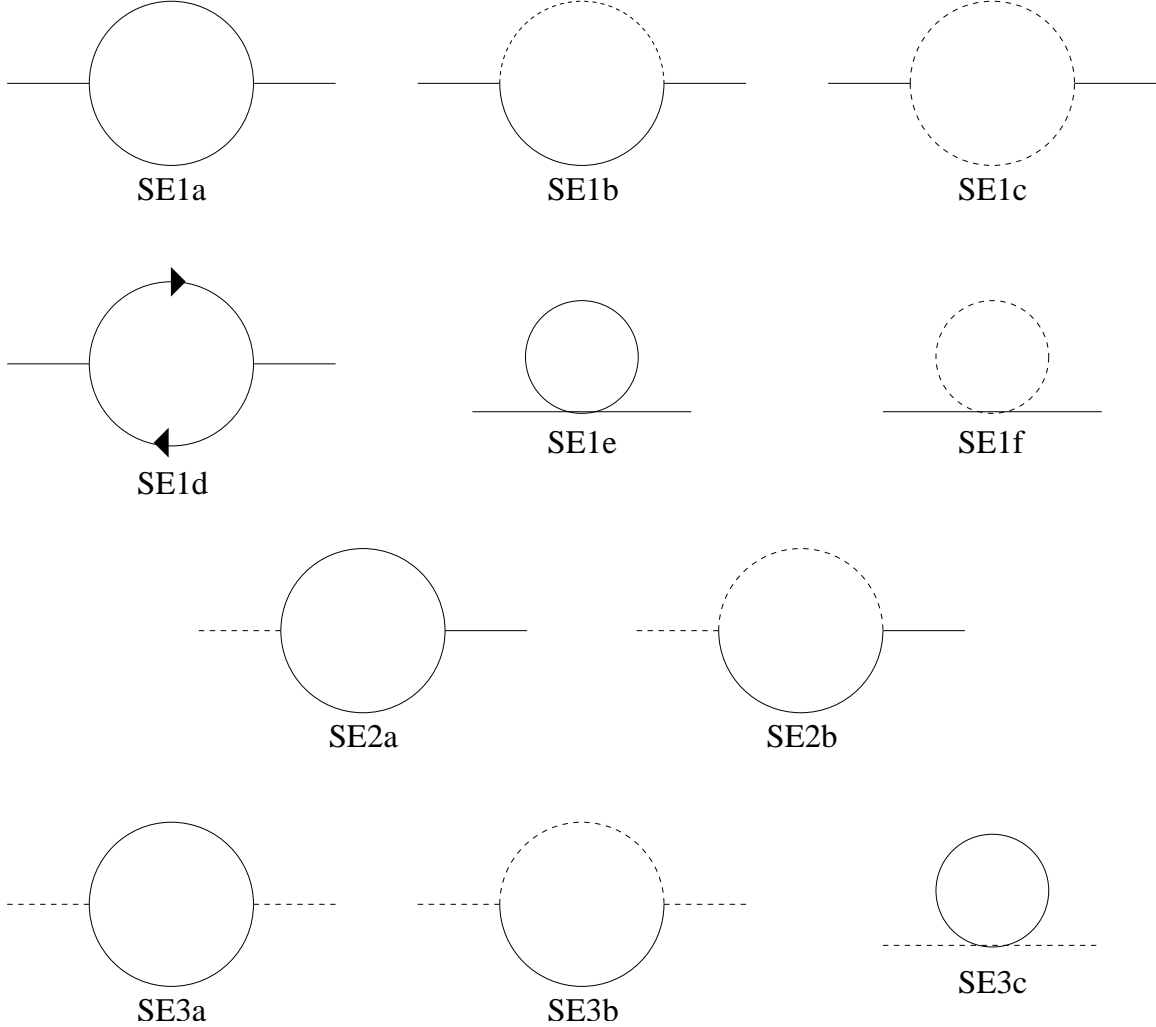


Figure 4: Diagrams contributing to the gauge boson self-energy at 1-loop. Solid lines denote A_i propagators, dashed lines denote A_0 propagators, and arrowed lines denote ghost propagators.

We now list the regulator dependent contribution, $\Pi_*^{(RD)}$, of each diagram in figure 4 to the self-energy $\Pi_{\mu\nu} = -\frac{1}{2}\langle A_\mu A_\nu \rangle$ at momentum p :

$$\begin{aligned} \frac{1}{\lambda} \left(\Pi_{SE1a}^{(RD)} \right)_{ij} &= -\frac{2}{3} M^2 C_2 g_{ij} + \left(\frac{1}{24\pi^2} p_0^2 g_{ij} - \frac{9}{40\pi^2} p^2 g_{ij} + \frac{31}{120\pi^2} p_i p_j \right) \ln \left(\frac{\mathcal{A}_2 M}{\mu} \right) \\ &\quad - \frac{1}{15} (p^2 g_{ij} + 4p_i p_j) F_2 + \frac{43}{450\pi^2} p_i p_j - \frac{19}{300\pi^2} p^2 g_{ij} - \frac{1}{72\pi^2} p_0^2 g_{ij}, \end{aligned} \quad (\text{A.4})$$

$$\begin{aligned} \frac{1}{\lambda} \left(\Pi_{SE1b}^{(RD)} \right)_{ij} &= \frac{2}{3} M^2 C_1 g_{ij} + \left(-\frac{1}{6\pi^2} p_0^2 g_{ij} + \frac{1}{10\pi^2} p^2 g_{ij} - \frac{2}{15\pi^2} p_i p_j \right) \ln \left(\frac{\mathcal{A}_1 M}{\mu} \right) \\ &\quad - \frac{1}{36\pi^2} p_0^2 g_{ij} + \frac{16}{225\pi^2} p_i p_j - \frac{31}{300\pi^2} p^2 g_{ij} + \Lambda M B_1 (\delta_i^m \delta_j^n - g^{mn} g_{ij}) (H_1)_{mn}, \end{aligned} \quad (\text{A.5})$$

$$\frac{1}{\lambda} \left(\Pi_{SE1c}^{(RD)} \right)_{ij} = \bar{\Lambda} \bar{B}_2 (p_i [\bar{J}_2]_j - 2\bar{M}(\bar{H}_2)_{ij}), \quad (\text{A.6})$$

$$\frac{1}{\lambda} \left(\Pi_{SE1d}^{(RD)} \right)_{ij} = \bar{\Lambda} \bar{B}_2 (\bar{M}[\bar{H}_2]_{ij} - p_i [\bar{J}_2]_j), \quad (\text{A.7})$$

$$\frac{1}{\lambda} \left(\Pi_{SE1e}^{(RD)} \right)_{ij} = \frac{4}{3} M^2 C_1 g_{ij}, \quad (\text{A.8})$$

$$\frac{1}{\lambda} \left(\Pi_{SE1f}^{(RD)} \right)_{ij} = 2\bar{\Lambda} \bar{M} \bar{B}_1 \bar{C}_1 g_{ij}, \quad (\text{A.9})$$

$$\frac{1}{\lambda} \left(\Pi_{SE2a}^{(RD)} \right)_{0i} = -\frac{p_0 p_i}{24\pi^2} \ln \left(\frac{\mathcal{A}_2 M}{\mu} \right) + \frac{p_0 p_i}{72\pi^2}, \quad (\text{A.10})$$

$$\frac{1}{\lambda} \left(\Pi_{SE2b}^{(RD)} \right)_{0i} = \frac{p_0 p_i}{3\pi^2} \ln \left(\frac{\mathcal{A}_1 M}{\mu} \right) + \frac{p_0 p_i}{18\pi^2}, \quad (\text{A.11})$$

$$\frac{1}{\lambda} \left(\Pi_{SE3a}^{(RD)} \right)_{00} = -2C_2 M^2 + \frac{5p^2}{24\pi^2} \ln \left(\frac{\mathcal{A}_2 M}{\mu} \right) - \frac{p^2}{3} F_2 + \frac{7}{72\pi^2} p^2, \quad (\text{A.12})$$

$$\frac{1}{\lambda} \left(\Pi_{SE3b}^{(RD)} \right)_{00} = -\frac{2p^2}{3\pi^2} \ln \left(\frac{\mathcal{A}_1 M}{\mu} \right) - \frac{1}{9\pi^2} p^2, \quad (\text{A.13})$$

$$\frac{1}{\lambda} \left(\Pi_{SE3c}^{(RD)} \right)_{00} = 2M^2 C_1. \quad (\text{A.14})$$

A.3. A check : the 2-loop free energy

We now proceed to compute a physical quantity, the free energy of Yang Mills theory at order λ , using our regularization scheme. We will find a result that agrees with the standard result obtained by traditional methods (utilizing dimensional regularization in Feynman gauge). We view this agreement as a significant check on the consistency of our regularization scheme.

The two-loop free energy of Yang Mills theory, at order λ , receives contributions from six graphs depicted in figure 5. A set of one-loop counterterm graphs also contribute to the same order. We will find it useful to group each two-loop graph with a set of one-loop counterterm graphs, in the manner (and for the reasons) that we now explain.

Consider the counterterm contributions to the free energy at order λ . For the purpose of this discussion, it will be useful to regard counterterms that cancel different one-loop

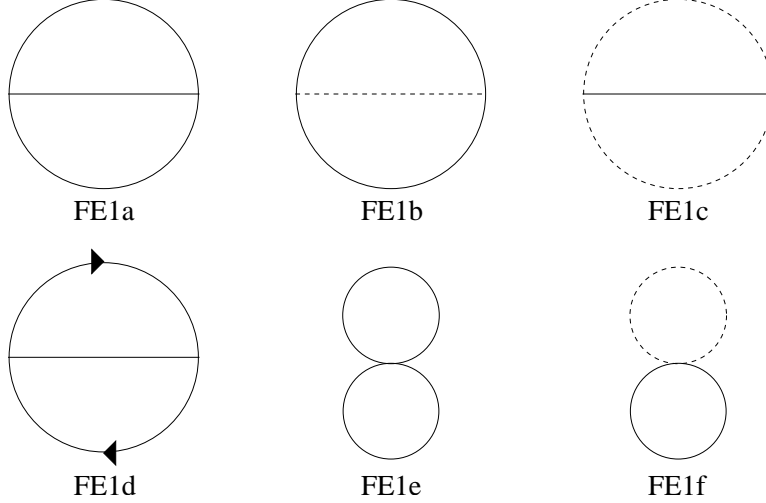


Figure 5: Diagrams contributing to the 2-loop free energy.

contributions to the self energy (see above) as distinct²⁴. Any one-loop contribution to the free energy with a counterterm insertion may uniquely be associated with one of the two-loop free energy graphs by “blowing up” the counterterm into its parent self-energy diagram. It is plausible (and true) that the sum of any particular 2-loop free energy graph with all its associated 1-loop counterterm graphs, is finite²⁵ and independent of the damping function $R(\frac{q}{\Lambda})$. This fact suggests a natural grouping of graphs that we will use.

Next, we list the results related to the diagrams, depicted in figure 5, that contribute to the 2-loop free energy. For each such diagram, we list the result of evaluating it in our damping function scheme, F_* , the contribution arising from its associated one-loop self-energy diagram (see section 4 and the previous subsection), $F_*^{(CT)}$, and the result obtained by direct evaluation in (split) dimensional regularization, $F_*^{(DR)}$ (all divided by λV , where

²⁴ Furthermore, it is easy to convince oneself that only the counterterm with external vector lines yields a temperature-dependent contribution to the free energy.

²⁵ It may also seem natural to guess that this sum will equal the corresponding diagram evaluated in split dimensional regularization, but this is not precisely the case, as we explain in detail in the next subsection.

V is the volume of space) :

$$\begin{aligned}
F_{FE1a} &= -\frac{1}{9}C_2M^2T^2 - \frac{4}{225}T^4 \ln\left(\frac{\mathcal{A}_2M}{a}\right) - \frac{\pi^2}{225}T^4F_2 + \frac{4}{15\pi^4} \int \frac{dp}{e^{p/T} - 1} p^3 \ln\left(\frac{p}{a}\right) \\
&\quad - \frac{4393}{216000}T^4 + \frac{1}{128\pi^4} \int_0^\infty \frac{dq}{q^2(e^{q/T} - 1)} \int_0^\infty \frac{dp}{p^2(e^{p/T} - 1)} \\
&\quad \quad \quad \times \left\{ 4q^5p + 4p^5q + (p^2 + q^2)(p^4 + 6p^2q^2 + q^4) \ln\left[\frac{(p-q)^2}{(p+q)^2}\right] \right\} \\
F_{FE1a}^{(CT)} &= \frac{1}{9}C_2M^2T^2 + \frac{4}{225}T^4 \ln\left(\frac{\mathcal{A}_2M}{\mu}\right) + \frac{\pi^2}{225}T^4F_2 + \frac{89}{27000}T^4 \\
F_{FE1a}^{(DR)} &= \frac{4}{15\pi^4} \int \frac{dp}{e^{p/T} - 1} p^3 \ln\left(\frac{p}{a}\right) + \frac{4}{225}T^4 \ln\left(\frac{a}{\mu}\right) - \frac{587}{72000}T^4 \\
&\quad + \frac{1}{128\pi^4} \int_0^\infty \frac{dq}{q^2(e^{q/T} - 1)} \int_0^\infty \frac{dp}{p^2(e^{p/T} - 1)} \\
&\quad \quad \quad \times \left\{ 4q^5p + 4p^5q + (p^2 + q^2)(p^4 + 6p^2q^2 + q^4) \ln\left[\frac{(p-q)^2}{(p+q)^2}\right] \right\}
\end{aligned} \tag{A.15}$$

$$\begin{aligned}
F_{FE1b} &= \frac{1}{9}M^2T^2C_1 + \frac{4}{225}T^4 \ln\left(\frac{\mathcal{A}_1M}{\mu}\right) - \frac{4}{15\pi^4} \int_0^\infty \frac{dp}{e^{p/T} - 1} p^3 \ln\left(\frac{p}{a}\right) + \frac{3593}{216000}T^4 \\
&\quad - \Lambda MB_1 \int \frac{d^3q}{(2\pi)^3} \frac{q^2 g_{ij} - q_i q_j}{q^3 (e^{-q/T} - 1)} H_1^{ij}(q) \\
&\quad - \frac{1}{128\pi^4} \int_0^\infty \frac{dq}{q^2(e^{q/T} - 1)} \int_0^\infty \frac{dp}{p^2(e^{p/T} - 1)} \\
&\quad \quad \quad \times \left\{ 4(p^5q + q^5p) + (p^2 + q^2)(p^4 + 6p^2q^2 + q^4) \ln\left[\frac{(p-q)^2}{(p+q)^2}\right] \right\} \\
F_{FE1b}^{(CT)} &= -\frac{1}{9}M^2T^2C_1 - \frac{4}{225}T^4 \ln\left(\frac{\mathcal{A}_1M}{\mu}\right) + \frac{17}{3375}T^4 \\
&\quad + \Lambda MB_1 \int \frac{d^3q}{(2\pi)^3} \frac{q^2 g_{ij} - q_i q_j}{q^3 (e^{-q/T} - 1)} H_1^{ij}(q) \\
F_{FE1b}^{(DR)} &= -\frac{4}{15\pi^4} \int \frac{dp}{e^{p/T} - 1} p^3 \ln\left(\frac{p}{a}\right) - \frac{4}{225}T^4 \ln\left(\frac{a}{\mu}\right) + \frac{2761}{216000}T^4 \\
&\quad - \frac{1}{128\pi^4} \int_0^\infty \frac{dq}{q^2(e^{q/T} - 1)} \int_0^\infty \frac{dp}{p^2(e^{p/T} - 1)} \\
&\quad \quad \quad \times \left\{ 4(p^5q + q^5p) + (p^2 + q^2)(p^4 + 6p^2q^2 + q^4) \ln\left[\frac{(p-q)^2}{(p+q)^2}\right] \right\}
\end{aligned} \tag{A.16}$$

$$\begin{aligned}
F_{FE1c} &= -2\bar{\Lambda}\bar{M}\bar{B}_2T \sum_{p_0} \int \frac{d^3p}{(2\pi)^3} \frac{(p^2 g^{ij} - p^i p^j) (\bar{H}_2)_{ij}(p)}{p^2(p^2 + p_0^2)} \\
F_{FE1c}^{(CT)} &= 2\bar{\Lambda}\bar{M}\bar{B}_2T \sum_{p_0} \int \frac{d^3p}{(2\pi)^3} \frac{(p^2 g^{ij} - p^i p^j) (\bar{H}_2)_{ij}(p)}{p^2(p^2 + p_0^2)} \tag{A.17}
\end{aligned}$$

$$F_{FE1c}^{(DR)} = 0$$

$$\begin{aligned}
F_{FE1d} &= \bar{\Lambda}\bar{M}\bar{B}_2T \sum_{p_0} \int \frac{d^3p}{(2\pi)^3} \frac{(p^2 g^{ij} - p^i p^j) (\bar{H}_2)_{ij}(p)}{p^2(p^2 + p_0^2)} \\
F_{FE1d}^{(CT)} &= -\bar{\Lambda}\bar{M}\bar{B}_2T \sum_{p_0} \int \frac{d^3p}{(2\pi)^3} \frac{(p^2 g^{ij} - p^i p^j) (\bar{H}_2)_{ij}(p)}{p^2(p^2 + p_0^2)} \tag{A.18}
\end{aligned}$$

$$F_{FE1d}^{(DR)} = 0$$

$$\begin{aligned}
F_{FE1e} &= \frac{2}{9}M^2T^2C_1 + \frac{1}{108}T^4 \\
F_{FE1e}^{(CT)} &= -\frac{2}{9}M^2T^2C_1 \tag{A.19}
\end{aligned}$$

$$F_{FE1e}^{(DR)} = \frac{1}{108}T^4$$

$$F_{FE1f} = \frac{1}{3}\bar{\Lambda}\bar{M}\bar{C}_1\bar{B}_1T^2$$

$$F_{FE1f}^{(CT)} = -\frac{1}{3}\bar{\Lambda}\bar{M}\bar{C}_1\bar{B}_1T^2 \tag{A.20}$$

$$F_{FE1f}^{(DR)} = 0$$

Summing the contributions of the individual diagrams, we find that the 2-loop free energy is

$$\frac{F_{2-loop}}{V} = \frac{\lambda}{72}T^4, \tag{A.21}$$

in agreement with results previously computed using dimensional regularization in Feynman gauge [16]^{26 27}.

²⁶ The result often seen in the literature is $\frac{\lambda}{144}T^4$, which differs from this by a factor of 2. The reason for this apparent difference arises from a choice of convention. Our definition of the propagators in (4.12) corresponds to a normalization of the basis matrices $(t^A)^{ab}$ such that $(t^A)^{ab}(t^A)^{cd} = \delta^{ad}\delta^{bc}$, which is equivalent to taking the quadratic Casimir of the fundamental representation as $C(N) = 1$. The convention most prevalent in the literature is $C(N) = \frac{1}{2}$. This difference amounts to an effective difference in the definition of λ which, when properly accounted for, gives an extra factor of 2.

²⁷ We also find the same result for the free energy evaluated directly in Coulomb gauge using split dimensional regularization.

We may explicitly verify the diagram by diagram cancellation of divergences discussed above. In addition, we note that adding the contributions from a free energy diagram in our damping function scheme and its associated self-energy diagram does not lead to full diagram by diagram agreement with the result of (split) dimensional regularization. We discuss this in greater detail in the next subsection.

A.4. Diagram by diagram comparison with split dimensional regularization

In this subsection, we will explain in detail how the sum of any particular two loop self energy graph plus all its associated 1-loop counterterm graphs differs from the same graph evaluated in dimensional regularization.

If we consider summing a free energy diagram computed in our scheme with its corresponding counterterm, this yields a result equivalent to evaluating the integral over the internal loop momentum from which the divergence arises *before* contracting the legs of this loop with the A_i propagator. After the evaluation, we perform this contraction but, at that point, the number of spatial dimensions is fixed at $d = 3$. On the other hand, when we compute the free energy diagram in pure (split) dimensional regularization, contraction of the divergent momentum integral with the final propagator is done at unspecified d , leading to additional dependence on $\epsilon = 3 - d$ and changing the finite result.

As a check on our calculations, we now compute the difference between the finite parts of diagrams evaluated with our scheme and with (split) dimensional regularization. Any factors of d that arise only affect the evaluation of the logarithmic divergences and thus we restrict attention to these. We write a generic logarithmically divergent integral that arises in the asymptotic expansion of a given self-energy diagram as

$$[f(p^2, \epsilon)g_{ij} + g(p^2, \epsilon)p_i p_j] \int \frac{d^3 q}{(2\pi)^3} \frac{1}{\sqrt{q^2}(q^2 + a^2)}. \quad (\text{A.22})$$

Contracting this with an A_i propagator at momentum p , and evaluating the integral in dimensional regularization, we obtain

$$(2 - \epsilon)f(p^2, \epsilon) \int \frac{d^3 q}{(2\pi)^3} \frac{1}{\sqrt{q^2}(q^2 + a^2)} = (2 - \epsilon) [f(p^2, 0) + \mathcal{O}(\epsilon)] \left[\frac{1}{\epsilon} - \ln \left(\frac{a}{\mu} \right) \right]. \quad (\text{A.23})$$

We see that the new finite contribution that arises due to the ϵ in the $(2 - \epsilon)$ factor is precisely $-\frac{1}{2}$ times the coefficient of $\ln \mu$ in the final result. This implies that, to get the (split) dimensional regularization result for diagram $FE1a$ ($FE1b$), we should add $\frac{2}{225}T^4$

$(-\frac{2}{225}T^4)$. It is easy to check that this is consistent with equations (A.15) and (A.16). Moreover, we see why this diagram by diagram discrepancy didn't ruin agreement in the final result for the free energy; the difference between our scheme and (split) dimensional regularization is proportional to the logarithmic divergence of a given diagram and all logarithmic divergences cancel when the diagrams are summed.

A.5. Coefficients of divergences in non-planar one-loop 4-point graphs

In this subsection, we consider details related to the computation of the $\text{tr}(A_i A_j)\text{tr}(A_k A_l)$ counterterm that is relevant for the computation of b in section 3. The relevant diagrams are depicted in figure 6. The seemingly chaotic ordering and labeling of diagrams was chosen for easy identification with 3-loop free energy diagrams via the correspondence discussed in the main text.

We compute the counter-term by computing four-point functions of gauge fields, with the color index structure $\langle \text{tr}(A_i A_j)\text{tr}(A_k A_l) \rangle$ which arises from one-loop non-planar diagrams. These diagrams generally have a logarithmic divergence proportional to

$$\int \frac{d^3 q}{4\pi \sqrt{q^2(q^2 + a^2)}}. \quad (\text{A.24})$$

We begin by listing the coefficient, M_{abcd}^* , of this logarithmically divergent integral for each diagram in figure 6 with the indices fixed as in the figure, computed in dimensional regularization with $d = 3 - \epsilon$:

$$\begin{aligned} M_{abcd}^{(3a)} &= \frac{1}{8\pi^2} \left[\frac{1}{d(d+2)} [(5+2d)g_{ab}g_{cd} + (5d-19)g_{ac}g_{bd} + (17-4d^2)g_{ad}g_{bc}] + (d-3)g_{ab}g_{cd} \right] \\ M_{abcd}^{(3b)} &= \frac{1}{8\pi^2} \left(\frac{1}{d(d+2)} \right) [(3-d-d^2)g_{ab}g_{cd} + (2d^2-7)g_{ac}g_{bd} + (5-d^2)g_{ad}g_{bc}] \\ M_{abcd}^{(3c)} &= -\frac{3}{8\pi^2} \left(\frac{1}{d(d+2)} \right) [g_{ab}g_{cd} + g_{ac}g_{bd} + (d^2-3)g_{ad}g_{bc}] \end{aligned} \quad (\text{A.25})$$

$$\begin{aligned} M_{abcd}^{(3d)} &= \frac{1}{4\pi^2} \left[\frac{1}{d(d+2)} [(d^2-2)g_{ab}g_{cd} + (d^2-2)g_{ad}g_{bc} + (4d+10)g_{ac}g_{bd}] + 2(d-3)g_{ac}g_{bd} \right] \\ M_{abcd}^{(3e)} &= \frac{1}{8\pi^2} \left(\frac{1}{d(d+2)} \right) [(d^2-2)g_{ab}g_{cd} + (d^2-2)g_{ad}g_{bc} + 2(3-d-d^2)g_{ac}g_{bd}] \\ M_{abcd}^{(3f1)} &= -\frac{3}{8\pi^2} \left(\frac{1}{d(d+2)} \right) [g_{ab}g_{cd} + g_{ac}g_{bd} + (d^2-3)g_{ad}g_{bc}] \\ M_{abcd}^{(3f2)} &= -\frac{3}{8\pi^2} \left(\frac{1}{d(d+2)} \right) [g_{ac}g_{bd} + g_{ad}g_{bc} + (d^2-3)g_{ab}g_{cd}] \end{aligned} \quad (\text{A.26})$$

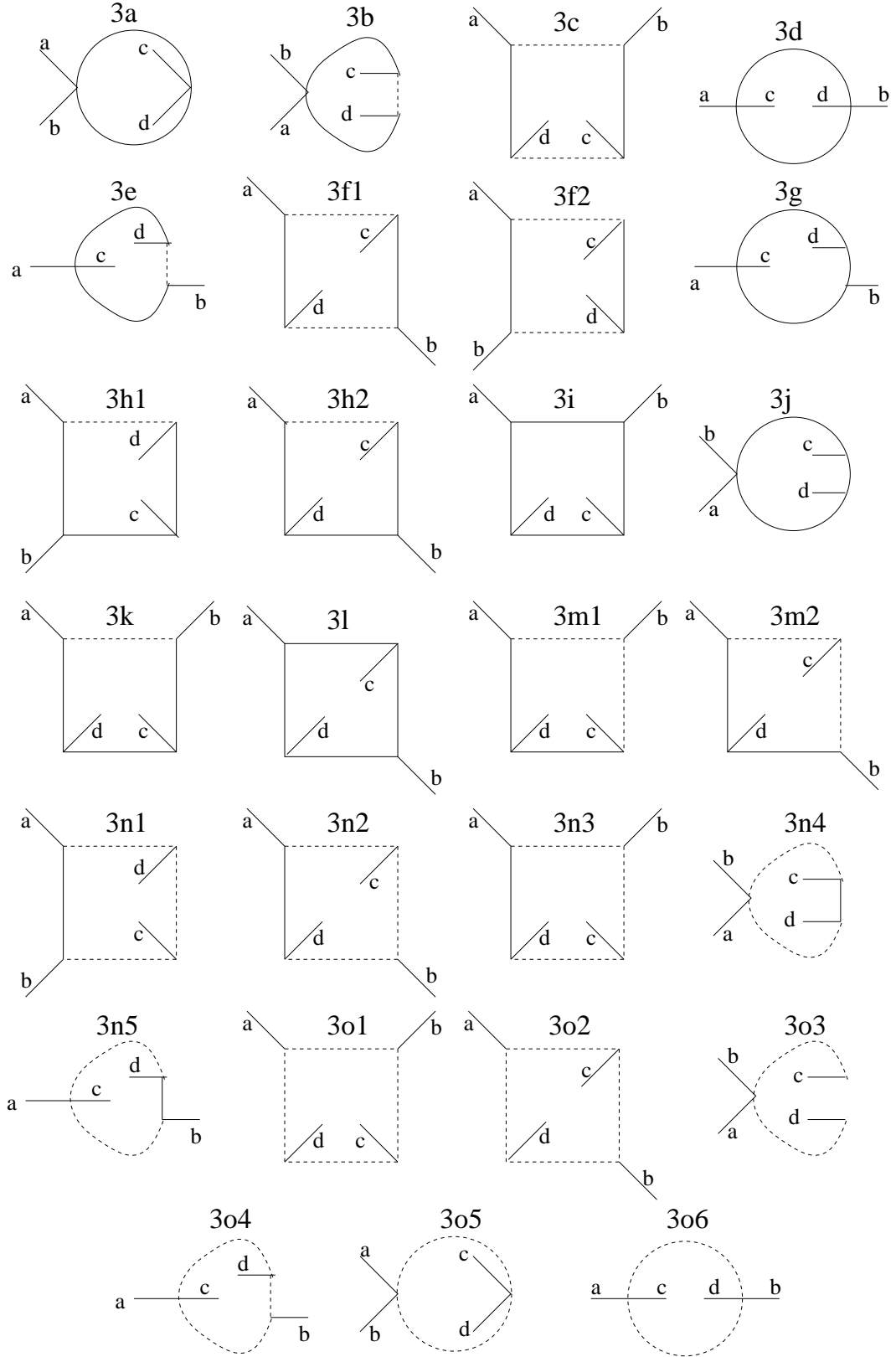


Figure 6: The diagrams contributing to $\langle \text{tr}(A_i A_j) \text{tr}(A_k A_l) \rangle$ at order λ^2/N^2 , whose corresponding counterterms are relevant to the calculation of b .

$$\begin{aligned}
M_{abcd}^{(3g)} &= -\frac{3}{4\pi^2} \left(\frac{1}{d(d+2)} \right) [(d^2 - 3)g_{ac}g_{bd} + g_{ab}g_{cd} + g_{ad}g_{bc}] \\
M_{abcd}^{(3h1)} &= \frac{1}{8\pi^2} \left(\frac{1}{d(d+2)} \right) [(d+1)g_{ad}g_{bc} - g_{ac}g_{bd} - g_{ab}g_{cd}] \\
M_{abcd}^{(3h2)} &= \frac{1}{8\pi^2} \left(\frac{1}{d(d+2)} \right) [(d+1)g_{ac}g_{bd} - g_{ab}g_{cd} - g_{ad}g_{bc}] \\
M_{abcd}^{(3i)} &= \frac{5}{4\pi^2} \left(\frac{d-1}{d(d+2)} \right) [g_{ab}g_{cd} + g_{ac}g_{bd} + g_{ad}g_{bc}] \\
M_{abcd}^{(3j)} &= -\frac{3}{8\pi^2} \left(\frac{1}{d(d+2)} \right) [g_{ac}g_{bd} + g_{ad}g_{bc} + (d^2 - 3)g_{ab}g_{cd}]
\end{aligned} \tag{A.27}$$

$$\begin{aligned}
M_{abcd}^{(3k)} &= \frac{1}{8\pi^2} \left(\frac{1}{d(d+2)} \right) [(d+1)g_{ab}g_{cd} - g_{ac}g_{bd} - g_{ad}g_{bc}] \\
M_{abcd}^{(3l)} &= \frac{5}{4\pi^2} \left(\frac{d-1}{d(d+2)} \right) [g_{ab}g_{cd} + g_{ac}g_{bd} + g_{ad}g_{bc}] \\
M_{abcd}^{(3m1)} &= \frac{1}{2\pi^2} \left(\frac{1}{d(d+2)} \right) [(d+1)g_{ac}g_{bd} - g_{ab}g_{cd} - g_{ad}g_{bc}] \\
M_{abcd}^{(3m2)} &= \frac{1}{2\pi^2} \left(\frac{1}{d(d+2)} \right) [(d+1)g_{ab}g_{cd} - g_{ac}g_{bd} - g_{ad}g_{bc}]
\end{aligned} \tag{A.28}$$

$$\begin{aligned}
M_{abcd}^{(3n1)} &= \frac{1}{\pi^2} \left(\frac{1}{d(d+2)} \right) [g_{ad}g_{cb} + g_{ac}g_{bd} - (d+1)g_{ab}g_{cd}] \\
M_{abcd}^{(3n2)} &= \frac{1}{\pi^2} \left(\frac{1}{d(d+2)} \right) [g_{ac}g_{bd} + g_{ab}g_{cd} - (d+1)g_{ad}g_{bc}] \\
M_{abcd}^{(3n3)} &= \frac{1}{\pi^2} \left(\frac{1}{d(d+2)} \right) [g_{ab}g_{cd} + g_{ac}g_{bd} - (d+1)g_{ad}g_{bc}] \\
M_{abcd}^{(3n4)} &= \frac{1}{4\pi^2} \left(\frac{d-1}{d} \right) g_{ab}g_{cd} \\
M_{abcd}^{(3n5)} &= \frac{1}{2\pi^2} \left(\frac{d-1}{d} \right) g_{ac}g_{bd} \\
M_{abcd}^{(3o1)} &= M_{abcd}^{(3o2)} = M_{abcd}^{(3o3)} = M_{abcd}^{(3o4)} = M_{abcd}^{(3o5)} = M_{abcd}^{(3o6)} = 0.
\end{aligned} \tag{A.29}$$

We now sum over the appropriate permutations of indices to obtain the coefficient, $R_{ijkl}^{(*)}$, of the logarithmic divergence (A.24) due to diagrams of each type. We list these

coefficients, as well as the contribution to the $\text{tr}(A_i A_j)\text{tr}(A_k A_l)$ counterterm $R_{CT}^{(*)}$:

$$\begin{aligned}
R_{ijkl}^{(3a)} &= \frac{1}{4\pi^2 d(d+2)} [(10+4d)g_{ij}g_{kl} + (d^2-2)g_{ik}g_{jl} + (d^2-2)g_{il}g_{jk}] + \frac{d-3}{2\pi^2} g_{ij}g_{kl} \\
&= \left[\frac{11}{30\pi^2} - \frac{167\epsilon}{450\pi^2} + \mathcal{O}(\epsilon^2) \right] g_{ij}g_{kl} + \left[\frac{7}{60\pi^2} - \frac{17\epsilon}{450\pi^2} + \mathcal{O}(\epsilon^2) \right] [g_{ik}g_{jl} + g_{il}g_{jk}] \\
R_{CT}^{(3a)} &= \left[\frac{11}{240\pi^2} \ln\left(\frac{\mathcal{A}_2 M}{\mu}\right) + \frac{167}{3600\pi^2} \right] \text{tr}(A_i A_i)\text{tr}(A_j A_j) \\
&\quad + 2 \left[\frac{7}{480\pi^2} \ln\left(\frac{\mathcal{A}_2 M}{\mu}\right) + \frac{17}{3600\pi^2} \right] \text{tr}(A_i A_j)\text{tr}(A_i A_j)
\end{aligned} \tag{A.30}$$

$$\begin{aligned}
R_{ijkl}^{(3b)} &= \frac{1}{2\pi^2 d(d+2)} [2(3-d-d^2)g_{ij}g_{kl} + (d^2-2)g_{ik}g_{jl} + (d^2-2)g_{il}g_{jk}] \\
&= \left[-\frac{3}{5\pi^2} + \frac{11\epsilon}{75\pi^2} + \mathcal{O}(\epsilon^2) \right] g_{ij}g_{kl} + \left[\frac{7}{30\pi^2} - \frac{17\epsilon}{225\pi^2} + \mathcal{O}(\epsilon^2) \right] [g_{ik}g_{jl} + g_{il}g_{jk}] \\
R_{CT}^{(3b)} &= \left[-\frac{3}{40\pi^2} \ln\left(\frac{\mathcal{A}_2 M}{\mu}\right) - \frac{11}{600\pi^2} \right] \text{tr}(A_i A_i)\text{tr}(A_j A_j) \\
&\quad + 2 \left[\frac{7}{240\pi^2} \ln\left(\frac{\mathcal{A}_2 M}{\mu}\right) + \frac{17}{1800\pi^2} \right] \text{tr}(A_i A_j)\text{tr}(A_i A_j)
\end{aligned} \tag{A.31}$$

$$\begin{aligned}
R_{ijkl}^{(3c)} &= -\frac{3}{4\pi^2 d(d+2)} [2g_{ij}g_{kl} + (d^2-2)(g_{ik}g_{jl} + g_{il}g_{jk})] \\
&= \left[-\frac{1}{10\pi^2} - \frac{4\epsilon}{75\pi^2} + \mathcal{O}(\epsilon^2) \right] g_{ij}g_{kl} + \left[-\frac{7}{20\pi^2} + \frac{17\epsilon}{150\pi^2} + \mathcal{O}(\epsilon^2) \right] [g_{ik}g_{jl} + g_{il}g_{jk}] \\
R_{CT}^{(3c)} &= \left[-\frac{1}{80\pi^2} \ln\left(\frac{\mathcal{A}_2 M}{\mu}\right) + \frac{1}{150\pi^2} \right] \text{tr}(A_i A_i)\text{tr}(A_j A_j) \\
&\quad + 2 \left[-\frac{7}{160\pi^2} \ln\left(\frac{\mathcal{A}_2 M}{\mu}\right) - \frac{17}{1200\pi^2} \right] \text{tr}(A_i A_j)\text{tr}(A_i A_j)
\end{aligned} \tag{A.32}$$

$$\begin{aligned}
R_{ijkl}^{(3d)} &= \frac{1}{4\pi^2 d(d+2)} [2(d^2-2)g_{ij}g_{kl} + (d^2+4d+8)g_{ik}g_{jl} + (d^2+4d+8)g_{il}g_{jk}] \\
&\quad + \frac{d-3}{2\pi^2} [g_{ik}g_{jl} + g_{il}g_{jk}] \\
&= \left[\frac{7}{30\pi^2} - \frac{17\epsilon}{225\pi^2} + \mathcal{O}(\epsilon^2) \right] g_{ij}g_{kl} + \left[\frac{29}{60\pi^2} - \frac{92\epsilon}{225\pi^2} + \mathcal{O}(\epsilon^2) \right] [g_{ik}g_{jl} + g_{il}g_{jk}] \\
R_{CT}^{(3d)} &= \left[\frac{7}{240\pi^2} \ln\left(\frac{\mathcal{A}_2 M}{\mu}\right) + \frac{17}{1800\pi^2} \right] \text{tr}(A_i A_i)\text{tr}(A_j A_j) \\
&\quad + 2 \left[\frac{29}{480\pi^2} \ln\left(\frac{\mathcal{A}_2 M}{\mu}\right) + \frac{92}{1800\pi^2} \right] \text{tr}(A_i A_j)\text{tr}(A_i A_j)
\end{aligned} \tag{A.33}$$

$$\begin{aligned}
R_{ijkl}^{(3e)} &= \frac{1}{2\pi^2 d(d+2)} [2(d^2 - 2)g_{ij}g_{kl} + (4 - 2d - d^2)g_{ik}g_{jl} + (4 - 2d - d^2)g_{il}g_{jk}] \\
&= \left[\frac{7}{15\pi^2} - \frac{34\epsilon}{225\pi^2} + \mathcal{O}(\epsilon^2) \right] g_{ij}g_{kl} + \left[-\frac{11}{30\pi^2} + \frac{16\epsilon}{225\pi^2} + \mathcal{O}(\epsilon^2) \right] [g_{ik}g_{jl} + g_{il}g_{jk}] \\
R_{CT}^{(3e)} &= \left[\frac{7}{120\pi^2} \ln \left(\frac{\mathcal{A}_2 M}{\mu} \right) + \frac{17}{900\pi^2} \right] \text{tr}(A_i A_i) \text{tr}(A_j A_j) \\
&\quad + 2 \left[-\frac{11}{240\pi^2} \ln \left(\frac{\mathcal{A}_2 M}{\mu} \right) - \frac{2}{225\pi^2} \right] \text{tr}(A_i A_j) \text{tr}(A_i A_j)
\end{aligned} \tag{A.34}$$

$$\begin{aligned}
R_{ijkl}^{(3f1)} &= R_{ijkl}^{(3c)} \\
R_{CT}^{(3f1)} &= R_{CT}^{(3c)}
\end{aligned} \tag{A.35}$$

$$\begin{aligned}
R_{ijkl}^{(3f2)} &= -\frac{3}{2\pi^2 d(d+2)} [(d^2 - 3)g_{ij}g_{kl} + g_{ik}g_{jl} + g_{il}g_{jk}] \\
&= \left[-\frac{3}{5\pi^2} + \frac{7\epsilon}{25\pi^2} + \mathcal{O}(\epsilon^2) \right] g_{ij}g_{kl} + \left[-\frac{1}{10\pi^2} - \frac{4\epsilon}{75\pi^2} + \mathcal{O}(\epsilon^2) \right] [g_{ik}g_{jl} + g_{il}g_{jk}] \\
R_{CT}^{(3f2)} &= \left[-\frac{3}{40\pi^2} \ln \left(\frac{\mathcal{A}_2 M}{\mu} \right) - \frac{7}{200\pi^2} \right] \text{tr}(A_i A_i) \text{tr}(A_j A_j) \\
&\quad + 2 \left[-\frac{1}{80\pi^2} \ln \left(\frac{\mathcal{A}_2 M}{\mu} \right) + \frac{1}{150\pi^2} \right] \text{tr}(A_i A_j) \text{tr}(A_i A_j)
\end{aligned} \tag{A.36}$$

$$\begin{aligned}
R_{ijkl}^{(3g)} &= -\frac{3}{\pi^2 d(d+2)} [2g_{ij}g_{kl} + (d^2 - 2)g_{ik}g_{jl} + (d^2 - 2)g_{il}g_{jk}] \\
&= \left[-\frac{2}{5\pi^2} - \frac{16\epsilon}{75\pi^2} + \mathcal{O}(\epsilon^2) \right] g_{ij}g_{kl} + \left[-\frac{7}{5\pi^2} + \frac{34\epsilon}{75\pi^2} + \mathcal{O}(\epsilon^2) \right] [g_{ik}g_{jl} + g_{il}g_{jk}] \\
R_{CT}^{(3g)} &= \left[-\frac{1}{20\pi^2} \ln \left(\frac{\mathcal{A}_3 M}{\mu} \right) + \frac{2}{75\pi^2} \right] \text{tr}(A_i A_i) \text{tr}(A_j A_j) \\
&\quad + 2 \left[-\frac{7}{40\pi^2} \ln \left(\frac{\mathcal{A}_3 M}{\mu} \right) - \frac{17}{300\pi^2} \right] \text{tr}(A_i A_j) \text{tr}(A_i A_j)
\end{aligned} \tag{A.37}$$

$$\begin{aligned}
R_{ijkl}^{(3h1)} &= \frac{1}{2\pi^2 d(d+2)} [-2g_{ij}g_{kl} + d(g_{ik}g_{jl} + g_{il}g_{jk})] \\
&= \left[-\frac{1}{15\pi^2} - \frac{8\epsilon}{225\pi^2} + \mathcal{O}(\epsilon^2) \right] g_{ij}g_{kl} + \left[\frac{1}{10\pi^2} + \frac{\epsilon}{50\pi^2} + \mathcal{O}(\epsilon^2) \right] [g_{ik}g_{jl} + g_{il}g_{jk}] \\
R_{CT}^{(3h1)} &= \left[-\frac{1}{120\pi^2} \ln \left(\frac{\mathcal{A}_3 M}{\mu} \right) + \frac{1}{225\pi^2} \right] \text{tr}(A_i A_i) \text{tr}(A_j A_j) \\
&\quad + 2 \left[\frac{1}{80\pi^2} \ln \left(\frac{\mathcal{A}_3 M}{\mu} \right) - \frac{1}{400\pi^2} \right] \text{tr}(A_i A_j) \text{tr}(A_i A_j)
\end{aligned} \tag{A.38}$$

$$\begin{aligned}
R_{ijkl}^{(3h2)} &= R_{ijkl}^{(3h1)} \\
R_{CT}^{(3h2)} &= R_{CT}^{(3h1)}
\end{aligned}
\tag{A.39}$$

$$\begin{aligned}
R_{ijkl}^{(3i)} &= \frac{5}{\pi^2} \left(\frac{d-1}{d(d+2)} \right) [g_{ij}g_{kl} + g_{ik}g_{jl} + g_{il}g_{jk}] \\
&= \left[\frac{2}{3\pi^2} + \frac{\epsilon}{45\pi^2} + \mathcal{O}(\epsilon^2) \right] [g_{ij}g_{kl} + g_{ik}g_{jl} + g_{il}g_{jk}] \\
R_{CT}^{(3i)} &= \left[\frac{1}{12\pi^2} \ln \left(\frac{\mathcal{A}_4 M}{\mu} \right) - \frac{1}{360\pi^2} \right] [\text{tr}(A_i A_i) \text{tr}(A_j A_j) + 2\text{tr}(A_i A_j) \text{tr}(A_i A_j)]
\end{aligned}
\tag{A.40}$$

$$\begin{aligned}
R_{ijkl}^{(3j)} &= -\frac{3}{\pi^2 d(d+2)} [(d^2 - 3)g_{ij}g_{kl} + g_{ik}g_{jl} + g_{il}g_{jk}] \\
&= \left[-\frac{6}{5\pi^2} + \frac{14\epsilon}{25\pi^2} + \mathcal{O}(\epsilon^2) \right] g_{ij}g_{kl} + \left[-\frac{1}{5\pi^2} - \frac{8\epsilon}{75\pi^2} + \mathcal{O}(\epsilon^2) \right] [g_{ik}g_{jl} + g_{il}g_{jk}] \\
R_{CT}^{(3j)} &= \left[-\frac{3}{20\pi^2} \ln \left(\frac{\mathcal{A}_3 M}{\mu} \right) - \frac{7}{100\pi^2} \right] \text{tr}(A_i A_i) \text{tr}(A_j A_j) \\
&\quad + 2 \left[-\frac{1}{40\pi^2} \ln \left(\frac{\mathcal{A}_3 M}{\mu} \right) + \frac{1}{75\pi^2} \right] \text{tr}(A_i A_j) \text{tr}(A_i A_j)
\end{aligned}
\tag{A.41}$$

$$\begin{aligned}
R_{ijkl}^{(3k)} &= \frac{1}{\pi^2 d(d+2)} [(d+1)g_{ij}g_{kl} - g_{ik}g_{jl} - g_{il}g_{jk}] \\
&= \left[\frac{4}{15\pi^2} + \frac{17\epsilon}{225\pi^2} + \mathcal{O}(\epsilon^2) \right] g_{ij}g_{kl} + \left[-\frac{1}{15\pi^2} - \frac{8\epsilon}{225\pi^2} + \mathcal{O}(\epsilon^2) \right] [g_{ik}g_{jl} + g_{il}g_{jk}] \\
R_{CT}^{(3k)} &= \left[\frac{1}{30\pi^2} \ln \left(\frac{\mathcal{A}_3 M}{\mu} \right) - \frac{17}{1800\pi^2} \right] \text{tr}(A_i A_i) \text{tr}(A_j A_j) \\
&\quad + 2 \left[-\frac{1}{120\pi^2} \ln \left(\frac{\mathcal{A}_3 M}{\mu} \right) + \frac{1}{225\pi^2} \right] \text{tr}(A_i A_j) \text{tr}(A_i A_j)
\end{aligned}
\tag{A.42}$$

$$\begin{aligned}
R_{ijkl}^{(3l)} &= \frac{5}{2\pi^2} \left(\frac{d-1}{d(d+2)} \right) [g_{ij}g_{kl} + g_{ik}g_{jl} + g_{il}g_{jk}] \\
&= \left[\frac{1}{3\pi^2} + \frac{\epsilon}{90\pi^2} + \mathcal{O}(\epsilon^2) \right] [g_{ij}g_{kl} + g_{ik}g_{jl} + g_{il}g_{jk}] \\
R_{CT}^{(3l)} &= \left[\frac{1}{24\pi^2} \ln \left(\frac{\mathcal{A}_4 M}{\mu} \right) - \frac{1}{720\pi^2} \right] [\text{tr}(A_i A_i) \text{tr}(A_j A_j) + 2\text{tr}(A_i A_j) \text{tr}(A_i A_j)]
\end{aligned}
\tag{A.43}$$

$$\begin{aligned}
R_{ijkl}^{(3m1)} &= \frac{4}{\pi^2 d(d+2)} [-2g_{ij}g_{kl} + d(g_{ik}g_{jl} + g_{il}g_{jk})] \\
&= \left[-\frac{8}{15\pi^2} - \frac{64\epsilon}{225\pi^2} + \mathcal{O}(\epsilon^2) \right] g_{ij}g_{kl} + \left[\frac{4}{5\pi^2} + \frac{4\epsilon}{25\pi^2} + \mathcal{O}(\epsilon^2) \right] [g_{ik}g_{jl} + g_{il}g_{jk}] \\
R_{CT}^{(3m1)} &= \left[-\frac{1}{15\pi^2} \ln\left(\frac{\mathcal{A}_2 M}{\mu}\right) + \frac{8}{225\pi^2} \right] \text{tr}(A_i A_i) \text{tr}(A_j A_j) \\
&\quad + 2 \left[\frac{1}{10\pi^2} \ln\left(\frac{\mathcal{A}_2 M}{\mu}\right) - \frac{1}{50\pi^2} \right] \text{tr}(A_i A_j) \text{tr}(A_i A_j)
\end{aligned} \tag{A.44}$$

$$\begin{aligned}
R_{ijkl}^{(3m2)} &= \frac{4}{\pi^2 d(d+2)} [(d+1)g_{ij}g_{kl} - g_{ik}g_{jl} - g_{il}g_{jk}] \\
&= \left[\frac{16}{15\pi^2} + \frac{68\epsilon}{225\pi^2} + \mathcal{O}(\epsilon^2) \right] g_{ij}g_{kl} + \left[-\frac{4}{15\pi^2} - \frac{32\epsilon}{225\pi^2} + \mathcal{O}(\epsilon^2) \right] [g_{ik}g_{jl} + g_{il}g_{jk}] \\
R_{CT}^{(3m2)} &= \left[\frac{2}{15\pi^2} \ln\left(\frac{\mathcal{A}_2 M}{\mu}\right) - \frac{17}{450\pi^2} \right] \text{tr}(A_i A_i) \text{tr}(A_j A_j) \\
&\quad + 2 \left[-\frac{1}{30\pi^2} \ln\left(\frac{\mathcal{A}_2 M}{\mu}\right) + \frac{4}{225\pi^2} \right] \text{tr}(A_i A_j) \text{tr}(A_i A_j)
\end{aligned} \tag{A.45}$$

$$\begin{aligned}
R_{ijkl}^{(3n1)} &= \frac{8}{\pi^2 d(d+2)} [-(d+1)g_{ij}g_{kl} + (g_{ik}g_{jl} + g_{il}g_{jk})] \\
&= \left[\frac{-32}{15\pi^2} - \frac{136\epsilon}{225\pi^2} + \mathcal{O}(\epsilon^2) \right] g_{ij}g_{kl} + \left[\frac{8}{15\pi^2} + \frac{64\epsilon}{225\pi^2} + \mathcal{O}(\epsilon^2) \right] [g_{ik}g_{jl} + g_{il}g_{jk}] \\
R_{CT}^{(3n1)} &= \left[-\frac{4}{15\pi^2} \ln\left(\frac{\mathcal{A}_1 M}{\mu}\right) + \frac{17}{225\pi^2} \right] \text{tr}(A_i A_i) \text{tr}(A_j A_j) \\
&\quad + 2 \left[\frac{1}{15\pi^2} \ln\left(\frac{\mathcal{A}_1 M}{\mu}\right) - \frac{8}{225\pi^2} \right] \text{tr}(A_i A_j) \text{tr}(A_i A_j)
\end{aligned} \tag{A.46}$$

$$\begin{aligned}
R_{ijkl}^{(3n2)} &= \frac{4}{\pi^2 d(d+2)} [2g_{ij}g_{kl} - d(g_{ik}g_{jl} + g_{il}g_{jk})] \\
&= \left[\frac{8}{15\pi^2} + \frac{64\epsilon}{225\pi^2} + \mathcal{O}(\epsilon^2) \right] g_{ij}g_{kl} + \left[-\frac{4}{5\pi^2} - \frac{4\epsilon}{25\pi^2} + \mathcal{O}(\epsilon^2) \right] [g_{ik}g_{jl} + g_{il}g_{jk}] \\
R_{CT}^{(3n2)} &= \left[\frac{1}{15\pi^2} \ln\left(\frac{\mathcal{A}_1 M}{\mu}\right) - \frac{8}{225\pi^2} \right] \text{tr}(A_i A_i) \text{tr}(A_j A_j) \\
&\quad + 2 \left[-\frac{1}{10\pi^2} \ln\left(\frac{\mathcal{A}_1 M}{\mu}\right) + \frac{1}{50\pi^2} \right] \text{tr}(A_i A_j) \text{tr}(A_i A_j)
\end{aligned} \tag{A.47}$$

$$\begin{aligned}
R_{ijkl}^{(3n3)} &= R_{ijkl}^{(3n2)} \\
R_{CT}^{(3n3)} &= R_{CT}^{(3n2)}
\end{aligned} \tag{A.48}$$

$$\begin{aligned}
R_{ijkl}^{(3n4)} &= \frac{2}{\pi^2} \left(\frac{d-1}{d} \right) g_{ij} g_{kl} \\
&= \left[\frac{4}{3\pi^2} - \frac{2\epsilon}{9\pi^2} + \mathcal{O}(\epsilon^2) \right] g_{ij} g_{kl}
\end{aligned} \tag{A.49}$$

$$\begin{aligned}
R_{CT}^{(3n4)} &= \left[\frac{1}{6\pi^2} \ln \left(\frac{\mathcal{A}_1 M}{\mu} \right) + \frac{1}{36\pi^2} \right] \text{tr}(A_i A_i) \text{tr}(A_j A_j) \\
R_{ijkl}^{(3n5)} &= \frac{2(d-1)}{\pi^2 d} [g_{ik} g_{jl} + g_{il} g_{jk}] \\
&= \left[\frac{4}{3\pi^2} - \frac{2\epsilon}{9\pi^2} + \mathcal{O}(\epsilon^2) \right] [g_{ik} g_{jl} + g_{il} g_{jk}]
\end{aligned} \tag{A.50}$$

$$R_{CT}^{(3n5)} = 2 \left[\frac{1}{6\pi^2} \ln \left(\frac{\mathcal{A}_1 M}{\mu} \right) + \frac{1}{36\pi^2} \right] \text{tr}(A_i A_j) \text{tr}(A_i A_j)$$

Summing these yields the following result for the order λ^2/N^2 double-trace counter-term which is needed in equation (3.48) :

$$\mathcal{L}_{CT} = \left(\frac{\lambda^2}{N^2} \right) \left(\frac{1}{120\pi^2} \ln \left(\frac{\mathcal{A}_1^4 \mathcal{A}_2^3 \mathcal{A}_4^{15}}{\mathcal{A}_3^{22}} \right) + \frac{1}{60\pi^2} \right) [\text{tr}(A_i A_i) \text{tr}(A_j A_j) + 2\text{tr}(A_i A_j) \text{tr}(A_i A_j)]. \tag{A.51}$$

Appendix B. Useful Spherical Harmonic Identities

In this appendix, we collect various properties of the S^3 spherical harmonics required to study field theory on S^3 . Many of the basic results were derived in [7].

B.1. Basic properties of spherical harmonics

Scalar functions on the sphere may be expanded in a complete set of spherical harmonics $S_j^{m m'}$ transforming in the $(j/2, j/2)$ representation of $SU(2) \times SU(2) \equiv SO(4)$, where j is any nonnegative integer, and $-j/2 \leq m, m' \leq j/2$. It is convenient to denote the full set of indices (j, m, m') by α . These obey an orthonormality condition (we take the radius of the S^3 to be one)

$$\int_{S^3} S^\alpha S^\beta = \delta^{\alpha\bar{\beta}}, \tag{B.1}$$

where $S^{\bar{\alpha}}$ denotes the complex conjugate of S^α ,

$$(S_j^{m m'})^* = (-1)^{m+m'} S_j^{-m -m'}. \tag{B.2}$$

The spherical harmonics are eigenfunctions of the Laplace operator on the sphere,

$$\nabla^2 S^\alpha = -j_\alpha(j_\alpha + 2) S^\alpha, \tag{B.3}$$

and under a parity operation transform with eigenvalue $(-1)^{j_\alpha}$.

A general vector field on the sphere may be expanded as a combination of gradients of the scalar spherical harmonics plus a set of vector spherical harmonics $\vec{V}_{j_\pm}^{m m'}$. These transform in the $(\frac{j_\pm+1}{2}, \frac{j_\pm-1}{2})$ representation of $SO(4)$, where j is a positive integer. Again, it is convenient to denote the full set of indices (j, m, m', ϵ) by a single index α . These obey orthonormality relations

$$\begin{aligned} \int_{S^3} V^\alpha \cdot V^\beta &= \delta^{\alpha\bar{\beta}}, \\ \int_{S^3} V^\alpha \cdot \nabla S^\beta &= 0. \end{aligned} \tag{B.4}$$

Again $V^{\bar{\alpha}}$ indicates the complex conjugate of V^α , given by

$$(\mathbf{V}_{j_\pm}^{m m'})^* = (-1)^{m+m'+1} \mathbf{V}_{j_\pm}^{-m -m'}. \tag{B.5}$$

The vector spherical harmonics are eigenfunctions of parity with eigenvalue $(-1)^{j+1}$, and satisfy

$$\begin{aligned} \nabla^2 V^\alpha &= -(j_\alpha + 1)^2 V^\alpha, \\ \nabla \times V^\alpha &= -\epsilon_\alpha (j_\alpha + 1) V^\alpha, \\ \nabla \cdot V^\alpha &= 0. \end{aligned} \tag{B.6}$$

Explicit expressions for the scalar and vector spherical harmonics may be found in [7].

B.2. Spherical harmonic integrals

In expanding the action in modes, we require the integrals over the sphere of products of various numbers of spherical harmonics. For two spherical harmonics, the integrals are given by the orthonormality relations. For products of three spherical harmonics, we require the set of integrals given in (2.18). These were calculated in [7], and the results may be expressed in terms of the functions (3.12) and (3.13) as²⁸

$$\begin{aligned} C^{\alpha\beta\gamma} &= \begin{pmatrix} \frac{j_\alpha}{2} & \frac{j_\beta+\epsilon_\beta}{2} & \frac{j_\gamma}{2} \\ m_\alpha & m_\beta & m_\gamma \end{pmatrix} \begin{pmatrix} \frac{j_\alpha}{2} & \frac{j_\beta-\epsilon_\beta}{2} & \frac{j_\gamma}{2} \\ m'_\alpha & m'_\beta & m'_\gamma \end{pmatrix} R_2(j_\alpha, j_\beta, j_\gamma), \\ D^{\alpha\beta\gamma} &= \begin{pmatrix} \frac{j_\alpha+\epsilon_\alpha}{2} & \frac{j_\beta+\epsilon_\beta}{2} & \frac{j_\gamma}{2} \\ m_\alpha & m_\beta & m_\gamma \end{pmatrix} \begin{pmatrix} \frac{j_\alpha-\epsilon_\alpha}{2} & \frac{j_\beta-\epsilon_\beta}{2} & \frac{j_\gamma}{2} \\ m'_\alpha & m'_\beta & m'_\gamma \end{pmatrix} R_{3\epsilon_\alpha\epsilon_\beta}(j_\alpha, j_\beta, j_\gamma), \\ E^{\alpha\beta\gamma} &= \begin{pmatrix} \frac{j_\alpha+\epsilon_\alpha}{2} & \frac{j_\beta+\epsilon_\beta}{2} & \frac{j_\gamma+\epsilon_\gamma}{2} \\ m_\alpha & m_\beta & m_\gamma \end{pmatrix} \begin{pmatrix} \frac{j_\alpha-\epsilon_\alpha}{2} & \frac{j_\beta-\epsilon_\beta}{2} & \frac{j_\gamma-\epsilon_\gamma}{2} \\ m'_\alpha & m'_\beta & m'_\gamma \end{pmatrix} R_{4\epsilon_\alpha\epsilon_\beta\epsilon_\gamma}(j_\alpha, j_\beta, j_\gamma). \end{aligned} \tag{B.7}$$

²⁸ The expression for C below differs by a factor of two from the expression in [7], but we believe that this expression is correct.

To evaluate integrals appearing in quartic terms, we do not require any additional information, since any product of two spherical harmonics may be expressed as a sum of single spherical harmonics using the completeness property and the integrals above. For example, we find

$$V^\alpha \cdot V^\beta = D^{\alpha\beta\bar{\gamma}} S^\gamma. \quad (\text{B.8})$$

B.3. Identities involving 3j symbols

The expressions for two and three loop vacuum diagrams involve products of the integrals in the previous subsection, with indices contracted and summed over in various ways. Since the m and m' indices appear only in 3j-symbols, we can always evaluate the sums over these using standard 3j-symbol identities.

For basic manipulations, we require the identities

$$\begin{pmatrix} j_1 & j_2 & j_3 \\ m_1 & m_2 & m_3 \end{pmatrix} = \begin{pmatrix} j_3 & j_1 & j_2 \\ m_3 & m_1 & m_2 \end{pmatrix} \quad (\text{B.9})$$

$$\begin{pmatrix} j_1 & j_2 & j_3 \\ m_1 & m_2 & m_3 \end{pmatrix} = (-1)^{(j_1+j_2+j_3)} \begin{pmatrix} j_1 & j_2 & j_3 \\ -m_1 & -m_2 & -m_3 \end{pmatrix} \quad (\text{B.10})$$

$$\begin{pmatrix} j_1 & j_2 & j_3 \\ m_1 & m_2 & m_3 \end{pmatrix} = (-1)^{(j_1+j_2+j_3)} \begin{pmatrix} j_2 & j_1 & j_3 \\ m_2 & m_1 & m_3 \end{pmatrix} \quad (\text{B.11})$$

To evaluate two-loop sums, we require

$$\sum_{m_1} \sum_{m_2} \begin{pmatrix} j_1 & j_2 & j_3 \\ m_1 & m_2 & m_3 \end{pmatrix} \begin{pmatrix} j_1 & j_2 & j_4 \\ m_1 & m_2 & m_4 \end{pmatrix} = \frac{\delta_{j_3 j_4} \delta_{m_3 m_4}}{2j_3 + 1} \quad (\text{B.12})$$

Finally, in three-loop computations we require

$$\begin{aligned} & \sum_{m's} (-1)^{m_1+m_2+m_3+m_4+m_5+m_6} \\ & \begin{pmatrix} j_1 & j_1 & j_3 \\ m_1 & -m_1 & m_3 \end{pmatrix} \begin{pmatrix} j_3 & j_4 & j_5 \\ -m_3 & m_4 & m_5 \end{pmatrix} \begin{pmatrix} j_5 & j_4 & j_6 \\ -m_5 & -m_4 & m_6 \end{pmatrix} \begin{pmatrix} j_6 & j_2 & j_2 \\ -m_6 & m_2 & -m_2 \end{pmatrix} \\ & = (-1)^{j_1+j_2} \sqrt{(2j_1+1)(2j_2+1)} \delta_{j_3,0} \delta_{j_6,0} \delta_{j_4,j_5} \end{aligned} \quad (\text{B.13})$$

$$\begin{aligned} & \sum_{m's} (-1)^{m_1+m_2+m_3+m_4+m_5+m_6} \\ & \begin{pmatrix} j_1 & j_1 & j_2 \\ m_1 & -m_2 & m_2 \end{pmatrix} \begin{pmatrix} j_2 & j_3 & j_4 \\ -m_2 & m_3 & m_4 \end{pmatrix} \begin{pmatrix} j_3 & j_5 & j_6 \\ -m_3 & m_5 & m_6 \end{pmatrix} \begin{pmatrix} j_4 & j_6 & j_5 \\ -m_4 & -m_6 & -m_5 \end{pmatrix} \\ & = (-1)^{j_1+j_3} \sqrt{\frac{2j_1+1}{2j_3+1}} \delta_{j_3,j_4} \delta_{j_2,0} \delta(j_4, j_5, j_6) \end{aligned} \quad (\text{B.14})$$

$$\begin{aligned}
& \sum_{m's} (-1)^{m_1+m_2+m_3+m_4+m_5+m_6} \\
& \begin{pmatrix} j_1 & j_2 & j_3 \\ m_1 & m_2 & m_3 \end{pmatrix} \begin{pmatrix} j_3 & j_2 & j_4 \\ -m_3 & -m_2 & m_4 \end{pmatrix} \begin{pmatrix} j_4 & j_5 & j_6 \\ -m_4 & m_5 & m_6 \end{pmatrix} \begin{pmatrix} j_6 & j_5 & j_1 \\ -m_6 & -m_5 & -m_1 \end{pmatrix} \\
& = \frac{1}{2j_1+1} \delta_{j_1, j_4} \delta(j_1, j_2, j_3) \delta(j_1, j_5, j_6)
\end{aligned} \tag{B.15}$$

$$\begin{aligned}
& \sum_{m's} (-1)^{m_1+m_2+m_3+m_4+m_5+m_6} \\
& \begin{pmatrix} j_1 & j_2 & j_3 \\ m_1 & m_2 & -m_3 \end{pmatrix} \begin{pmatrix} j_3 & j_4 & j_5 \\ m_3 & m_4 & -m_5 \end{pmatrix} \begin{pmatrix} j_5 & j_6 & j_1 \\ m_5 & m_6 & -m_1 \end{pmatrix} \begin{pmatrix} j_2 & j_6 & j_4 \\ -m_2 & -m_6 & -m_4 \end{pmatrix} \\
& = (-1)^{j_1+j_2+j_3+j_4+j_5+j_6} \left\{ \begin{matrix} j_1 & j_2 & j_3 \\ j_4 & j_5 & j_6 \end{matrix} \right\}
\end{aligned} \tag{B.16}$$

In equations (B.14) and (B.15), the delta function with three arguments is either 1 or 0, depending on whether or not the triangle relation is satisfied. In equation (B.16), $\left\{ \begin{matrix} j_1 & j_2 & j_3 \\ j_4 & j_5 & j_6 \end{matrix} \right\}$ is the 6j symbol.

B.4. Identities for sums of spherical harmonics

Using the 3j-identities, it is straightforward to derive expressions for sums over m, m' , and ϵ in various products of the spherical harmonic integrals. For the two loop diagrams, we require:

$$\begin{aligned}
& \sum_{m's} D^{\alpha\bar{\alpha}\gamma} D^{\beta\bar{\beta}\bar{\gamma}} = \frac{1}{2\pi^2} j_\alpha(j_\alpha+2) j_\beta(j_\beta+2) \delta_{\gamma,0}, \\
& \sum_{m's, \epsilon's, j_\gamma} D^{\alpha\bar{\alpha}\gamma} D^{\beta\bar{\beta}\bar{\gamma}} = \frac{2}{\pi^2} j_\alpha(j_\alpha+2) j_\beta(j_\beta+2), \\
& \sum_{m's, \epsilon's} D^{\alpha\beta\gamma} D^{\bar{\alpha}\bar{\beta}\bar{\gamma}} = 2R_{3+}^2(j_\alpha, j_\gamma, j_\beta) + 2R_{3-}^2(j_\alpha, j_\gamma, j_\beta), \\
& \sum_{m's, \epsilon's, j_\gamma} D^{\alpha\beta\gamma} D^{\bar{\alpha}\bar{\beta}\bar{\gamma}} = \frac{2}{3\pi^2} j_\alpha(j_\alpha+2) j_\beta(j_\beta+2), \\
& \sum_{m's} E^{\alpha\beta\gamma} E^{\bar{\alpha}\bar{\beta}\bar{\gamma}} = R_{4\epsilon_\alpha\epsilon_\beta\epsilon_\gamma}^2(j_\alpha, j_\beta, j_\gamma).
\end{aligned} \tag{B.17}$$

For the three-loop diagrams it is useful first to note the basic relations (related to

those above):

$$\begin{aligned}
\sum_{m's,\epsilon} D^{\alpha\bar{\alpha}\lambda} &= \frac{\sqrt{2}}{\pi} \delta_{\lambda,0} j_\alpha (j_\alpha + 2), \\
\sum_{m's,\epsilon's} D^{\alpha\beta\gamma} D^{\bar{\alpha}\bar{\beta}\bar{\tau}} &= 2\delta_{\gamma\bar{\tau}} \frac{1}{(j_\gamma + 1)^2} (R_{3+}^2(j_\alpha, j_\gamma, j_\beta) + R_{3-}^2(j_\alpha, j_\gamma, j_\beta)), \\
\sum_{m's,\epsilon's} D^{\alpha\gamma\tau} D^{\beta\bar{\gamma}\bar{\tau}} &= \delta_{\alpha\bar{\beta}} \frac{1}{j_\alpha(j_\alpha + 2)} (R_{3+}^2(j_\alpha, j_\tau, j_\gamma) + R_{3-}^2(j_\alpha, j_\tau, j_\gamma)), \\
\sum_{m's,\epsilon's} C^{\alpha\delta\gamma} C^{\bar{\gamma}\bar{\delta}\beta} &= -2\delta_{\alpha\bar{\beta}} \frac{1}{(j_\alpha + 1)^2} R_2^2(j_\alpha, j_\delta, j_\gamma), \\
\sum_{m's} E^{\alpha\gamma\delta} E^{\bar{\delta}\bar{\gamma}\beta} &= -\delta_{\alpha\bar{\beta}} \frac{1}{j_\alpha(j_\alpha + 2)} R_{4\epsilon_\delta\epsilon_\gamma\epsilon_\alpha}^2(j_\delta, j_\gamma, j_\alpha), \\
\sum_{m's} D^{\gamma\tau\alpha} E^{\bar{\tau}\bar{\gamma}\beta} &= 0, \\
\sum_{m's} C^{\alpha\gamma\tau} D^{\bar{\gamma}\beta\bar{\tau}} &= 0.
\end{aligned} \tag{B.18}$$

In each of these, we are summing over m , m' , and ϵ for each of the contracted indices only.

Using these basic relations and the results of the previous subsection, we find the following results for the non-vanishing spherical harmonic sums that appear in the three loop calculations:

$$\begin{aligned}
\sum_{m's,\epsilon's,j_\lambda,j_\tau} D^{\alpha\bar{\alpha}\lambda} D^{\gamma\delta\bar{\lambda}} D^{\bar{\gamma}\bar{\delta}\bar{\tau}} D^{\beta\bar{\beta}\bar{\tau}} &= \delta_{j_\gamma,j_\delta} \frac{2}{\pi^4} j_\alpha (j_\alpha + 2) j_\beta (j_\beta + 2) j_\gamma (j_\gamma + 2), \\
\sum_{m's,\epsilon's,j_\lambda} D^{\alpha\bar{\alpha}\lambda} D^{\gamma\delta\bar{\lambda}} D^{\beta\bar{\gamma}\tau} D^{\bar{\beta}\bar{\delta}\bar{\tau}} &= \delta_{j_\gamma,j_\delta} \frac{2}{\pi^2} j_\alpha (j_\alpha + 2) (R_{3+}^2(j_\gamma, j_\tau, j_\beta) + R_{3-}^2(j_\gamma, j_\tau, j_\beta)), \\
\sum_{m's,\epsilon's} D^{\alpha\gamma\lambda} D^{\bar{\alpha}\delta\bar{\lambda}} D^{\beta\bar{\delta}\tau} D^{\bar{\beta}\bar{\gamma}\bar{\tau}} &= \delta_{j_\gamma,j_\delta} \frac{2}{j_\gamma(j_\gamma + 2)} (R_{3+}^2(j_\gamma, j_\lambda, j_\alpha) + R_{3-}^2(j_\gamma, j_\lambda, j_\alpha)) \\
&\quad \cdot (R_{3+}^2(j_\gamma, j_\tau, j_\beta) + R_{3-}^2(j_\gamma, j_\tau, j_\beta)), \\
\sum_{m's,\epsilon's} D^{\alpha\gamma\lambda} D^{\bar{\alpha}\bar{\gamma}\tau} D^{\delta\beta\bar{\lambda}} D^{\bar{\delta}\bar{\beta}\bar{\tau}} &= \delta_{j_\lambda,j_\tau} \frac{4}{(j_\lambda + 1)^2} (R_{3+}^2(j_\alpha, j_\lambda, j_\gamma) + R_{3-}^2(j_\alpha, j_\lambda, j_\gamma)) \\
&\quad \cdot (R_{3+}^2(j_\beta, j_\lambda, j_\delta) + R_{3-}^2(j_\beta, j_\lambda, j_\delta)), \\
\sum_{m's} D^{\alpha\beta\lambda} D^{\gamma\delta\bar{\lambda}} D^{\bar{\beta}\bar{\delta}\tau} D^{\bar{\alpha}\bar{\gamma}\bar{\tau}} &= (-1) \sum_{j's} \left\{ \begin{array}{ccc} \frac{j_\gamma + \epsilon_\gamma}{2} & \frac{j_\lambda}{2} & \frac{j_\delta + \epsilon_\delta}{2} \\ \frac{j_\beta + \epsilon_\beta}{2} & \frac{j_\tau}{2} & \frac{j_\alpha + \epsilon_\alpha}{2} \end{array} \right\} \left\{ \begin{array}{ccc} \frac{j_\gamma - \epsilon_\gamma}{2} & \frac{j_\lambda}{2} & \frac{j_\delta - \epsilon_\delta}{2} \\ \frac{j_\beta - \epsilon_\beta}{2} & \frac{j_\tau}{2} & \frac{j_\alpha - \epsilon_\alpha}{2} \end{array} \right\} \\
&\quad \cdot R_{3\epsilon_\alpha\epsilon_\beta}(j_\alpha, j_\lambda, j_\beta) R_{3\epsilon_\gamma\epsilon_\delta}(j_\gamma, j_\lambda, j_\delta) R_{3\epsilon_\beta\epsilon_\delta}(j_\beta, j_\tau, j_\delta) R_{3\epsilon_\alpha\epsilon_\gamma}(j_\alpha, j_\tau, j_\gamma),
\end{aligned} \tag{B.19}$$

$$\begin{aligned}
\sum_{m's, \epsilon's, j_\lambda} D^{\rho\bar{\rho}\lambda} D^{\alpha\beta\bar{\lambda}} \widehat{E}^{\bar{\alpha}\tau\sigma} \widehat{E}^{\bar{\beta}\bar{\sigma}\bar{\tau}} &= -\delta_{j_\alpha, j_\beta} \frac{1}{\pi^2} j_\rho (j_\rho + 2) \sum_{\epsilon's} (\widehat{R}_{4\epsilon_\sigma\epsilon_\tau\epsilon_\alpha}(j_\sigma, j_\tau, j_\alpha))^2, \\
\sum_{m's, \epsilon's} C^{\sigma\gamma\rho} C^{\bar{\rho}\bar{\gamma}\bar{\tau}} D^{\alpha\beta\bar{\sigma}} D^{\bar{\alpha}\bar{\beta}\bar{\tau}} &= -\delta_{j_\sigma, j_\tau} \frac{4}{(j_\sigma + 1)^2} R_2^2(j_\sigma, j_\gamma, j_\rho) \\
&\quad \cdot (R_{3+}^2(j_\alpha, j_\sigma, j_\beta) + R_{3-}^2(j_\alpha, j_\sigma, j_\beta)), \\
\sum_{m's, \epsilon's} D^{\alpha\beta\lambda} D^{\bar{\alpha}\gamma\bar{\lambda}} \widehat{E}^{\bar{\beta}\delta\rho} \widehat{E}^{\bar{\delta}\bar{\gamma}\bar{\rho}} &= -\delta_{j_\beta, j_\gamma} \frac{1}{j_\beta(j_\beta + 2)} (R_{3+}^2(j_\alpha, j_\lambda, j_\beta) + R_{3-}^2(j_\alpha, j_\lambda, j_\beta)) \\
&\quad \cdot \sum_{\epsilon's} (\widehat{R}_{4\epsilon_\beta\epsilon_\delta\epsilon_\rho}(j_\beta, j_\delta, j_\rho))^2, \\
\sum_{m's, \epsilon's} \widehat{E}^{\gamma\alpha\rho} \widehat{E}^{\bar{\rho}\bar{\alpha}\bar{\delta}} \widehat{E}^{\bar{\gamma}\tau\beta} \widehat{E}^{\bar{\beta}\bar{\tau}\bar{\delta}} &= \delta_{j_\gamma, j_\delta} \frac{1}{j_\gamma(j_\gamma + 2)} \sum_{\epsilon_\gamma} [\sum_{\epsilon's} (\widehat{R}_{4\epsilon_\alpha\epsilon_\rho\epsilon_\gamma}(j_\alpha, j_\rho, j_\gamma))^2 \\
&\quad \cdot \sum_{\epsilon's} (\widehat{R}_{4\epsilon_\beta\epsilon_\tau\epsilon'_\gamma}(j_\beta, j_\tau, j_\gamma))^2],
\end{aligned} \tag{B.20}$$

$$\begin{aligned}
\sum_{m's} D^{\alpha\gamma\rho} D^{\beta\delta\bar{\rho}} \widehat{E}^{\bar{\alpha}\bar{\beta}\bar{\tau}} \widehat{E}^{\bar{\delta}\bar{\gamma}\bar{\tau}} &= -(-1) \sum j's \left\{ \begin{array}{ccc} \frac{j_\alpha + \epsilon_\alpha}{2} & \frac{j_\beta + \epsilon_\beta}{2} & \frac{j_\tau + \epsilon_\tau}{2} \\ \frac{j_\delta + \epsilon_\delta}{2} & \frac{j_\gamma + \epsilon_\gamma}{2} & \frac{j_\rho}{2} \end{array} \right\} \left\{ \begin{array}{ccc} \frac{j_\alpha - \epsilon_\alpha}{2} & \frac{j_\beta - \epsilon_\beta}{2} & \frac{j_\tau - \epsilon_\tau}{2} \\ \frac{j_\delta - \epsilon_\delta}{2} & \frac{j_\gamma - \epsilon_\gamma}{2} & \frac{j_\rho}{2} \end{array} \right\} \\
&\quad \cdot R_{3\epsilon_\alpha\epsilon_\gamma}(j_\alpha, j_\rho, j_\gamma) R_{3\epsilon_\beta\epsilon_\delta}(j_\beta, j_\rho, j_\delta) \widehat{R}_{4\epsilon_\alpha\epsilon_\beta\epsilon_\tau}(j_\alpha, j_\beta, j_\tau) \widehat{R}_{4\epsilon_\delta\epsilon_\gamma\epsilon_\tau}(j_\delta, j_\gamma, j_\tau), \\
\sum_{m's} \widehat{E}^{\rho\sigma\tau} \widehat{E}^{\bar{\alpha}\bar{\beta}\bar{\tau}} \widehat{E}^{\bar{\beta}\bar{\gamma}\bar{\rho}} \widehat{E}^{\bar{\gamma}\bar{\alpha}\bar{\sigma}} &= (-1) \sum j's \left\{ \begin{array}{ccc} \frac{j_\rho + \epsilon_\rho}{2} & \frac{j_\sigma + \epsilon_\sigma}{2} & \frac{j_\tau + \epsilon_\tau}{2} \\ \frac{j_\alpha + \epsilon_\alpha}{2} & \frac{j_\beta + \epsilon_\beta}{2} & \frac{j_\gamma + \epsilon_\gamma}{2} \end{array} \right\} \left\{ \begin{array}{ccc} \frac{j_\rho - \epsilon_\rho}{2} & \frac{j_\sigma - \epsilon_\sigma}{2} & \frac{j_\tau - \epsilon_\tau}{2} \\ \frac{j_\alpha - \epsilon_\alpha}{2} & \frac{j_\beta - \epsilon_\beta}{2} & \frac{j_\gamma - \epsilon_\gamma}{2} \end{array} \right\} \\
&\quad \cdot \widehat{R}_{4\epsilon_\rho\epsilon_\sigma\epsilon_\tau}(j_\rho, j_\sigma, j_\tau) \widehat{R}_{4\epsilon_\alpha\epsilon_\beta\epsilon_\tau}(j_\alpha, j_\beta, j_\tau) \widehat{R}_{4\epsilon_\beta\epsilon_\gamma\epsilon_\rho}(j_\beta, j_\gamma, j_\rho) \widehat{R}_{4\epsilon_\gamma\epsilon_\alpha\epsilon_\sigma}(j_\gamma, j_\alpha, j_\sigma), \\
\sum_{m's} D^{\alpha\gamma\rho} D^{\beta\bar{\gamma}\bar{\sigma}} C^{\bar{\rho}\bar{\beta}\bar{\tau}} C^{\bar{\tau}\bar{\alpha}\bar{\sigma}} &= -(-1) \sum j's \left\{ \begin{array}{ccc} \frac{j_\rho}{2} & \frac{j_\tau}{2} & \frac{j_\beta + \epsilon_\beta}{2} \\ \frac{j_\sigma}{2} & \frac{j_\gamma + \epsilon_\gamma}{2} & \frac{j_\alpha + \epsilon_\alpha}{2} \end{array} \right\} \left\{ \begin{array}{ccc} \frac{j_\rho}{2} & \frac{j_\tau}{2} & \frac{j_\beta - \epsilon_\beta}{2} \\ \frac{j_\sigma}{2} & \frac{j_\gamma - \epsilon_\gamma}{2} & \frac{j_\alpha - \epsilon_\alpha}{2} \end{array} \right\} \\
&\quad \cdot R_2(j_\rho, j_\beta, j_\tau) R_2(j_\tau, j_\alpha, j_\sigma) R_{3\epsilon_\alpha\epsilon_\gamma}(j_\alpha, j_\rho, j_\gamma) R_{3\epsilon_\beta\epsilon_\gamma}(j_\beta, j_\sigma, j_\gamma), \\
\sum_{m's} \widehat{E}^{\alpha\beta\gamma} C^{\rho\bar{\gamma}\bar{\sigma}} D^{\bar{\beta}\bar{\tau}\bar{\sigma}} D^{\bar{\alpha}\bar{\tau}\bar{\rho}} &= (-1) \sum j's \left\{ \begin{array}{ccc} \frac{j_\alpha + \epsilon_\alpha}{2} & \frac{j_\beta + \epsilon_\beta}{2} & \frac{j_\gamma + \epsilon_\gamma}{2} \\ \frac{j_\sigma}{2} & \frac{j_\rho}{2} & \frac{j_\tau + \epsilon_\tau}{2} \end{array} \right\} \left\{ \begin{array}{ccc} \frac{j_\alpha - \epsilon_\alpha}{2} & \frac{j_\beta - \epsilon_\beta}{2} & \frac{j_\gamma - \epsilon_\gamma}{2} \\ \frac{j_\sigma}{2} & \frac{j_\rho}{2} & \frac{j_\tau - \epsilon_\tau}{2} \end{array} \right\} \\
&\quad \cdot R_2(j_\rho, j_\gamma, j_\sigma) \widehat{R}_{4\epsilon_\alpha\epsilon_\beta\epsilon_\gamma}(j_\alpha, j_\beta, j_\gamma) R_{3\epsilon_\beta\epsilon_\tau}(j_\beta, j_\sigma, j_\tau) R_{3\epsilon_\alpha\epsilon_\tau}(j_\alpha, j_\rho, j_\tau).
\end{aligned} \tag{B.21}$$

Finally, in certain cases, we may simplify expressions further by using the relations

$$\begin{aligned}
\sum_c R_{3+}^2(a, c, b) &= \sum_c R_{3-}^2(a, c, b) = \frac{1}{6\pi^2} a(a+2)b(b+2), \\
\sum_c (R_2(a, b, c))^2 &= \frac{1}{3\pi^2} b(b+2)a(a+2)(a+1)^2.
\end{aligned} \tag{B.22}$$

References

- [1] B. Lucini, M. Teper and U. Wenger, “The deconfinement transition in $SU(N)$ gauge theories,” *Phys. Lett. B* **545**, 197 (2002) [arXiv:hep-lat/0206029].
- [2] B. Lucini, M. Teper and U. Wenger, “The high temperature phase transition in $SU(N)$ gauge theories,” *JHEP* **0401**, 061 (2004) [arXiv:hep-lat/0307017].
- [3] G. 't Hooft, “A planar diagram theory for strong interactions,” *Nucl. Phys. B* **72**, 461 (1974).
- [4] B. Sundborg, “The Hagedorn transition, deconfinement and $N = 4$ SYM theory,” *Nucl. Phys. B* **573**, 349 (2000) [arXiv:hep-th/9908001].
- [5] O. Aharony, J. Marsano, S. Minwalla, K. Papadodimas and M. Van Raamsdonk, “The Hagedorn / deconfinement phase transition in weakly coupled large N gauge theories,” arXiv:hep-th/0310285, to appear in *ATMP*.
- [6] D. J. Gross and E. Witten, “Possible third order phase transition in the large N lattice gauge theory,” *Phys. Rev. D* **21**, 446 (1980); S. Wadia, “A study of $U(N)$ lattice gauge theory in two-dimensions,” preprint EFI-79/44-CHICAGO; S. R. Wadia, “ $N = \infty$ phase transition in a class of exactly soluble model lattice gauge theories,” *Phys. Lett. B* **93**, 403 (1980).
- [7] R. E. Cutkosky, “Harmonic functions and matrix elements for hyperspherical quantum field models,” *J. Math. Phys.* **25**, 939 (1984).
- [8] G. 't Hooft, “Renormalization of massless Yang-Mills fields,” *Nucl. Phys. B* **33**, 173 (1971).
- [9] This file is available at <http://www.fas.harvard.edu/~papadod/3loop/3loop.html>.
- [10] A. Adams and E. Silverstein, “Closed string tachyons, AdS/CFT, and large N QCD,” *Phys. Rev. D* **64**, 086001 (2001) [arXiv:hep-th/0103220].
- [11] O. Aharony, M. Berkooz and E. Silverstein, “Multiple-trace operators and non-local string theories,” *JHEP* **0108**, 006 (2001) [arXiv:hep-th/0105309].
- [12] G. Leibbrandt and J. Williams, “Split dimensional regularization for the Coulomb Gauge,” *Nucl. Phys. B* **475**, 469 (1996) [arXiv:hep-th/9601046].
- [13] Y. H. Chen, R. J. Hsieh and C. I. Lin, “Split dimensional regularization for the temporal gauge,” arXiv:hep-th/9610165.
- [14] G. Leibbrandt, “The three-point function in split dimensional regularization in the Coulomb gauge,” *Nucl. Phys. B* **521**, 383 (1998) [arXiv:hep-th/9804109].
- [15] G. Heinrich and G. Leibbrandt, “Split dimensional regularization for the Coulomb gauge at two loops,” *Nucl. Phys. B* **575**, 359 (2000) [arXiv:hep-th/9911211].
- [16] J. Kapusta, “Finite temperature field theory” (Cambridge University Press, 1989) and references therein.
- [17] D. J. Gross, R. D. Pisarski and L. G. Yaffe, “QCD and instantons at finite temperature,” *Rev. Mod. Phys.* **53**, 43 (1981).

- [18] K. Kajantie, M. Laine, K. Rummukainen and Y. Schroder, “The pressure of hot QCD up to $g^6 \ln(1/g)$,” *Phys. Rev. D* **67**, 105008 (2003) [arXiv:hep-ph/0211321].
- [19] S. Hadizadeh, B. Ramadanovic, G. W. Semenoff and D. Young, “Free energy and phase transition of the matrix model on a plane-wave,” arXiv:hep-th/0409318.
- [20] O. Aharony, J. Marsano, S. Minwalla, K. Papadodimas, M. Van Raamsdonk and T. Wiseman, to appear.
- [21] S. W. Hawking and D. N. Page, “Thermodynamics of black holes in anti-de Sitter space,” *Commun. Math. Phys.* **87**, 577 (1983).
- [22] E. Witten, “Anti-de Sitter space, thermal phase transition, and confinement in gauge theories,” *Adv. Theor. Math. Phys.* **2**, 505 (1998) [arXiv:hep-th/9803131].